

A Design of A Mobile Application for Thalang's Historical Sites Representation

Pita Jarupunphol*, Wipawan Buathong†
 Department of Digital Technology,
 Phuket Rajabhat University Phuket, Thailand, 83000
 Email: *p.jarupunphol@pkru.ac.th, †w.buathong@pkru.ac.th

Abstract— This article proposes a design of a historical background searching application of Thalang's historical sites in Phuket. Thalang's historical information and images were adopted from different offline and online sources. A design process is based on using Z Schemata of Z-notation to represent logical arguments in state schema and operation schema associated with the system. The historical sites were determined by the referred location in history and GPS. The GPS coordinates are set to the centre for users to view historical data and images. If the user takes a photo within the designated area, he/she will be able to view historical data and images associated with the taken photo. The experimental results revealed that the users could view historical background and images of the historical sites properly.

Keywords— Application, GPS, Historical Background, Smart City, Z-notation.

I. Introduction

Phuket is a province located in the south of Thailand and has been widely recognised as a world tourist destination because of a variety of tourism natural resources. Nowadays, the current growth of digital technology has facilitated the management of government agencies, private organizations, and individuals. This province has become a key national economic sector. For instance, Phuket is a government strategic province of Thailand that has been promoted to be driven by digital technology with the availability of ICT infrastructure capacity in the race for the country under the Thailand 4.0 policy [1], [2]. Besides, Phuket Smart City is one of the most prominent national projects to support Thailand as the country's first smart city [3], [4], [5]. According to Giffinger et al. [6], smart city comprises six components, including smart economy, smart mobility, smart environment, smart living, smart people, and smart governance. These six components were also included in Thailand Smart Cities Development Strategic Plan [3]. In this case, several provincial strategic projects were proposed by the stakeholders from public and private sectors. For example, enabling software developers from abroad to conduct business with the 8-year tax exemption, encouraging the use of digital technology to enhance the tourism industry, developing applications to facilitate the tourism, providing security services in the province, using IoTs (Internet of Things) to enhance the living quality, and extending the high-speed Internet infrastructure for the public [7]. In the meantime, different types of tourism were also introduced to support a tremendous growth of the Phuket tourism industry. In addition to beach tourism, which is the most popular tourism type, cultural tourism also captures tourist interests since this type of tourism is concerned with the culture, history, and lifestyle

of the people in a geographical area. Other attributes contribute to the way of life (e.g., architecture, art, food, and religion) are also considered as part of cultural tourism.

Thalang district was once the historical significance of Phuket. It was among the former cities of the West Coast of the South Central region. Thalang is also reputable as the city of two heroines, including Lady Chan and Lady Mook. Nevertheless, the historical sites in this area have changed dramatically. Not only were significant changes of the outline of the past to the present, a number of historical images and information of Thalang landmarks have disappeared. It is difficult for individuals to search and obtain these historical images. Recently, the use of digital technology together with Global Positioning System (GPS) has become an essential feature in the destination navigation [8]. Google Map, for example, is an example of the use of GPS technology that has gained popularity around the world. The system has improved the image attributes responding to users who need to travel to tourist sites or check the near landmark. While Google Map is not purposely designed for tracing historical events in the past, this article proposes an application capable of representing the historical backgrounds of tourist attractions in Thalang district. The application represents the historical image of the user current position connected to GPS via the Internet in the specified area. The tourists can observe the images displaying the Thalang's historical sites from past to present.

II. Literature Reviews

There were several application designed to facilitate tourism industry. In Jarupunphol et al. [2], Phuket Tourism Planning Model (PTPM) was proposed to obtain a traveling path of tourist sites under limited distance and time. The application is based on the QR Code to organises raw kitchen materials in a household. The user can add, delete, and adjust the number of products in the kitchen or refrigerator. In terms of cultural and historical tourism, "Culture Explorer" is an application for android mobile platform developed by Flexmedia [9]. The application was introduced to bridge today people with the cultural and historical heritage. The current version 2.0 includes several contents about Thailand's key tourist sites and most of them are in Bangkok. There are several features in the application for enhancing user experience. For instance, the user can selfie and overlay with the displayed historical images. The application allows the user to share his/her photos to popular social media applications. The application also provides a nearby notification feature to alert the user when he/she is near historical sites. However, all cultural sites and themes are defined by Samsung's authorised agents. Then, users are

allowed to add images and videos related to the specified destinations in the application. Since this application involves a distance measurement between two points, the following equations should also be reviewed in this section.

A. Minkowski distance

Minkowski distance is a measure of a vector space on a plane space, which is the fundamental principle of the Euclidean distance and Manhattan distance based on the equation 1, given that: 1) x and y are points on m dimension; 2) $p \geq 1$ and i contains values from 1 to m ; and 3) $d(x, y)$ is the distance from x to y .

$$d(x, y) = \left(\sum_{i=1}^m |x_i - y_i|^p \right)^{\frac{1}{p}} \quad (1)$$

B. Canberra distance

Canberra distance, which was invented in 1966 and updated in 1967 by Lance Williams (Lance and Williams) Canberra, is a measure of the numerical distance between two points in space vector. The Canberra is similar to Manhattan distance, which has a wide space and is generally used as a measure for rank comparison. Canberra distance is also used for intrusion detection in computer network [10]. It is based on the equation 2 in which x and y are points on m dimension, and i contains values from 1 to m , where $d(x; y)$ is the distance from x to y .

$$d(x, y) = \sum_{i=1}^m \frac{|x_i - y_i|}{|x_i + y_i|} \quad (2)$$

C. Chebyshev distance

Chebyshev distance is a measure specified in the vector space where the distance between the two vectors is the difference on most dimensions harmonization. The name is conceptualised and named after Pafnuty Chebyshev. Chebyshev distance is also recognised as chessboard distance since the minimum number of moves required of the king to the next square on the chessboard is equivalent to the Chebyshev. The centre of the square is a rectangle with a representative side length of the coordinates of spatial 2-D axis corresponding to the edge of the board. The term Chebyshev between f6 and e2 is equal to 4 on the basis of equation (3) in which x and y are points on m dimension, and i contains values from 1 to m , where $d(x; y)$ is the distance from x to y .

$$d(x, y) = \max_{i=1}^m |x_i - y_i| \quad (3)$$

D. Euclidean distance

Euclidean distance, derived from the Pythagoras theory, is the distance between two points, which is a straight line that can be measured with a ruler. Equation (4) represents x and y points on m dimension, where i ranges from 1 to m and $d(x; y)$ is the distance from x to y .

$$d(x, y) = \sqrt{\sum_{i=1}^m (x_i - y_i)^2} \quad (4)$$

E. Manhattan distance

Manhattan distance is the distance between two points in the table on the horizontal and vertical grid lines strictly based on the diagonal. The name comes from the area of the square of streets in Manhattan with the shortest path between two points in the city. The distance of Manhattan is a simple summary of the horizontal and vertical. The Manhattan has been applied to evaluate the differences in discrete frequency distributions. While the distance diagonally may be calculated by using the Pythagoras theory. The equation (5) on the x and y are spots on the m dimensions, and i contains values from 1 to m , where $d(x; y)$ is the distance from x to y .

$$d(x, y) = \sum_{i=1}^m |x_i - y_i| \quad (5)$$

F. Haversine formula

Haversine formula is an important equation in determining the distance between two points on the circle sphere defined by longitude and latitude. The Haversine is a special case of the general rules of spherical trigonometry according to Haversine formula, which is related to sides and angles of a triangle sphere. The equation 6 requires that 1) φ is the latitude 2) ω is the longitude 3) a space is half the distance between two points, 4) c is the angular distance in Radian 5) d is the distance and 6) R is the radius of the Earth. The Haversine differs from the above equations, which are suitable for finding the distance between two points on a common plane, but ineffective for locating GPS coordinates on the world oval surface.

$$a = \sin^2\left(\frac{\Delta\varphi}{2}\right) + \cos\varphi_1 \cdot \cos\varphi_2 \cdot \sin^2\left(\frac{\Delta\omega}{2}\right)$$

$$c = 2 \cdot \text{atan2}(\sqrt{a}, \sqrt{1-a})$$

$$d = R \cdot c \quad (6)$$

III. Methodology

Since this research emphasises an adaptive process of the application design to obtain a workable application, there are few methodological steps involved in the application development.

A. Data Collection

A related set of Thalang's historical attractions in Phuket province, including requirements and boundaries, were defined according to the historical book of Thalang and Phuket [11], [12]. Desired input and output are determined in this initial step. Thalang National Museum in Phuket is also a major sources of historical information of Thalang primarily used in this research. Besides Phuket and Thalang historical books, the internet, journal articles, historical data and images related to Thalang historical sites are also essential for defining and comparing the sites locations. For instance, Southern Historical Encyclopedia includes a number of images and information related to Phuket history, which has been widely used by many history researchers and manipulated by PhuketData.Net [13]. Nevertheless, there are also several historical sites that do not clearly specify the location and pinpoint coordinates based on a historic visit to the items specified in the above references must be conducted.

B. Analysis and Design

Administrator and user are two main entities involved in the system utilisation. While administrator is the person who can determine the location of historical sites and also add, edit and delete historical images and information linking to Google Map based on the GPS coordinates, user is the person, who can take pictures of Thalang's historical sites. Then, the pictures will be compared with the historical images stored in the system. In this section, the Z notation schemata [14], [15] is used to provide formal descriptions of major attributes and their roles in the system.

1) Administrator

The ADMIN state schema below represents the ADMIN static view in which the upper part consists of variable declarations of the ADMIN and the lower part comprises the operational statements.

ADMIN
location: \square LOCATION
image: \square IMAGE
history: LOCATION \leftrightarrow IMAGE
location \subseteq dom history
image \subseteq ran history

The initialisation schema ADMIN_{INIT} illustrates an initial stage before an admin adds an image to a system. Two variables, including system and image are set at \emptyset . The ADMIN in the upper part enforces that all defined statements in the ADMIN state scheme will be included in the initialization schema ADMIN_{INIT}.

ADMIN _{INIT}
ADMIN
location = \emptyset
image = \emptyset

The ADMINAdd operation schema includes the state schema Δ ADMIN. The operation schema ADMINAdd updates the component *history* in the schema ADMIN. The $add \subseteq history$ enforces that the storage function in the schema ADMIN will always be updated when the image is added ($\forall l? \mapsto i? \in add \bullet l? \mapsto i? \in history$). The predicate $history' = history \cup l? \mapsto i?$ represents that *l?* has been updated in location and *i?* has been updated in image.

ADMINAdd
ADMIN
<i>l?</i> : LOCATION
<i>i?</i> : IMAGE
add: LOCATION \leftrightarrow IMAGE
add \subseteq history
history' = history $\cup \{l? \mapsto i?\}$

Similar to the ADMINAdd, the ADMINDelete operation schema includes the state schema Δ ADMIN. The delete \subseteq history enforces that delete activity is a subset of history. The predicate $history' = history \setminus \{l? \mapsto i?\}$ represents that *l?* and *i?* have been updated in history and image.

ADMINDelete
ADMIN
<i>l?</i> : LOCATION
<i>i?</i> : IMAGE
delete: LOCATION \leftrightarrow IMAGE
delete \subseteq history
history' = history $\setminus \{l? \mapsto i?\}$

The ADMINUpdate is used to update the ingredient. The predicate $system' = system \oplus s? \mapsto i?$ represents that *i?* has been updated in image.

ADMINUpdate
ADMIN
<i>l?</i> : LOCATION
<i>i?</i> : IMAGE
update: LOCATION \leftrightarrow IMAGE
update \subseteq history
history' = history $\oplus \{l? \mapsto i?\}$

2) User

The USER includes the state schema \exists ADMIN to represent the retrieval of location and image with the postcondition remain unchanged. The operation schema USER will not update the component location and image in the schema ADMIN. The predicate $retrieve' = retrieve \cup \{l? \mapsto i?\}$ represents a condition when the location and image are scanned by the user, but no operations will update location and image at this stage.

<p><i>USER</i></p> <hr/> <p>$\exists ADMIN$</p> <p>$l?: LOCATION$</p> <p>$i!: IMAGE$</p> <p>$retrieve: LOCATION \rightarrow IMAGE$</p> <hr/> <p>$retrieve \subseteq history$</p> <p>$l? \in location$</p> <p>$i! \in image$</p> <p>$retrieve' = retrieve \cup \{l? \mapsto i!\}$</p>
--

The initialisation schema $USER_{INIT}$ is an initial stage before a user starts using the application. Variables *location* and *image* are set at \emptyset in the first stage when location and image have not yet been retrieved. All variables and logical statements in the *ADMIN* state scheme will be used in the initialisation schema $USER_{INIT}$.

<p><i>USER_{INIT}</i></p> <hr/> <p><i>ADMIN</i></p> <hr/> <p>$location = \emptyset$</p> <p>$image = \emptyset$</p>
--

C. Development

After the design phase had completed, an application prototype was built. The application development tools consisted of a smartphone capable of pinpointing the GPS coordinates based on the defined historical sites. Android Studio was used as a primary tool for the application development [16]. Firebase Realtime Database, a non-SQL database, was used to collect images and information of historical sites and respond to user queries in realtime [17].

D. System Testing

The application was pre-tested with three historical sites of Thalang at least 10 times for each destination. There were some minor errors in which the locations of the historical destination images determined by the administrator according to historical reference sources were inaccurate with the current location of those historical attractions.

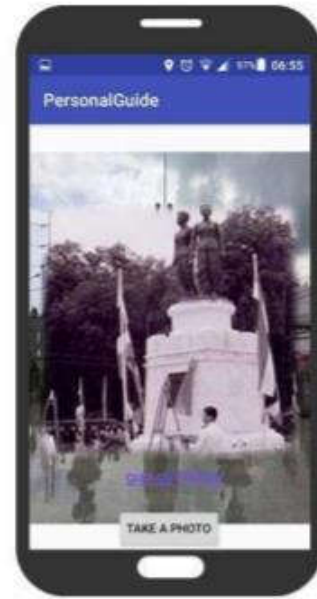


Fig 1. Past Image of Phuket Heroines Monument

IV. Results and Discussion

The students could use the application effortlessly without any hindrance. The images of historical places defined by the administrator could be retrieved correctly. The application was capable of retrieving historical images according to the user's current location on the map. Since the application relies upon the Internet, the application speed is varied according to the coverage of Internet Service Provider (ISP) and distribution of wireless access points in the Thalang's historical sites. Nevertheless, there were minor errors in the accuracy of the location of some historical places defined by the formula. The dislocation caused by the measured position of the application function. This discrepancy is between the image retrieved from the user's current location and that from the historical location specified by the administrator.

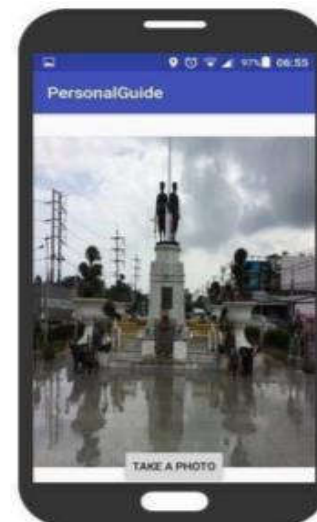


Fig. 2. Present Image of Phuket Heroines Monument

V. Conclusions and Future Work

More accurate equations for comparing current and historical locations of users should be adopted. Multimedia sources such as video files should be added to make the data more diverse. In addition, the application should be equipped with contemporary technologies to enhance user experience. For example, using Geofence, a perimeter around a physical location, to show the extent of the historical place that has been defined. AR (Augmented Reality) technology can also be used to manipulate the images that have been assigned to historical sites to be realistic and compatible with historical location environments.

However, the application should be tested with tourists using appropriate questionnaires for the more accurate data in terms of usability or user experience. For example, a USE questionnaire comprises question items for measuring measure usability [18]. According to Lund [18], subjective reactions to the software product usability were often ignored despite being closely related to user behavior concerning the software adoption. Thirty question items, based on seven-point Likert scales ranging from strongly disagree to strongly agree, are proposed to evaluate user attitudes towards four dimensions of usability, e.g., ease of use, ease of learning, usefulness, and satisfaction [19]. Furthermore, using TAM (Technology Acceptance Model) [20], [21] can also be considered as a promising tool for measuring the user's intention towards an innovation adoption as it contains certain psychological constructs to forecast the user adoption likelihood of an innovation, including perceived ease of use, perceived usefulness, attitude towards using, and intention to use. The relationships of these constructs are considered as a human-computer interaction theoretical model.

Acknowledgment

I would like to express my special thanks to the ICNGC for inviting me to be part of ICNGC programme committee and giving me a wonderful opportunity to present my paper.

References

- [1] P. Jarupunphol, W. Buathong, and T. Chansaeng, "The MTAS for addressing motorcycle theft," in The 13th International Conference on Electrical Engineering/Electronics, Computer, Telecommunications and Information Technology (ECTI-CON 2016), Chiang Mai, Thailand, June 2016, pp. 1–6.
- [2] P. Jarupunphol, W. Buathong, T. Chansaeng, and N. Laosen, "A combination of GA and Fuzzy Set for a Phuket tourism planning model (PTPM)," in 2016 International Computer Science and Engineering Conference (ICSEC), Dec 2016, pp. 1–6.
- [3] "Thailand smart cities development strategic plan – draft (in Thai)," Department of Economy and Promotion Agency, May 2018. [Online]. Available: <http://www.depa.or.th/th/publications>
- [4] A. Pornwasin, "Plan to make Phuket and Chiang Mai 'smart cities'," The Nation, September 2015. [Online]. Available: <http://www.nationmultimedia.com/national/Plan-to-make-Phuket-and-Chiang-Mai-smart-cities-30268781.html>
- [5] P. Jarupunphol, W. Buathong, T. Chansaeng, and N. Laosen, "A descriptive design for a smart kitchen management application (SKM)," in Proceedings of the 2018 IEEE International Conference on Information and Computer Technologies (ICICT 2018), DeKalb, USA, March 2018, pp. 61–66.
- [6] R. Giffinger, H. Gudrun, G., and G. Haindlmaier, "Smart cities ranking: An effective instrument for the positioning of the cities," vol. 4, 02 2010.
- [7] A. Maierbrugger, "Phuket to become Thailand's first smart city, Chiang Mai to follow," Investvine, January 2016. [Online]. Available: <http://investvine.com/phuket-to-become-thailands-first-smart-city-chiang-mai-to-follow/>
- [8] A. El-Rabbany, Introduction to GPS: the Global Positioning System. Boston: Artech House, 2006.
- [9] "Culture Explorer (Thailand)," Google Play, September 2016. [Online]. Available: <https://play.google.com/store/apps/details?id=com.samsung.culture.thailand>
- [10] G. B. Regulwar and P. R. Deshmukh, "Extraction of texture features using euclidean, canberra and both distance," International Journal of Advanced Research in Computer Science, vol. 2, no. 3, pp.228–234, 2017. [Online]. Available: <http://www.ijarcs.info/index.php/Ijarcs/article/view/526>
- [11] S. Pinbuddhasilpa, Supplementary Phuket City Knowledge (in Thai). Phuket: Phuket Cultural Center, 1983.
- [12] Thalang Historical Sites (in Thai). Phuket: Phuket Cultural Office, 2016.
- [13] "All about cultures in phuket," PHUKETDATA.NET. [Online]. Available: <https://www.phuketdata.net/>
- [14] J. Jacky, The Way of Z: Practical Programming with Formal Methods. Cambridge: Cambridge University Press, 1997.
- [15] J. M. Spivey, The Z Notation: A Reference Manual. University of Oxford, 1998.
- [16] J. Horton, H. Vasconcelos, and R. Portales, Android: programming for developers: develop your own responsive, reactive, and ready-to-deploy Android applications. Birmingham: Packt Publishing, 2016.
- [17] F. Cheng, Build mobile apps with Ionic 2 and Firebase: hybrid mobile app development. New York: Apress, 2017.
- [18] A. M. Lund, "Measuring usability with the use questionnaire," Usability Interface, vol. 8, pp. 3–6, 2001. [Online]. Available: <http://www.stcsig.org/usability/newsletter/index.html>
- [19] "USE questionnaire: Usefulness, satisfaction, and ease of use," garyperlman.com. [Online]. Available: <http://garyperlman.com/quest/quest.cgi?form=USE>
- [20] F. D. Davis, "Perceived usefulness, perceived ease of use, and user acceptance of information technology," MIS Quarterly, vol. 13, no. 3, pp. 319–340, 1989.
- [21] —, "User acceptance of information technology: system characteristics, user perceptions and behavioral impacts," International Journal of Man-Machine Studies, vol. 38, no. 3, pp. 475–487, March 1993.

Session IV : IoT

- Smart Transportation: The Role of Big Data and Internet of Things
/ Phuong Dinh
/ BaRia VungTau University, Vietnam
- Semi-Automatic Construction of Field Maps for Fingerprint-based Indoor Positioning System
/ HanJun Bae, Lynn Choi
/ Korea University, Korea
- A real-time relay selection scheme for MAC protocol in smart farm systems
/ Sam, Nguyen-Xuan, Nguyen Hong Son
/ Posts and Telecoms Institute of Technology HCM, Vietnam
- Study for Cycle Control Method of Publisher using PUBACK packet in MQTT
/ Yeon Ju Lee, Min Chang Lee, Pan Koo Kim
/ Chosun University, Korea
- Managing Home IoT Device using Smart Contract on A BlockChain Platform
/ Jae Geun Song, Eung Seon Kang, Seung Jae Pee, Ju Wook Jang
/ Sogang University, Korea

Smart Transportation: The Role of Big Data and Internet of Things

Thu Phuong Dinh

Logistics and Supply Chain Management
 Ba Ria – Vung Tau University
 Vungtau City, Socialist Republic of Vietnam
 Dinhthuphuong0908@gmail.com

Abstract— Industrial revolution 4.0 has brought the world to a new trend called "smart trend". Countries have been building smart cities, which is also the orientation of the Vietnamese government. There are many factors that make up a smart city, in which the most important component is the smart transportation. This paper provides the basics of smart transportation, and the role of Big Data and Internet of Things in improving transportation system to become smarter.

Keywords— Big Data; Internet of Things (IoT); Smart Transportation; Smart City

I. Introduction

The history of transportation development is closely related to the history of human development from the earliest days, when humans used labor and animals as the main means of transport. It plays an important role in the economy, society and politics of a country. As transportation demand has been increasing leads to challenges such as the land uses, traffic accidents or environmental pollution. That requires countries to find a solution, and smart transportation seems to be the best solution in the context of the Fourth industrial revolution. The paper answer following question:

1. What is smart transportation
2. What makes smart transportation?
3. What are the benefits of smart transportation?
4. What is the role of Big Data and Internet of Things (IoT) in application smart transportation?

II. Smart Transportation

“Smart transportation (and its cousin, intelligent transportation system) offers a means of providing innovative services on different modes of transportation and traffic management. It is an important area in the smart grid and an extension of smart cities. Its components include infrastructure, vehicles, and users.” (Sadiku et al., 2017).

Intelligent transportation system (ITS) or smart transportation optimises existing infrastructure to make transport more efficient, and helps improve transportation in many ways, as belowing:

- Health, safety and environmental benefits: Reducing accidents
- Public transport benefits: Reducing congestion, optimising route of bus
- Driver and traffic management benefits: Traffic control, gathering traffic data, parking management

- Economic benefits: Reducing infrastructure damage.

The elements of smart transportation are shown in Figure 1. Smart transportation system is the integration of many systems such as Automated Vehicle Location System, Real-Time Traffic Information System, Automated Fare Collection System, Car Sharing Cycle Sharing Systems, Intelligent Signaling System, Real-time Monitoring System, Parking Information System, ... Technology is the best tool to connect all above systems effectively, including Big data and IoT which are mentioned in the next section of the article.

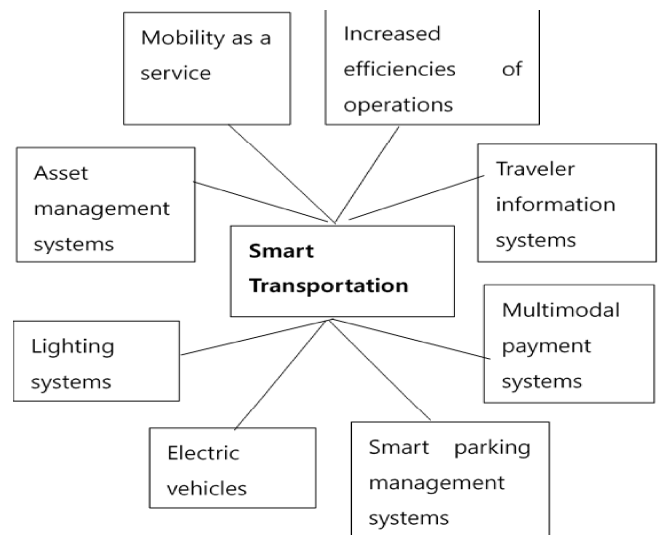


Fig 1. Elements of Smart Transportation in Smart city (Source: Author’s work based on Neil Pedersen, 2017)

III. Big Data and Internet of Things in Smart Transportation

After the invention of the Internet, the Internet of Things (IoT) is a technology that has created maximum impact in the way businesses and corporates function. IoT can be defined as the network of interconnected computer devices embedded in various objects, ranging from mobile devices and household appliances to vehicles and even structures. The IoT has already had a huge positive impact on all industries such as healthcare, agriculture, etc ... and transportation is not an exception. Smart transportation includes the use of IoT in transportation systems.

IoT applications in transportation deliver not only the following benefits:

- Cost-savings: Operating data and diagnostics drive preventive maintenance to decrease costs and improve

warranty as well as service processes

- Operational and supply chain efficiencies
- Increased driver safety and job satisfaction.

Figure 2 is an example of benefit from application IoT in transportation. Drivers are alerted to hazardous conditions in real-time to avoid crashes and traffic congestion. Fuel consumption can be monitored and evaluated for efficiencies. Trucks can be monitored for wear and tear so that potential problems can be addressed before a vehicle breaks down. This helps reduce repair costs. Freight conditions can be tracked and monitored throughout the driver’s journey. Drivers can be alerted about the change of cargo environmental to resolve immediately. Drivers can be monitored for physical condition and performance. Every abnormal and unsafe expression like speeding, getting drowsy will be sent to managers, who can take the appropriate action. This enables crash avoidance safety applications. Transport managers can track their fleet status such as location, delivery status, schedules, ...via positioning and sensing systems, in conjunction with the navigation system determines the optimal route based on weather and traffic conditions so that drivers can be rerouted in real time (if necessary).



Fig 2. Application of IoT in Transportation (Source: <https://data-flair.training/blogs>)

In the digital age, the amount of data increases with the multiplier. In smart transportation, the need of data collection and data analytics is priority to answer the questions: Where do the traffic streams go? Where is the danger? What is the status of cargo in real time? etc ... Data sets can be so large and complex that they become difficult to process using traditional data processing applications and existing data management tools. This huge data is so-called Big data. Table 1 is an example for traffic management in Hochiminh City. It points out that the transport managers must collect at least five belowing data domains: Traffic operation, Traffic incident, Vehicle, Infrastructure, Weather condition. It also includes data of driver status, passenger information and their behavior, etc..

TABLE I. Traffic Management Data Matrix

Data Domain	Type of Data		
	Fixed	Historical	Real-time
Traffic Operation	Map Route Regulation	Rush hour Traffic jam	Vehicle flow Axle load Traffic density
Traffic Incident	Congestion Accident	Regular place Causation factors	Date/ time Location Type of impact
Vehicle	Amount Age Specification (length, weight, height, ...)	Emissions Fuel consumption	Position Speed Route
Infrastructure	Map fixed data layers (width of road, amount of bridge, ...)	Traffic history	Pavement occupancy Road maintenance Tides
Weather Condition	Sunny season Rainy season	Weather condition at the same period years before	Wind speed Temperature

All parties of transportation industry like airlines, airports, freight logistics, transportation agencies, and others are enjoying the benefits of Big Data. The benefits of Big Data and analytics help the transportation managers to precisely enhance the model capacity, demand, revenue, pricing, customer sentiments, cost and urban or public transportation.

In many countries, the implementation of Big Data in Transportation is one of the leading solutions for smart transportation. Better data can help transport managers understand the behavior of traffic participants, provide information and identify policy interventions. In fact, the biggest benefit from using Big Data can come from changing user behavior. For example, in Singapore, use real-time local traffic data to determine toll rates. This encourages the driver to avoid driving in the most congested time and optimizes the use of the road network.

Table 2 points of the benefits from IoT and Big Data application in some countries.

IV. Applications of Big Data and Internet of Things in Transportation

Application of IoT and Big Data extends to all aspects of transportation systems. Big Data is used not only in traffic management, but also in informing travelers, public authorities and transport industry, developing automated vehicles, etc ... On the other hand, Big Data is useful for all transportation industry parties. Governments are using big data for traffic controlling, transport planning and modeling, route planning, congestion management, and Intelligent Transport Systems. The private sector like travel industry, logistics and supply chain management also gets benefit from Big Data. Individuals can save their time and money by using Big Data because of increasing fuel-efficiency or easily travel planning.

The IoT and Big Data application is dramatically accelerating the pace of innovation and transforming the way of operations in transportation and infrastructure. Some of the key applications of IoT in transport can be listed as below:

- Fleet Management
- Optimal Asset Utilization
- Smart Toll Collection
- Smart Parking
- Vehicle manufacturing.

TABLE II. The benefits of IoT and Big Data Implementation in Transportation

<i>(Bus)</i>	<i>Passenger comfort</i>	Infotainment, Wi-Fi, LED lighting and signage, charging
	<i>Electrical system</i>	Power distribution, computers, sensors, micro chargers
	<i>Processing</i>	Engine control, energy optimisation, driving behavior, safety monitoring
	<i>Steering</i>	Driving assistance, cruise control, radio/ phone

Countries	Problems (before the implementation of IoT and Big data)	Results (after the implementation of IoT and Big data)
<i>Portugal</i>	Recurring cases of fatal accidents due to non-compliance with speed limits	Behavioral change in the drivers' ecodriving, then drastic reduction in the cases of fatal car accidents
<i>Germany</i>	Road safety concern, traffic congestion, and pollution.	Eco-friendliness, and hitch-free traffic flow
<i>England</i>	Operational waste and workers' safety	Operational waste reduction and safe working environment
<i>Singapore</i>	Unpleasant passenger's booking experience	Better passenger's booking experience

(Source: Hussein et al, 2017)

We can see that IoT applications are large and complex. The following are common IoT application areas for smart transportation:

- Smart Driver Advisory Systems: IoT can play a proactive role in helping drivers to stay on track of safe driving habits
- Smart Car Technology: Connected and Autonomous Vehicles
- Smart Traffic Management
- Smart Infrastructure Maintenance: IoT sensors can monitor and detect the structural status of roads and bridges under dynamic conditions and alert government about deficiencies for fixing them before they become less safe and more expensive to repair.

Table 3 is an example of Big Data and IoT application in freight transportation and public transportation.

TABLE III. Application of IoT and Big Data in Transportation

Type of transport	Application areas	Detail
<i>Freight Transport</i>	<i>Inventory management</i>	Real-time capacity availability
	<i>Human resources</i>	Reduction in driver turnover, driver assignment, using sentiment data analysis
	<i>Transport management</i>	Optimal routing, weather conditions, traffic congestion, and driver characteristics
	<i>Forecasting</i>	Time of delivery, factoring in weather, driver characteristics, time of day and date
<i>Public Transport</i>	<i>Fleet management</i>	Bus location, technical diagnostic, fuel monitoring, route optimisation

V. Conclusion

The article presents an overview of the role of IoT and Big Data in smart transportation. The government of Vietnam has realized the benefits of using Big Data and IoT to solve traffic problems. A €37 million-project in collaboration with IBM to set up a Traffic Management System has begun in 2013 in Danang City to solve the problem of traffic congestion throughout the city with a fast-growing population. However, there are challenges for application of IoT and Big Data in transportation which are listed as below: lack of appropriate skills and common standards in collecting and connecting data, software complexity, financial capability, security and privacy, data sources and characteristics, data quality, etc ... This requires that countries (including Vietnam) should have suitable policies and criteria to select the transportation aspect which is appropriate to their available conditions to apply Big Data and IoT.

Acknowledgment

I would like to give my thank to all who in one way or another contributed in the completion of this article. This paper would never have completed without the guidance of various scientists from many professional areas. I would also like to give thanks to websites of individuals and organizations for providing me the latest trend and technology regarding my research.

References

- [1] Matthew N.O. Sadiku, Adebowale E. Shadare, Sarhan M. Musa, "Smart Transportation: A Primer", International Journal of Advanced Research in Computer Science and Software Engineering 7(3), pp. 6-7, March- 2017.
- [2] ITS United Kingdom, " Intelligent transport systems (ITS) and their benefits," Published by Mouchel Ltd, September 2016.
- [3] Neil Pedersen, " Smart Transportation in a Smart City," Transportation Research Board Annual Meeting, Washington DC, 2017
- [4] Waleed Noori Hussein, L.M. Kamarudin, Haider N. Hussain, A. Zakaria, R Badlishah Ahmed, N.A.H. Zahri, " The Prospect of Internet of Things and Big Data Analytics in Transportation System," 1st International Conference on Big Data and Cloud Computing, IOP Publishing, 2017
- [5] Ed Kuzemchak, " The benefits of IoT in transportation: An industry case study," <https://softwaredesignsolutions.com/>, Jul 22, 2018.
- [6] Naveen Joshi, " This is why big data in transportation is a big deal", <https://www.allerin.com/blog/>, 20, September 2017.
- [7] International Transport Forum, "Big Data and Transport: Overview," <https://www.slideshare.net/>, Oct 2013
- [8] Patrick Le Fèvre, "Climb aboard Automotive 4.0," <http://www.newelectronics.co.uk/electronics-technology/>, 28 March 2017
- [9] Xiao-Feng Xie, "Key Applications of the Smart IoT to Transform Transportation," <http://www.wiomax.com/>, September 2016

Semi-Automatic Construction of Field Maps for Fingerprint-based Indoor Positioning System

Han Jun Bae and Lynn Choi
 School of Electrical Engineering
 Korea University
 Seoul, Korea
 {qwerty2901, lchoi}@korea.ac.kr

Abstract— Fingerprinting has been one of the most popular techniques used for both magnetic and RF-based indoor positioning systems. It requires the preconstruction of a field map such as radio map that records the received signal strengths at predetermined positions. Although the localization performance is closely related to the precision and accuracy of the underlying field maps, generating a good field map is still a bottleneck of the fingerprinting since it requires a walking survey that often includes point-by-point manual calibration. In this paper we propose two semi-automatic techniques that can reduce the time and cost of such walking survey without losing too much accuracy. We first introduce a semi-automatic signal sampling method called *linear sampling* assuming linear and constant movement of a pedestrian. Then, we present a PDR (pedestrian dead reckoning) based signal sampling method called *PDR sampling* assuming a random waypoint model of a pedestrian movement. In addition, we discuss how to handle missing values that can occur due to the distortion caused by the semi-automatic measurement. To evaluate the accuracy of the proposed signal sampling techniques, we construct various versions of geomagnetic field maps on our campus test-bed by using the proposed methods as well as the manual walking survey. From our experimentation results, we find that linear sampling can produce a relatively high quality data with only 40.4% of data collection time. In contrast, PDR sampling increases the error rate by 15.7% and 23.9% compared to linear sampling and walking survey although it can substantially reduce the data collection time depending on the position reset interval.

Keywords—Indoor positioning system, magnetic field map, radio map, fingerprinting.

I. Introduction

As people spend most of their time in indoor rather than in outdoor environment, the demand for indoor location based services (LBS) have grown substantially. The key enabling technology for LBS is an accurate yet economical indoor positioning system like the outdoor counterpart such as Global Navigation Satellite System (GNSS). Due to the proliferation of IoT sensors and smart devices such as smartphones, various indoor positioning schemes using ultrasonic, RF, magnetic, image, and LIDAR sensors have been proposed for the last few decades. Among these, magnetic and RF-based localization schemes are usually employed for indoor positioning due to their availability in low-cost sensors and applicability to smartphones. Although various distance estimation algorithms from the signal sources have been proposed including angle-of-arrival (AoA), time-of-arrival (ToA), time-difference-of-arrival (TDoA), and inverse square law [1, 4, 11], all of these techniques suffer from complex synchronization mechanisms and/or from unstable and time-varying signal strengths caused by reflection and diffraction inherent in indoor RF signals. Instead, fingerprinting technique is widely used for both RF and magnetic positioning,

since pre-collected signals strengths at the reference points already account for such signal distortion caused by indoor environment.

Fingerprinting requires the construction of a field map that records the signal strengths of predetermined positions called reference points. By comparing signal strengths of an unknown position to those of the reference points, it can estimate the location of the position. Actually, the field map has the role of recording the environmental characteristics of the site since the recorded signal strengths already reflect the environmental variables. Thus, it can give a higher accuracy compared to other solutions. Fingerprinting is widely used for RF-based solutions such as Wi-Fi [3] positioning and BLE (Bluetooth Low Energy) positioning.

Like RF signals, RSS (Received Signal Strength) values of 3-axis of geomagnetic field vector are also distorted by various structures inside buildings such as steel structures, steel shelter doors, elevators, and generators. There are different ways to measure environment variables. Many of the existing studies use their own customized sensor or robot [5]. However, the custom-made sensor and robot are vulnerable to “Kidnapped robot problem”, a situation where an autonomous robot in operation is carried to an arbitrary location [6]. For this reason, smartphone with its built-in sensors is usually more preferred to measure the magnetic field signals. There is currently no de facto standard method for the construction of field maps. But, smartphone obviously offers a benefit that it can be held by users and its sensor data is more appropriate for localizing each person. It can be also used for large-scale data mining. Crowdsourcing sensor data from each user let the process of field map construction more easy and accurate. Even with a smartphone, each reference point should be measured individually and manually, which is very time consuming and an arduous process.

In this paper we automate the process of field map construction by using a smartphone, focusing on reducing the time spent on measurement yet acquiring accurate and reliable sensor data. We target geomagnetic positioning and apply our techniques to geomagnetic field map construction. The reason we choose magnetic field is three-fold. First, unlike RF-based positioning methods no infrastructure such as access points or beacons are required to generate sensor signals since the geomagnetic field is a natural magnetic field flow created by the Earth’s movement. Second, the signal strengths of magnetic field vectors are very stable in indoor environment unlike RF or ultrasonic signal strengths, which potentially enables a more accurate indoor positioning. Despite its advantages, magnetic positioning still requires a walking survey to create a magnetic field map for each site we target for indoor localization service. This is a very time consuming process, especially in a large-scale environment such as airports and complex shopping malls.

We propose two different semi-automatic techniques that can accelerate the construction of magnetic field maps, reducing time and cost. The first technique assumes that a smartphone user walks straightly in a constant speed. The user first selects a start point and an end point before collecting magnetic data. A smartphone application can record sensor data sequentially while the user is walking along the line. After recording data, the application computes the location of each position that sampled the data by dividing the distance between start and end points by the number of recorded data, generating uniform equal interval among the locations. A constant walking speed of the user is a prerequisite for getting reliable data. We call this technique *linear sampling*.

The second technique does neither assume the constant walking speed nor the straight line movement of the user. It relies on a technique called Pedestrian Dead Reckoning (PDR), which is a relative positioning method that can compute the step count and the direction of the pedestrian movement by using Inertial Measurement Unit (IMU) sensor of a smartphone. PDR cannot compute the absolute position of a smartphone user directly but it can compute the relative position of the user with respect to the initial start point by using accelerometer, magnetometer, and gyro sensors that are integrated in the IMU sensor. Like linear sampling, this technique also requires the user selects the initial position. However, the user can freely move in any direction during walking. But, to avoid the accumulation of the positioning errors, the user needs to reset the start position in constant interval. Therefore, there is a tradeoff between the measurement time and the accuracy of the measurement depending on this interval length. With a smartphone, we can measure the magnetic field data while performing PDR simultaneously during walking. All of this process can be programmed in the smartphone application. We call this technique *PDR sampling*.

An important issue in the automatic generation of field maps is how to handle missing or out-of-range values that are created by the distortion of the semi-automatic process. Unlike the manual survey of measuring magnetic field data at the predetermined positions such as grid points in the field map, the semi-automatic techniques collect magnetic field data at random points and estimates their locations. Due to the positioning errors caused by the automatic process, they may generate reference points whose positions can be outside of the field map. Or, some area of the field map may not contain sufficient reference points. Therefore, we need a policy on handling such missing or out-of-range values generated from the semi-automatic process. In this paper we introduce two conversion methods that can transform the raw filed map data into a normalized matrix form where the data points of all the reference points are filled in. The first technique fills in the missing values of the matrix with nearest point value from each reference point while the second technique fills in the matrix with the results of k-nearest neighbors (k-NN) algorithm.

To evaluate the performance of our proposed data collection techniques, we have implemented all the proposed in an Android application and conducted the experimentation using Samsung Galaxy S7 smartphone. We construct various versions of magnetic field maps on our campus test-bed by using the proposed methods as well as the manual walking survey. Our experimentation results show that linear sampling can produce a reasonably good quality data with only a fraction of data collection time. In addition, with PDR sampling we can

substantially reduce the cost of data collection. However, it results in reduced data quality, increasing the error rate by 15.7% and 23.9% compared to linear sampling and walking survey. We also demonstrate how to handle missing and out-of-range values in case of data distortion in semi-automatic techniques.

In the following we discuss the existing studies related to our work in Section II. Then, in Section III we introduce two semi-automatic field map generation techniques that can accelerate the existing manual survey process. We also discuss algorithms that can convert distorted field maps into a normalized matrix form and how we handle missing or out-of-range values. In Section IV we present our experimentation methodology and discuss the evaluation results of the proposed semi-automatic techniques compared to the existing manual survey method in terms of accuracy as well as the time spent on the field map construction. Section V concludes the paper.

II. Related Works

There is still no standard procedure in constructing the magnetic field map. The existing magnetic positioning schemes [2, 7, 8] usually employ manual field survey technique where the administrator collects magnetic sensor data at predetermined reference points. Instead of dedicated sensors, they often use magnetic sensors embedded in smart devices such as smartphones.

A few recent studies [9, 13, 14] have tried to automate the field map construction process. Rai, Anshul, et al. [9] proposed an algorithm which can predict the location of a smartphone user by tracing the user's movement path using a technique similar to PDR. They can infer the location of a user by comparing the user's movement path to the pre-studied patterns of corridors and walls in the site map and eliminating the paths of low possibility. Once the position is predicted, the system can collect RSS data automatically. But, this algorithm still requires a walking survey of the target site to record the positions of corridors and walls. So this method cannot be applied to an indoor environment where no obstacles are present, such as a lobby of a building.

In [13], they focused on improving the data quality of a radio map by using crowdsourced Wi-Fi fingerprints which are post processed offline along with the logged pedestrian trajectory. The crowdsourcing process is automatically carried out by individual users who carry smart devices in the indoor area. But this study also requires a manual survey of corridors and Wi-Fi radio map beforehand.

III. Field map construction process

A smartphone periodically records the magnetic vector in the 3 dimensional (X, Y, Z) space. Since X, Y and Z axes are relative to the smartphone's orientation, if we turn the smartphone, the axis is changed, which makes the geomagnetic field values change. It can be fixed by using the orientation value. The orientation value shows us how much the smartphone has been rotated by the absolute 3-dimensional cardinal dimension, namely north, east, south, west, up and down. This orientation value can be estimated by the smartphone's IMU sensor.

The first semi-automatic technique for the field map construction is called linear sampling where a smartphone application measures magnetic field vector along with straight lines. The smartphone user sets both the starting and end points of a line, and then he or she walks along the line. Assume that n signal samples are recorded and the positions of the first and the

last sample are predetermined and denoted by two vectors $P^0(P_x^0, P_y^0)$ and $P^{n-1}(P_x^{n-1}, P_y^{n-1})$ assuming 2-dimensional field map. After the smartphone user arrives at the end point, our algorithm calculates the position of k^{th} sampling point as in (1). This assumes a constant walking speed and straight line movement of the user.

$$P^k = P^0 + \frac{k(P^{n-1} - P^0)}{n-1} \quad (n \geq 1, 0 \leq k \leq n-1, k \in \mathbf{Z}) \quad (1)$$

The second semi-automatic technique we use for the field map construction is called PDR sampling where PDR estimates the step count, the step length and the orientation of the movement by using the IMU sensor with a smart device such as smartphone. It usually determines the step by analyzing the pattern of the accelerometer sensor data and estimates the direction of the user movement by analyzing the IMU sensor data, i.e. gyroscope, magnetometer, and accelerometer sensor signals of the device. Even with PDR, we still have to reset the starting position in constant time interval since PDR cannot provide an absolute positioning result and the positioning errors are usually accumulated as times go by due to the inaccuracy of the sensors.

Like linear sampling, we simply assume that each step of a pedestrian moves the same distance and set it as a constant value d . But, unlike linear sampling, PDR does not presume the position of an end point. Instead, it estimates the current position by computing the step count and the movement direction. Equation (2) shows the x-axis and y-axis positions of a user when k steps are counted. Here we simply compute x-axis and y-axis position by adding the sum of $\cos\theta_i$ multiplied by the step distance to the starting point.

$$P_x^k = P_x^0 + \sum_{i=1}^k d \cos\theta_i, \quad P_y^k = P_y^0 + \sum_{i=1}^k d \sin\theta_i \quad (2)$$

With PDR sampling, we can collect sensor data almost automatically. But this model has two problems. First, the position predicted by PDR could be different from the real position because indoor magnetic field distorts the orientation of sensed data. In other words, due to the distortion caused by indoor building structures, the magnetometer no longer accurately finds the absolute north direction in indoor environment. Second, the positioning errors are accumulated as times go by. To avoid these problems, the user needs to input the current correct position in constant interval. The lower the reset interval, the higher is the accuracy of the collected data.

After the signal collection step, we have a raw magnetic field map. But, note that the two proposed techniques collect sensor data at random points, which cannot be directly compared with the sensor data at predetermined reference points collected by manual walking survey. Therefore, we cannot determine how accurate the data is. Furthermore, due to the positioning errors caused by the semi-automatic process, the raw field map may contain holes of missing reference points or out-of-range reference points. Therefore, we need to arrange the raw field map of scattered data and convert them into a form that is in line with the manual field map. In the following we present two different algorithms that can select representative sensor values for each corresponding reference point in the manual field map.

The first solution we propose is selecting the nearest point of each reference point. This assumes that the closer the point is to the reference point, the more accurate it is. This method is represented by the following formula.

$$tmp = \arg \min_{0 \leq k \leq n} \left(\sqrt{\{(R_{i,j})_x - P_x^k\}^2 + \{(R_{i,j})_y - P_y^k\}^2} \right) \quad (0 \leq i \leq \text{The number of row of Matrix R})$$

$$(0 \leq j \leq \text{The number of column of Matrix R}) \quad (3)$$

$$N_{i,j} = (P_x^{tmp}, P_y^{tmp}) \quad (4)$$

$R_{i,j}$ is a matrix of reference points and the number of its rows and columns are predefined before the measurement, i.e. the number of reference points is $(i+1) \times (j+1)$, (if i and j starts at 0). $N_{i,j}$ is a matrix composed of the nearest points at each reference point (i, j) . Figure 1 (a) illustrates the idea of this algorithm. Note that this is quite close to K-NN ($k=1$) except the fact that it only finds the nearest point when the distance is less than a given threshold (half of the distance between reference points).

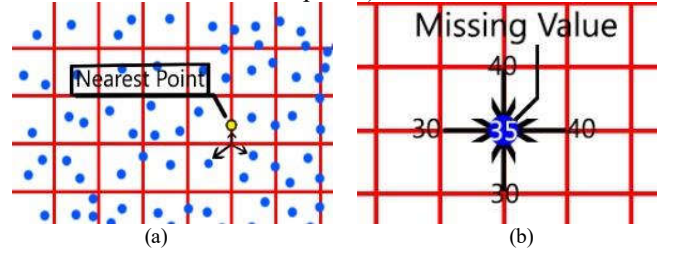


Fig 1. Conversion methods that can transform the raw filed map data into all the reference points.

The second solution we use is the k-NN algorithm where for each reference point the algorithm finds k nearest neighboring data points and computes the weighted average of them to fill in the missing values. This process is shown in the following formula.

$$d_t = \sqrt{\{(R_{i,j})_x - P_x^t\}^2 + \{(R_{i,j})_y - P_y^t\}^2} \quad (8)$$

$$w_n = \frac{\frac{1}{d_n}}{\sum_{t=1}^k \frac{1}{d_t}} \quad (9)$$

$$KNN_{i,j} = (\sum_{t=1}^k \{P_x^t \times w_t\}, \sum_{t=1}^k \{P_y^t \times w_t\}) \quad (10)$$

The d_t is the distance between the data point and its k nearest reference point. And w_n is the weight depends on the distance d_n . After getting weight, we can get the position of x and y by computing the weighted average of distance.

After mapping the raw sensor data to reference points, we can directly compare the accuracy of the semi-automatic field map data with the manual magnetic field map data to evaluate their accuracy. However, the converted field map can still have missing values, in case there is no collected data near the reference points. This circumstance occurs when there are not sufficient measured data sets either due to the random movement or due to the inaccurate position estimation done by the semi-automatic data collection procedures. We fill the missing values with the arithmetic mean of neighboring reference point data sets as illustrated in Figure 2 (a). In addition, a subset of the exterior data sets can be pushed to the outside of the site map. These out-of-range data sets are also caused by the random movement or by the inaccurate position estimation. These out-of-range data are pushed back within the site map by simply taking the arithmetic mean of these out-of-range values with the values in the nearby reference points.

IV. Experimental Environment

A. Environment

We have implemented all the algorithms described in Section III in an Android application. To evaluate the accuracy

and the duration of the semi-automatic data collection process, we construct various versions of magnetic field maps using linear sampling, PDR sampling, and manual survey in our campus test-bed shown in Figure 2 (a). We use Samsung Galaxy S7 as a magnetic sensor and also as an Android application device.

All of the experiments are implemented at same location in Figure 2 (a). Our experiment measure magnetic field with Samsung Galaxy S7. We first make point-by-point manual calibration as reference points. Engineering Building testbed has 629 reference points that are spaced every 57cm interval. And the dimension of the testbed is 20.52 meters by 9.12 meters. The x axis is vertical and the y axis is horizon. We fix slope and orientation of the smartphone while measuring and collect magnetic data stand on each reference point. After measuring reference point, we start experiment about linear sampling and PDR sampling. The walking path is shown in Figure 2 (b) and (c).

In both methods, we start collecting data at (0, 0). The linear sampling method measures magnetic field vector from the left side to the right side, and into the other direction in the zig-zag style as shown in Figure 2 (c). The smartphone user manually records both the start and the end position of each linear movement before starting the movement. In contrast, PDR sampling assumes random way point mobility model and randomize its movement paths freely assuming linear and constant speed movement. Linear sampling collects data at intervals of 6ms while PDR sampling collects data at each step. We also vary the reset interval of PDR sampling from 25 steps, 50 steps, to 100 steps. After measurement, we extract data from the smartphone, and then apply conversion procedures described in Section III on the raw field map data considering both missing and out of bounds data.

B. Result

We evaluate the accuracy and time cost of each technique by comparing with manually measured calibration data. Figure 3, 4 and 5 show the final magnetic field maps generated by manual survey, linear sampling, and PDR sampling respectively.

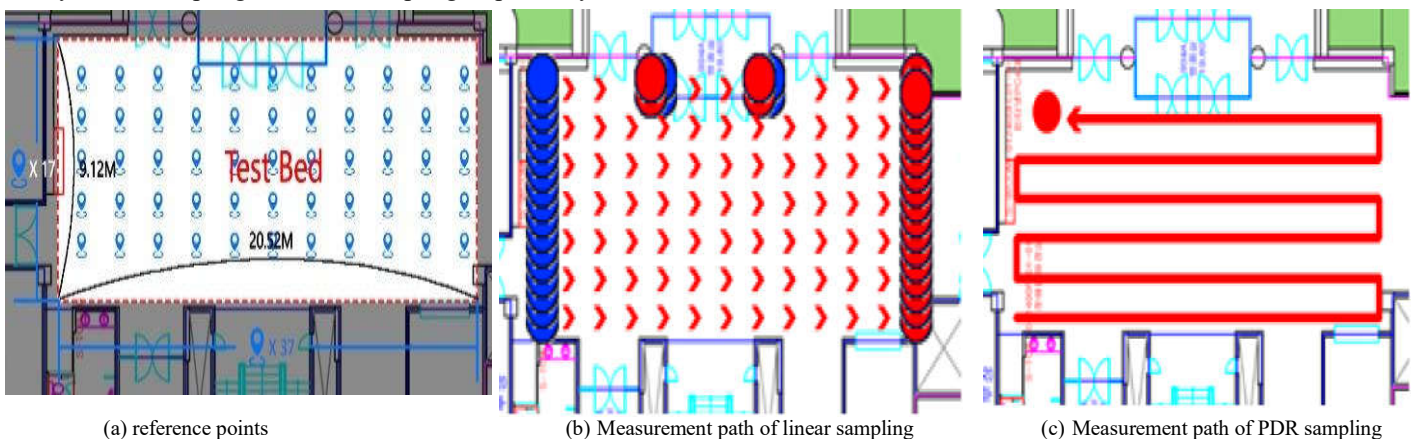


Fig 2. Test Bed, 1st floor of College of Engineering Building, Korea University.

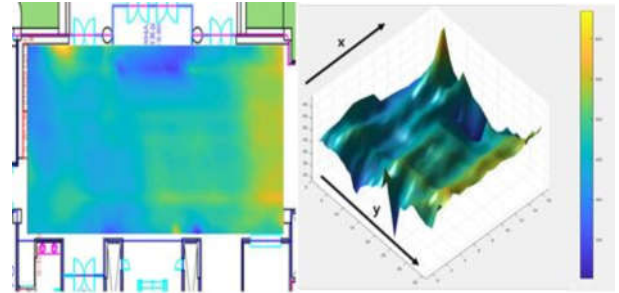


Fig 3. Magnetic field map produced by manual survey.

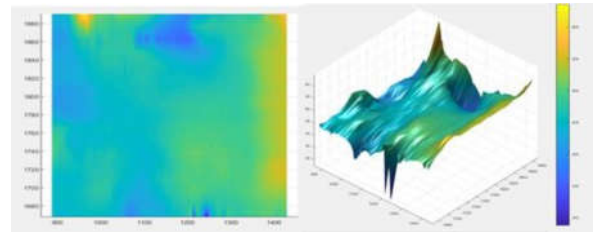


Fig 4. Magnetic field map produced by linear sampling.

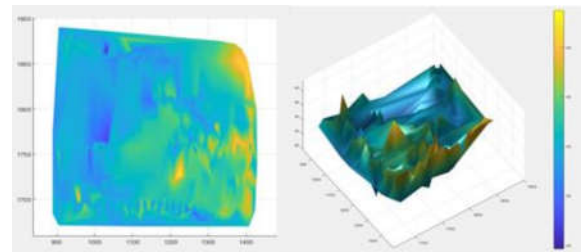


Fig 5. Magnetic field map produced by PDR sampling (using position reset at every 100 steps).

As shown in Figure 3 and 4, the data set collected by linear sampling is very similar to those of manual survey. However, the data set produced by PDR sampling is distorted and quite different from those of the other two methods as illustrated in Figure 5. This is probably caused by the inaccurate position estimation of PDR sampling. We have filled the missing values by using K-NN algorithm which basically computes the

weighted average from data sets of neighboring points. Figure 6 is the result of converting data in Figure 5 to a normalized matrix form by using the K-NN algorithm.

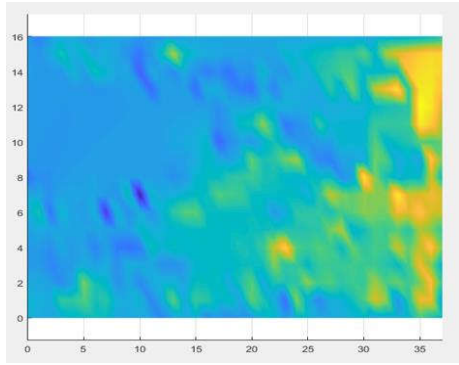


Fig. 6. Converted magnetic field map from Figure 5 by using k-NN.

Table 1 shows the measured data collection time and the average data error of 3 data collection techniques. The error is the average of differences between the data set of manual survey and those of linear and PDR sampling.

TABLE I. Measured collection time and average data error with each sampling method. The numbers shown in the parentheses of PDR sampling denote the position reset intervals in step counts.

	Time rate (time cost)	Nearest point Error rate	k-NN Error-rate
manual	100%(52min.)	0%(0 μ T)	0%(0 μ T)
Linear sampling	40.4%(21min.)	3.2%(1.436728 μ T)	3.1%(1.422695 μ T)
PDR sampling (25)	50%(26min.)	16.1%(7.579367 μ T)	15.7%(7.416036 μ T)
PDR sampling (50)	34.6%(18min.)	22.6%(10.54272 μ T)	22.4%(10.48805 μ T)
PDR sampling (100)	21.2%(11min.)	24.0%(11.3032 μ T)	23.9%(11.24748 μ T)

As shown in Table 1, linear sampling is quite effective, reducing the data collection time by 40.4% but only with 3.1% of marginal error compared to the manual survey technique. In contrast, PDR sampling increases the inaccuracy of the data by as much as 23.9% although it may substantially reduce the data collection time by increasing the position reset interval. Compared to the nearest neighbor algorithm, K-NN improves the accuracy of the data set by slight margin. There is a negative correlation between the data collection time and the data error in case of PDR sampling. The higher the position reset interval, then the lower the data collection time but the error also goes higher.

V. Conclusion

Generating a good field map has been a bottleneck of the fingerprinting used in RF-based and magnetic positioning because it requires a manual survey of the site map with point-by-point data calibration, which is a very time consuming and arduous process. In this paper we propose two semi-automatic techniques that can substantially reduce the time and cost in field map construction. Linear sampling automatically samples data by assuming a constant speed and linear movement of a pedestrian. PDR sampling can also automatically sample data by estimating the current location based on PDR. It allows more flexible movement of a pedestrian such as a random waypoint model while sampling. We also discuss how to handle missing and out-of-range values when the inaccurate position estimation causes the distortion of the data set.

From our Galaxy S7 experimentation on our campus test-bed, we find that linear sampling effectively reduces the time spent in data collection with a minor degradation of the data quality. In contrast, PDR sampling can substantially reduce the time cost but it produces a data set with relatively higher error rates. We also show how to produce a normalized data set in case of data distortion by using two conversion methods including the K-NN algorithm. In our future work, we will apply these techniques to a more large-scale indoor environment.

Acknowledgement

This work was supported by the National Research Foundation of Korea(NRF) grant funded by the Korea government (MSIP) (NRF- 2017R1A2B2009641) and by the MSIT(Ministry of Science and ICT), Korea, under the ITRC(Information Technology Research Center) support program (IITP-2018-2015-0-00363) supervised by the IITP (Institute for Information & communications Technology Promotion).

REFERENCES

- [1] Niculescu, Dragos, and Badri Nath. "Ad hoc positioning system (APS) using AOA." INFOCOM 2003. Twenty-Second Annual Joint Conference of the IEEE Computer and Communications. IEEE Societies. Vol. 3. Ieee, 2003.
- [2] An, Jae Hyung, and Lynn Choi. "Inverse fingerprinting: Server side indoor localization with Bluetooth low energy." Personal, Indoor, and Mobile Radio Communications (PIMRC), 2016 IEEE 27th Annual International Symposium on. IEEE, 2016.
- [3] Xiao, Wendong, Wei Ni, and Yue Khing Toh. "Integrated Wi-Fi fingerprinting and inertial sensing for indoor positioning." IPIN. 2011.
- [4] Huang, B., Xie, L., & Yang, Z. (2015). TDOA-based source localization with distance-dependent noises. IEEE Transactions on Wireless Communications, 14(1), 468-480.
- [5] Haverinen, Janne, and Anssi Kempainen. "Global indoor self-localization based on the ambient magnetic field." Robotics and Autonomous Systems 57.10 (2009): 1028-1035.
- [6] Engelson, Sean P., and Drew V. McDermott. "Error correction in mobile robot map learning." Robotics and Automation, 1992. Proceedings., 1992 IEEE International Conference on. IEEE, 1992.
- [7] Pritt, Noah. "Indoor navigation with use of geomagnetic anomalies." Geoscience and Remote Sensing Symposium (IGARSS), 2014 IEEE International. IEEE, 2014.
- [8] Faragher, Ramsey, and Robert Harle. "An analysis of the accuracy of bluetooth low energy for indoor positioning applications." Proceedings of the 27th International Technical Meeting of the Satellite Division of the Institute of Navigation (ION GNSS+ '14). 2014.
- [9] Rai, Anshul, et al. "Zee: Zero-effort crowdsourcing for indoor localization." Proceedings of the 18th annual international conference on Mobile computing and networking. ACM, 2012.
- [10] Do Yun Kim, and Lynn Choi. "Correction Algorithm for PDR Performance Improvement through Smartphone Motion Sensors." KIISE Transactions on Computing Practices. Vol.23.3 (2017): 148-155.
- [11] Hoskins, J. K., Newman, R. D., Spero, R., & Schultz, J. (1985). Experimental tests of the gravitational inverse-square law for mass separations from 2 to 105 cm. Physical Review D, 32(12), 3084.
- [12] Liu, Z., Zhang, L., Liu, Q., Yin, Y., Cheng, L., & Zimmermann, R. (2017). Fusion of Magnetic and Visual Sensors for Indoor Localization: Infrastructure-Free and More Effective. IEEE Transactions on Multimedia, 19(4), 874-888.
- [13] Wilk, P., Karciaz, J., & Swiatek, J. (2015, October). Indoor radio map maintenance by automatic annotation of crowdsourced Wi-Fi fingerprints. In Indoor Positioning and Indoor Navigation (IPIN), 2015 International Conference on (pp. 1-8). IEEE.
- [14] Liu, T., Li, Q., & Zhang, X. (2016). AUTOMATIC CONSTRUCTION OF WI-FI RADIO MAP USING SMARTPHONES. ISPRS-International Archives of the Photogrammetry, Remote Sensing and Spatial Information Sciences, 309-312.

A real-time relay selection scheme for MAC protocol in smart farm systems*

Sam, Nguyen-Xuan

Faculty of Information Technology
Posts and Telecoms Institute of Technology
HCM city campus, Vietnam
e-mail: samnx@ptithcm.edu.vn

Nguyen Hong Son

Faculty of Information Technology
Posts and Telecoms Institute of Technology
HCM city campus, Vietnam
e-mail: ngson@ptithcm.edu.vn

Abstract— We propose a relay selection scheme to improve end-to-end delay and reliable data transmission for agriculture monitoring systems involving large volumes of data and timing constraints because their properties such as temperature, humidity, light intensity, pH, water level, and quality of water change rapidly. By exploiting dual-hop cooperative communications, our proposal maximizes candidate nodes in the first phase and minimizes the candidate nodes to forwarding data to destination in the second phase. Specifically, the candidate nodes forward the packet only if they receive feedback message in second phase and its timer expires. The selection scheme not only decreases end-to-end delay of forwarding packets and but also increase packet delivery ratio comparing to the single relay scheme.

Keywords— end-to-end delay (E2ED); packet delivery ratio (PDR); relay selection scheme (RSS); smart farm system (SFS).

I. Introduction

The fourth industrial revolution is offering great opportunities to smart agriculture and systems based internet of things are now an important key to connect farms to famers by using smartphones or tablets [1]. However, there are many current issues relating with the systems due to climate change. Thus, we need smart systems that monitor the environmental conditions as such as temperature, humidity, light intensity, pH, water level, and quality of water in real-time so that they can support real-time alert, early warning and monitoring. Moreover, the sensors and actuators used in the systems are able to collect the environmental data, control the deployed devices, and forward them to end users quickly and accuracy by using smartphones or tablets.

In general, the architecture of the smart farm systems including three tiers as shown in figure 1 [2], where tier 1 is farm side, providing actuator and sensor devices, tier 2 stores and processes data at sever or cloud, tier 3 is client side, providing data visualization. In these systems, data generated from the sensor devices is forwarded to gateway and then it is stored, processed and analyzed at cloud or server. The data is then transformed into information which presents at end user's interface as smartphones or smart tablets. The information visualizations map data in the form of charts, graphs, maps, etc. to help the end users to take corrective decisions.

The smart farm systems, built with diverse wireless sensor devices and actuators, are able to the transmits the data through wireless technologies such as Wi-Fi ZigBee, Bluetooth. In order to make it easy to connect to current IoT devices and realize low cost systems, the Wi-Fi devices, known as the technical standards of IEEE 802.11, are used widely. These devices typically act as the network infrastructure to forward data to other nodes from a source to

the destination. However, several constraints such as noise, disconnections, packets lost affect the overall system performance, especially end-to-end delay.

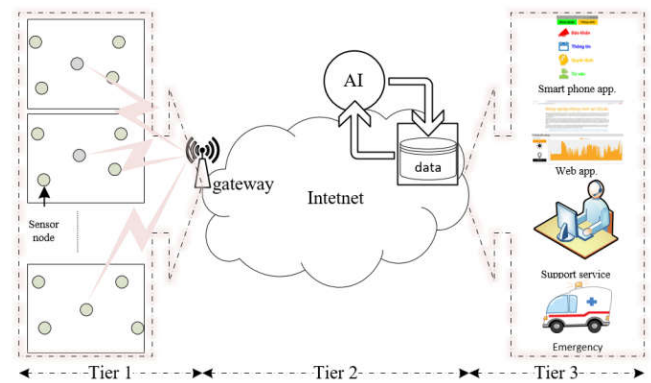


Fig. 1. The architecture of smart agriculture system.

In the work, we propose a selection scheme to exploit the broadcast nature of the wireless devices. By exploiting dual-hop cooperative communications, our proposal 1) maximizes candidate nodes in the first phase and 2) minimizes the candidate nodes to forwarding data to destination in the second phase. Specifically, the candidate nodes forward the packet only if they receive feedback message in second phase and its timer expires. It is necessary notice that key objective of the scheme is to minimize the transmission delay of data packets, therefore, reducing in exchanging data handshaking and a short back-off timer is necessary to decrease end-to-end delay.

Related work: Recently, IEEE 802.11 standards [3-7], are known popular, cheap. They are used in a diverse range of applications including smart cities, smart home, smart environment, smart agriculture, so on. The wireless local area networks (WLANs) devices access Internet services and communicate an access point (AP) or communicate directly with each other. In the WLANs, the devices usually overhear the communication of nearby neighbors. In this sense, cooperative strategies appeared as a solution that focuses on increasing network connectivity, reliability, and energy efficiency.

Many cooperative strategies are proposed to enhance energy efficiency. In, the destination combines the full signals received in both phases to decode the packet by using maximal-ratio combining (MRC) technique, which provides a maximum diversity gain. However, it did not consider real-time transmission problems. In [8-10], authors provide guidelines how to select the “good” relay nodes, which assist data transmission in a fading environment by using amplify-

and-forward (AaF), decode-and-forward (DaF), incremental relaying, etc.

In [11], simple opportunistic relaying with decode-and-forward (DaF) and amplify-and-forward (AaF) strategies known as proactive relay assignment has investigated. Though proactive relay assignment schemes simplify the algorithm design and overall network operations, as well as reducing the probability of channel access contention. However, proactive relay selection schemes cannot guarantee optimal performance in dynamic environments. Therefore, the NACK messages from the destination, is often used to trigger the cooperative communication. By this way, the relaying transmission is invoked only when the direct link between the source and the destination experiences fading environment. However, the use of triggered cooperative scheme increases the cooperative algorithm design complexity and computational overhead.

The remainder of this paper is organized as follows: Section II describes the proposed the scheme, Section III present and evaluates the performance of the proposed scheme, and Section IV is our conclusions.

II. Proposal Description

A. Mathematic Model

The cooperative communication techniques are developed widely for wireless communication, they offer the benefits of a natural broadcast. In general, the techniques can be realized as follows: in the first phase, a source node broadcasts a packet to the destination. It also starts timers to account for the event that the destination node cannot decode successfully the data packet. Neighbor nodes of the source node can overhear the packet as well. If the timers end with receiving NACK or without ACK packets. The packet is forwarded by the neighbor nodes to node D in the second phase.

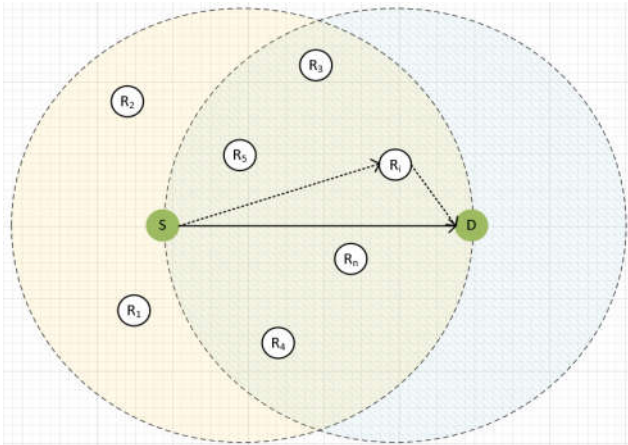


Fig. 2. Cooperative communication Model.

We consider the scenario with N IEEE 802.11 stations, including a source node (S), a destination (D) and set of help node $H = \{H_1, H_2, \dots\}$. Candidates $H_i \in H$ acting as a help node if they can decode the data packets from S in first phase and NACK packet from D in second phase. We define the help sets $H \subseteq N$ as the subset nodes located on constraint area within transmission range of S and D . H can be expressed as follows:

$$H = \{H(S) \cap H(D)\} \quad (1)$$

where $H(S)$ symbolizes the set of help nodes can decode the packet from S and $H(D)$ symbolizes the set of help nodes have been decoded NACK packets of node D . To decode the data and NACK packets, the instantaneous SNRs of the source-relay (γ_{SR_i}) and relay-destination (γ_{R_iD}) links are larger than a certain threshold (γ_{th}). The certain threshold value is determined according to the bit error rate (BER) requirement of applications. It should be noticed that the higher SNR value refers to high requirement of BER value. Therefore, the chance to select help nodes from subset H is smaller. For example, for a given BPSK modulation and targets $BER = 10^{-3}$ and $BER = 10^{-5}$, we can determine the range of threshold values for the QoS requirements by the probability of bit error. In BPSK modulation, $P_b = \frac{1}{2} * erfc(S/N)^{1/2}$ [3], where $erfc$ is an exponential function. From Figure. 3, the SNR threshold values are determined from 8.2dB to 9.4dB, respectively. Therefore, the R_i can act as a help node if and only if the SNR values of SR_i and R_iD links are higher than SNR threshold values. In order to find out more chance to forward the data packets, the SNR value of source-relay link should select as lower bound of SNR threshold range while the SNR value of source-relay link should select as upper bound of SNR threshold range to reduce collision at the destination node.

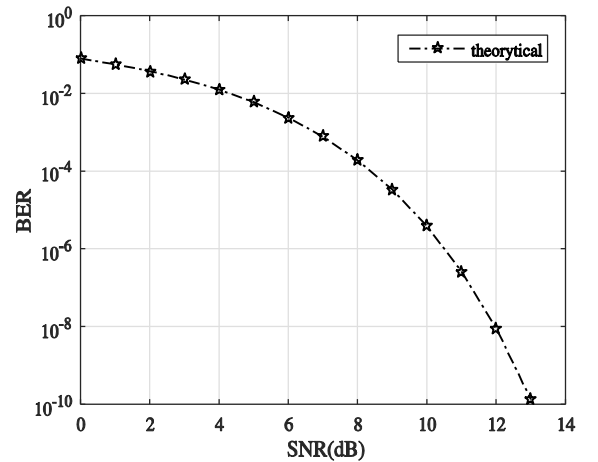


Fig. 3. Threshold selection based on BER in BPSK.

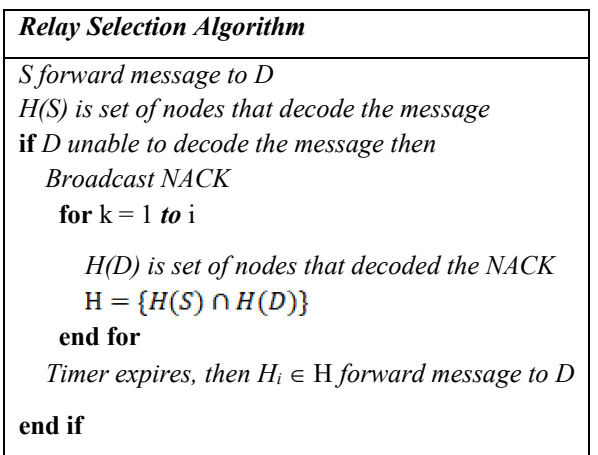


Fig. 4. Relay Selection Algorithm.

B. Proposed scheme

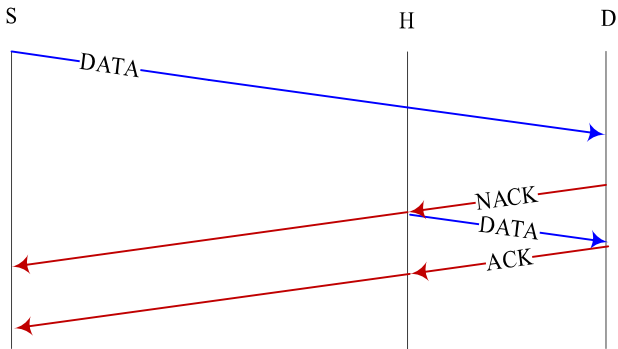


Fig. 5. Sequence flow chart of our proposal.

In IEEE 802.11 standards, when a relay node wants to forward the data packet to the receiver, it waits for a back-off (BO) period, ranging from $[0, CW]$. If the CW period is small, it will ensure that the devices will not spend too much time waiting for channel access, but the collision probability is increased and reverse. In default, the CW is set from 15 (CW_{Min}) to 1023 (CW_{Max}). In our proposal, The CW value is set to CW_{Min} because the number of sensor nodes in agriculture applications is small.

As shown in Figure 5, our proposed scheme used two-way handshake, including four steps, namely, decode and forward (DaF), information feedback (IF), real-time relay selection (RTRS), and relay forwarding (RF).

The DaF step: At first, when a source has a data packet, it transmits the packet to the destination with the power P_s . The overhearing nodes can store the packet in their buffer. If the destination can fully decode the packet, it broadcasts an ACK packet, and then the relaying nodes keep idle. In order to meet the QoS requirements, the relay nodes decide to decode the packet if their received signal strength is larger than a given threshold of the source node. Then, the relay nodes encode the packet in the same way as the source.

The IF step: If the destination cannot decode the source's packet, it sends a NACK packet and to request for help. We used the NACK packet to declare the failed data packet causing fading. One flag bit in the ACK packet is used to distinguish the NACK packet from the ACK packet. Otherwise, the destination sends an ACK packet to inform the source and relay nodes that it decoded the packet successfully. It is worth mentioning that the source node and relay nodes may receive neither ACK nor NACK packets after a short time interval. In this case, the source node concludes that the packet loss is caused by hidden terminal problem, and then it will trigger retransmission procedure to retransmit the failed data packet or data packet collision.

The RTRS step: the CW_{Min} period is set because the small number of sensor nodes is distributed in agriculture applications, the step includes a back-off period and a relay timer competition process. In order to select a relay which has the smallest latency among help nodes H , all help nodes choose CW_{Min} and wait for forwarding the packet after receiving the NACK packet or time out. Because the help nodes at different locations may receive NACK packet at different timestamp due to propagation delay. Thus, delay is decreased.

The RT step: Once the destination receives the packet, it broadcasts an ACK packet to the relay node and the source node.

III. Simulation Results

A. Simulation Environment

An agriculture monitoring system, including 9 sensor nodes (8 source nodes and 1 destination node), is investigated by ns2 simulation [12]. The nodes are distributed randomly in square area $500m \times 500m$. In order to value performance of the system, we have modified PHY and MAC parameters of 802.11g standard in ns2 such as CW, SNR thresholds, so on. The simulating parameters are presented in table 1.

TABLE 1. Simulation parameters

Parameter	Value
Simulation space size	500 m × 500 m
Source nodes	8
Destination	1
Simulation time	200 s
packet size	50 bytes
N_0	-100 dBm
CW	15

B. Results

• End-to-end delay (E2ED)

In this investigation, the end-to-end delay is the sum of delays experiences such as transmission delay, propagation delay, and processing time. We analyze and compare the average time for receiving 3903 packets at the destination for our proposal and the single relay scheme. In figure 6, our proposal reduces end-to-end delay comparing to the single relay scheme [11]. This result implies that SNR based optimal relay selection, two-way handshaking, and short back-off timer in our proposal can quickly find out the potential relays that have its timer reduced to zero first.

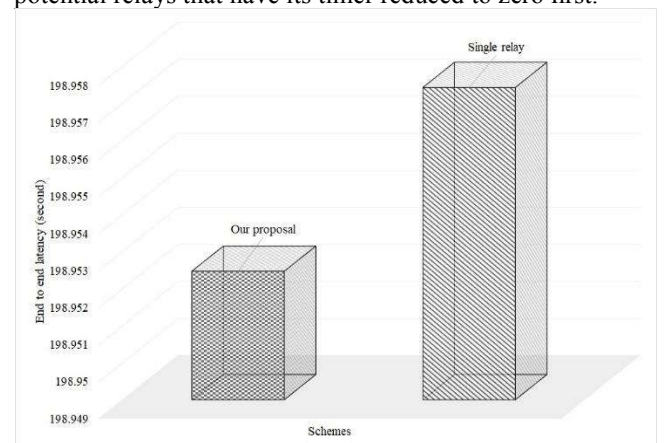


Fig. 6. E2ED of our proposal and single relay scheme.

• Packet delivery ratio (PDR)

Acknowledgment

This work was supported by Posts and Telecoms Institute of technology (PTIT), HCM city campus, Vietnam.

References

- [1] J.-S. Lin and C.-Z. Liu, "A monitoring system based on wireless sensor network and an SoC platform in precision agriculture," in *Communication Technology, 2008. ICCT 2008. 11th IEEE International Conference on*, 2008, pp. 101-104.
- [2] T. Popović, N. Latinović, A. Pešić, Ž. Zečević, B. Krstajić, and S. Djukanović, "Architecting an IoT-enabled platform for precision agriculture and ecological monitoring: A case study," *Computers and Electronics in Agriculture*, vol. 140, pp. 255-265, 2017.
- [3] "IEEE Std 802.11g-2003. Part 11: Wireless LAN medium access control (MAC) and physical layer (PHY) specifications: Further higher data rate extension in the 2.4 GHz band."
- [4] "IEEE Std 802.11n-2009. Part 11: Wireless LAN medium access control (MAC) and physical layer (PHY) specifications: Enhancements for higher throughput."
- [5] "IEEE Std. 802.11b-1999 Part 11: Wireless LAN medium access control (MAC) and physical layer (PHY) specifications: High-speed physical layer extension in the 2.4 GHz band."
- [6] "IEEE Std. 802.11e-2002. Part 11: Wireless medium access control (MAC) and physical layer (PHY) specifications: Medium access control (MAC) enhancements for quality of service (QoS)."
- [7] "IEEE Std. 802.11i-2004. Part 11: Wireless medium access control (MAC) and physical layer (PHY) specifications, Amendment 6: Medium access control (MAC) security enhancements."
- [8] J. N. Laneman, D. N. Tse, and G. W. Wornell, "Cooperative diversity in wireless networks: Efficient protocols and outage behavior," *IEEE Transactions on Information Theory*, vol. 50, pp. 3062-3080, 2004.
- [9] R. Madan, N. B. Mehta, A. F. Molisch, and J. Zhang, "Energy-efficient cooperative relaying over fading channels with simple relay selection," *IEEE Transactions on Wireless Communications*, vol. 7, pp. 3013-3025, 2008.
- [10] A. Bletsas, A. Khisti, D. P. Reed, and A. Lippman, "A simple cooperative diversity method based on network path selection," *IEEE Journal on Selected Areas in Communications*, vol. 24, pp. 659-672, 2006.
- [11] A. Bletsas, H. Shin, and M. Z. Win, "Cooperative communications with outage-optimal opportunistic relaying," *IEEE Transactions on Wireless Communications*, vol. 6, 2007.
- [12] "The Network Simulator."

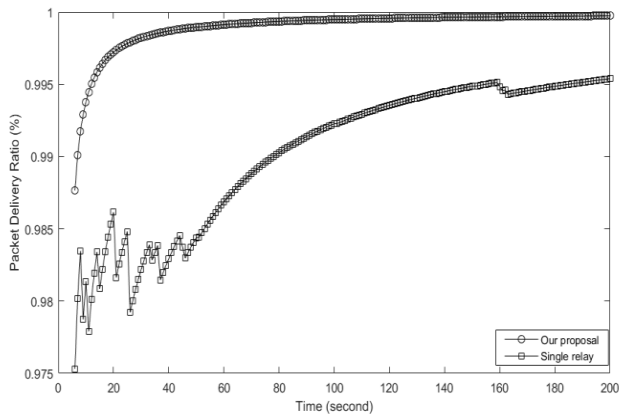


Fig. 7. PDR of our proposal and single relay scheme.

Packet delivery ratio is computed as the ratio between the total number of packets received at the destination and the total number of packets broadcast from the source nodes. The metric aims to evaluate how much our proposed scheme can provide reliable data transmission comparing to the single relay scheme. Figure. 7 presented the comparison of packet delivery ratio of our proposal and the single relay scheme [11]. Packet delivery ratio of our proposal is higher than the single relay scheme, respectively. It can be explained by the fact that our proposed scheme only selects small reliable nodes in the two phases because a small number of sensor nodes are used in in distribution area.

IV. Conclusions

In this paper, a relay selecting scheme is proposed to provide end-to-end delay and reliable data transmission for smart farm systems that their properties such as temperature, humidity, light intensity, pH, water level, and quality of water change rapidly. The work is a part of our project that allows end users not only to remotely monitor and control the physical devices, but also provide users visual information in a real-time manner.

Session V : Emerging Topics

- Performance Analysis of Partitioning based Real-Time Separation Kernel
/ Sihyeong Park, Daeyoung Song, Hyeeksoo Jang, Hyungshin Kim, Mi-Young Kwon, Sang-Hun Lee, Hoon-Kyu Kim
/ Chungnam National University, Agency for Defense Development, Korea
- A Design of Chao Phraya Express Boat Route and Tourist Attraction Application on Android
/ Supakit Thurapan, Sireethorn Phadlom, Hathairat Ketmaneechairat
/ King Mongkut's University of Technology North Bangkok, Thailand
- Sharing Experience and Knowledge: How to verify Secure Boot Against Modify Attack
/ Yangjae Lee, Daesun Choi, Ki-woong Park
/ Sejong University, Kongju National University Korea
- A fine-tuning CNN model for art painting style classificati
/ Tuong Le, Mi Young Lee, Sung Wook Baik / Sejong University, Korea
- Stock Selection by using an improved quick Artificial Bee Colony Algorithm
/ Dit Suthiwong, Maleerat Sodanil / King Mongkut's University, Thailand

Performance Analysis of Partitioning based Real-Time Separation Kernel

Sihyeong Park, Daeyoung Song, Hyeoksoo Jang and Hyungshin Kim*

Dept. Computer Science and Engineering
Chungnam National University
Daejeon, Korea
{sihyeong, daeyoungsong, hyeoksoojang, hyungshin}@cnu.ac.kr

*corresponding author

Mi-Young Kwon, Sang-Hun Lee and Hoon-Kyu Kim

The 2nd R&D Institute
Agency for Defense Development
Seoul, Korea
{kmyadd, shljhl, hunk}@add.re.kr

Abstract—In safety-critical embedded systems, a separation kernel is used to provide real-time performance, high reliability, and security. Partitioning-based separation kernels, in particular, provide temporal, spatial isolation and control inter-partition data flow. However, performance degradation can occur due to the hierarchical scheduling architecture. Therefore, it is necessary to measure and analyze the performance of kernel features to prevent performance deterioration of the separation kernel and to meet real-time performance requirements. In this paper, we have measured timing properties related to inter-partition communication, context switch, and interrupt latency at a monolithic kernel and a partition based separation kernel for comparison.

Keywords—embedded system; separation kernel; real-time; partitioning kernel; performance analysis

I. Introduction

In aerospace and weapon systems, real-time kernels are used to support mission-critical applications. Recently, security threats to software in these environments have increased, so the demand for security has increased [1].

Separation kernel provides isolation and security to real-time system [2]. This kernel provides temporal, spatial isolation and controls information flow between partitions. Embedded systems such as aerospace systems are evolving into the Integrated Modular Avionics (IMA) architecture that integrates distributed systems into a single chip [3]. Partitioning Kernels are proposed for IMA architecture [4]. They divide system resources into multiple partitions, and each partition consists of several processes. Therefore, partitioning kernels use a two-level hierarchical scheduler to guarantee the execution time of partitions and processes in each partition.

In this paper, we compare real-time properties of a general monolithic kernel and a separation kernel. We selected the VxWorks, a widely used real-time kernel in the aerospace field, and the RTWORKS [5], a separation kernel for evaluation.

This partitioning architecture may cause unwanted overhead to the real-time properties of the kernel [6].

To find out how the separation kernel architecture affects behavior of the scheduler, we measure the timing properties related to the context switching, inter-partition communication (IPC), and interrupt latency time for each kernel. Timing overheads are measured by varying the

number of partitions and processes. For the measurement, the cycle counter of the processor's performance management unit (PMU) was used.

The measurement shows that, as the number of processes and partitions increases, the execution time for IPC and context switch increases in both kernels. In the partitioning kernel, the transition between the partitions takes more time than the inter-process transition because the partition and the process structure of the partition need to be managed. Furthermore, the process scheduler is also called in the context switching between partitions, resulting in additional overhead. For IPC, both VxWorks and RTWORKS affected by the number of processes (or partition). RTWORKS has shown about 4 times shorter interrupt latency than VxWorks. This seems to be caused by differences in measurement setup.

From the analysis, we found that the partitioning architecture affects the inter-partition switching overhead the most. Therefore, design of the inter-partition context switching must be optimized for real-time performance in the partition-based separation kernel.

The rest of this paper is organized as follows. Section II describes the separation kernel and RTWORKS, and Section III address the performance analysis result. Section IV discusses related works and we conclude in Section V.

II. Separation Kernel and RTWORKS

Separation kernels provide the temporal and spatial separation of software and control the flow of information between partitions to ensure safe execution. Based on the Common Criteria (CC) [7], the Separation Kernel Protection Profile (SKPP) [8] released by the U.S. National Security Agency (NSA) specifies isolation, partitioning, and information flow between hardware, firmware, and software. The separation kernel aims to provide multiple security level operations in a typical multi-user system. Separation kernels are an extension of the concept of partitions to existing security kernels [9]. Security kernel provides protection for the creation of processes and memory objects and the management of resources on the hardware [10]. The security kernel categorizes sensitive works through the policy module within the kernel and controls access to objects by label. Based on this concept, the separation kernel controls information flow between each partition and resources.

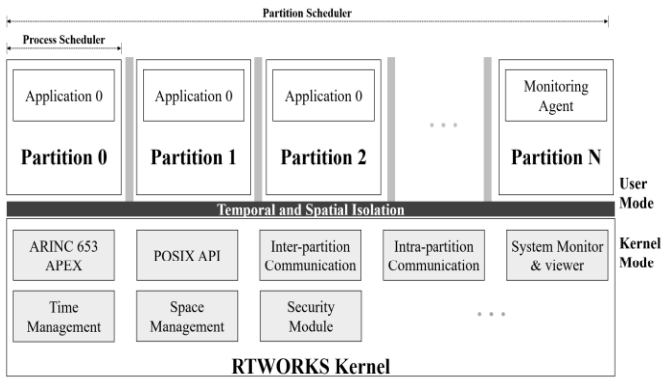


Fig. 1. RTWORKS architecture

The separation kernel requires the following security attributes:

- Data Separation: Each partition is implemented using separate resources. An application on one partition can not directly access the data on another partition.
- Temporal Separation: The kernel guarantees the execution time required by each partition.
- Information Flow Control: Block unauthorized accesses from a partition to the other partition.
- Fault Isolation: The kernel should make sure that errors occurring on one partition do not affect other partitions.

RTWORKS [5] is a real-time partitioning-based kernel that has DO-178B Level A certification. RTWORKS complies ARINC 653 and supports ARM, PowerPC and x86. RTWORKS has the architecture as the Fig 1. RTWORKS provides temporal and spatial partitioning. RTWORKS uses a channel, which is a logical communication link between the partitions, for inter-partition data transfer. It accesses the channel through the port.

III. Kernel Performance Analysis

For performance analysis, we choose VxWorks 6.9, a real-time operating system widely used in aerospace, and RTWORKS, a partitioning-based separation kernel. Performance parameters measured for analysis are shown in the Table I. Measurements were carried out on a SABRE Lite (BD-SL-I.MX6) board. The SABRE board uses an ARM Cortex A9 (ARMv7A) processor running at 792MHz and provides 1GB of DDR3 RAM and 1MB cache. For our measurement, the cache was disabled. Test program reads the counter register value of the PMU provided by the processor and uses the cycle value as the execution time. We ran the test for 1,000 iterations. We analyzed the factors affecting real-time performance of separation kernels from the result.

TABLE I. Kernel performance measurement setup

		VxWorks	RTWORKS
Scheduling Policy	Partition	-	Round-Robin
	Process	Priority-based Preemption, Round-Robin	Priority-based Preemption
IPC	Inter-partition	-	Queuing port
	Intra-partition	Message queue	Buffer
Interrupt Latency		Timer interrupt ISR	GPIO interrupt ISR

TABLE II. Context switching overhead (Cycles)

Context Switching – Process	# of Process ¹			# of Partition ²		
	2	4	8	1	2	4
VxWorks	7,109	7,260	7,553	-		
RTWORKS	2,152	2,850	3,648	2,152	2,819	3,287
Context Switching – Partition	# of Process ¹			# of Partition ²		
	2	4	8	2	3	4
RTWORKS	5,653	6,061	6,650	5,653	6,129	6,485

¹One Process, Multiple Partitions.
²Multiple Partitions, One Partition.

Context Switching

We compared the context switching overhead of VxWorks and RTWORKS. VxWorks provides a priority-based preemptive scheduling and a round-robin scheduling. RTWORKS has a two-level scheduling structure, a partition level and a process level.

The procedure for measuring the context switching time is as follows:

- Process 1 continues to update the cycle value during the time slice.
- Process 1 consumes all of the budget, and when it switches to Process 2, Process 2 measures the cycle value.
- Store the difference of the measured values.

We used various settings to determine the impact of the number of partitions and processes on context switching. The measurement results are shown in the Table II. In case of process switching, VxWorks takes 7,109 cycles when there are two processes, and RTWORKS takes 2,152 cycles, which is 3.5 times faster than VxWorks. As the number of processes and partitions increases, the time required for context switching increases for each kernel. In RTWORKS, the number of partitions did not affect the process switching time. In the case of partition switching, it was shown that the partition switching time increased when the number of process and the partitions were increased. This indicates that partition switching overhead is larger than process switching overhead. It is because the partitioning scheduler needs to manage the more number of data structures and complex hierarchical scheduler. When partition switching occurs, the process scheduler is invoked to check the process state. Therefore, there is a need to improve the invocation of the hierarchical scheduler in context switching.

TABLE III. Inter- and Intra-partition communication overhead (Cycles)

Inter-partition Communication	# of Process ¹			# of Partition ²		
	2	4	8	1	2	4
VxWorks ³	35,105	35,676	35,952	-		
RTWORKS	-			13,930	15,071	16,192
Intra-partition Communication	# of Process ¹			# of Partition ²		
	2	4	8	2	3	4
RTWORKS	46,158	47,259	53,064	46,158	51,655	53,150

³Inter-process Communication.

Inter- and Intra-Partition Communication

We analyzed the communication performance between processes and between partitions. In VxWorks, message queues are used for inter-process communication. In RTWORKS, queuing ports and buffers are used for inter-

partition communication and intra-partition communication, respectively. For intra-partition communication, queuing ports provides the port structures shared by processes in a partition. For inter-partition communication, a buffer object is used.

The IPC performance measurement procedure is as follows:

- Process 1 sends a message to a process via a shared object. At this time, the message content is the cycle value at the time of message transmission.
- After sending the message, Process 1 suspends the execution.
- The destination process acquires CPU time, checks and fetches messages.
- Measure the cycle when the message was retrieved and compare it with the value stored in the message.

We varied the number of processes and partitions to see how they affect IPC. Furthermore, we used a 4-byte message to measure the performance of RTWORKS's inter-partition communication. In the remaining cases, an 8-byte message was transmitted. The measurement results are shown in the Table III. In average, inter-process communication of VxWorks takes about 35,500 cycles. On RTWORKS, it is about 2.4 times smaller than VxWorks. This difference is caused by the difference in the length of the message for communication. In the intra-partition communication, it took about 49,000 and 50,000 cycles, respectively, depending on the process and partition varies.

Experiments show that both cases are affected by the number of processes and partitions. Context switch occurs in the execution of IPC. Based on context switching performance measurements, IPC execution time is affected by the number of processes and partitions. Therefore, reducing context switching time also reduces IPC execution time.

Interrupt Latency

If the interrupt processing time is delayed, there is a problem in guaranteeing real-time performance of the application.

The process of measuring the interrupt latency is as follows:

- Register an interrupt service routine for an interrupt.
- The user application generates the interrupt and reads the cycle counter.
- In the ISR, the cycle counter is read and the difference is calculated.

In VxWorks, the interrupt latency was measured with a timer interrupt and a user mode ISR. On the other hand, RTWORKS does not support a user mode ISR for the timer interrupt, so a GPIO interrupt is used. Therefore, we measured the latency by registering an interrupt handler inside the RTWORKS kernel. VxWorks took 10,530 cycles and 1,600 cycles were used in RTWORKS. In the case of VxWorks, the context switch is performed twice because the interrupt mode is changed to the kernel mode and then the user mode ISR is entered. This explains why we got 10 times larger value for the VxWorks.

IV. Related Work

The separation kernel can be implemented with a

microkernel [11]. The microkernel implements only core functionality in the kernel. This can increase the size of the trusted computing base (TCB). sel4 [12] is a microkernel that provides safety-critical features. This kernel provides a fine-grain access control of read / write / grant to all objects in the system. However, it is necessary to check the authority when accessing each object. Therefore, frequent access to objects may result in overhead due to repeated authorization.

The hypervisor [13] can be used as a separation kernel. The hypervisor runs applications in multiple platforms with virtualization on the single system. This reduces code redevelopment and testing costs for other environments. In the system, the application consists of several virtual machines (VM). In particular, the hypervisor manages VMs to prevent them from accessing resources or accessing others. However, virtualization may lead to overhead in hardware access and system call operations.

V. Conclusions

The separation kernel provides security and reliability to the safety-critical embedded systems. Especially, in aerospace systems, partitioning kernels are being introduced as existing systems evolve into IMA architecture. The partitioning kernel is also a sort of separation kernel that provides time, space isolation, and inter-partition communication. Partitioning kernels may affect real-time performance of the underlying system.

In this paper, we have measured and analyzed the real-time performances of a partitioning kernel. IPC, context switching, and interrupt latency are measured. From the analysis, we found that the partitioning architecture affects the inter-partition switching overhead the most. Therefore, design of the inter-partition context switching must be optimized for real-time performance in the partition-based separation kernel.

Acknowledgment

This work was supported by Agency for Defense Development under the contract UD180002ED.

References

- [1] G. Klein, "Operating system verification overview," *Sadhana*, vol. 34, no. 1, pp. 27–69, 2009.
- [2] D. Greve, M. Wilding, and W. M. Vanfleet, "A separation kernel formal security policy," in *Proc. Fourth International Workshop on the ACL2 Theorem Prover and Its Applications*. Citeseer, 2003.
- [3] C. B. Watkins and R. Walter, "Transitioning from federated avionics architectures to integrated modular avionics," in *Digital Avionics Systems Conference, 2007. DASC'07. IEEE/AIAA 26th. IEEE, 2007*, pp. 2-A.
- [4] J. Windsor and K. Hjortnaes, "Time and space partitioning in spacecraft avionics," in *Space Mission Challenges for Information Technology, 2009. SMC-IT 2009. Third IEEE International Conference on. IEEE, 2009*, pp. 13–20.
- [5] D. Son, H. Lee, and D. Lim, "Highly reliable partitioning real-time operating system and case studies on weapon system applications," *Communications of the Korean Institute of Information Scientists and Engineers*, vol. 34, no. 10, pp. 53–59, 2016.
- [6] R. Inam, J. Maki-Turja, M. Sjodin, S. M. Ashjaei, and S. Afshar, "Support for hierarchical scheduling in freertos," in *Emerging Technologies & Factory Automation (ETFA), 2011 IEEE 16th Conference on. IEEE, 2011*, pp. 1–10.
- [7] P. K. Infrastructure and T. P. Profile, "Common criteria for information technology security evaluation," National Security Agency, 2002.
- [8] Directorate, "Protection profile for separation kernels in environments requiring high robustness," US Government, 2007.

- [9] S. R. Ames Jr, M. Gasser, and R. R. Schell, "Security kernel design and implementation: An introduction." *IEEE computer*, vol. 16, no. 7, pp. 14–22, 1983.
- [10] Y. Zhao, Z. Yang, and D. Ma, "A survey on formal specification and verification of separation kernels," *Frontiers of Computer Science*, vol. 11, no. 4, pp. 585–607, 2017.
- [11] D. B. Golub, D. P. Julin, R. F. Rashid, R. P. Draves, R. W. Dean, A. Forin, J. Barrera, H. Tokuda, G. Malan, and D. Bohman, "Microkernel operating system architecture and mach," in *In Proceedings of the USENIX Workshop on Micro-Kernels and Other Kernel Architectures*, 1992, pp. 11–30.
- [12] G. Klein, K. Elphinstone, G. Heiser, J. Andronick, D. Cock, P. Derrin, D. Elkaduwe, K. Engelhardt, R. Kolanski, M. Norrish et al., "sel4: Formal verification of an os kernel," in *Proceedings of the ACM SIGOPS 22nd symposium on Operating systems principles*. ACM, 2009, pp. 207–220.
- [13] R. Sailer, T. Jaeger, E. Valdez, R. Caceres, R. Perez, S. Berger, J. L. Griffin, and L. Van Doorn, "Building a mac-based security architecture for the xen open-source hypervisor," in *Computer Security Applications Conference, Annual(ACSAC)*. IEEE, 2005, pp. 276–285.

A DESIGN OF CHAO PHRAYA EXPRESS BOAT ROUTE AND TOURIST ATTRACTION APPLICATION ON ANDRIOD

Supakit Thurapan

The College of Industrial Technology
King Mongkut's University of
Technology North Bangkok
Bangkok, Thailand
supakit.thurapan@gmail.com

Sireethorn Phadlom

The College of Industrial Technology
King Mongkut's University of
Technology North Bangkok
Bangkok, Thailand
ffangisiree@gmail.com

Hathairat Ketmaneechairat

The College of Industrial Technology
King Mongkut's University of
Technology North Bangkok
Bangkok, Thailand
hathairatk@kmutnb.ac.th

Abstract—This paper aims to develop a design of Chao Phraya Express Boat Application and evaluate user's satisfaction with Chao Phraya Express Boat Application. In this paper, Chao Phraya Express Boat Application is developed to search Chao Phraya Express Boat route, tourist attractions information and travel guide information. This application has been designed to present travel information, route map, time table and emergency call. The results show that the users can search Chao Phraya Express Boat trip information by using name of pier or map of pier. The application can show the detail of Chao Phraya Express Boat trip information such as type of flag, distance between starting point to end point, time table, transfer connection, fares and tourist attractions. The conclusion of assessment of user satisfaction on Chao Phraya Express Boat Application for all the environments, the users have high satisfied.

Keywords— *Tourist Attraction; Chao Phraya Express Boat; Application; Android;*

I. Introduction

Nowadays, People can easily access the technology. The smartphones are another alternative to the popular choice. There are a lot of function on smartphone such as camera, monitor and Internet technology. The users can be used the smartphone to provide benefits in them lifestyle [1]. The September 2017 statistics also revealed that iOS and Android 6.0 remain the most widely-used mobile operating systems, with more devices moving to Android 7.0. Mobile OS numbers show that Android is more popular than iOS, followed by Windows Phone in third [2]. Android is a mobile operating system developed by Google, based on a modified version of the Linux kernel and other open source software and designed primarily for touchscreen mobile devices such as smartphones and tablets [3].

Chao Phraya Express Boat Co., Ltd. (CPEX) was established by Khunying Supatra Singhulaka in September 1971. A concession right was granted to CPEX to provide river transportation service to passengers by the Harbor Department. Throughout the years of dedication, CPEX continues to provide quality services by improving routes, safety and operation standard to better serve the general public, and in accordance to the Thai Government's policy. Our total fleet size of 65 boats comprises of 15 super size boats, which were granted the Boar of Invest (BOI) privileges and 50 regular size boats. On average each boat has carrying capacity of 200 people. With a vision to achieve the highest standards

in river transportation operation and safety, CPEX continues to lead, with current operation accommodating approximately 35,000 to 40,000 passengers each day or 13.5millions passengers per year [4]. The Chao Phraya Express Boat service is a water bus which carries passengers along the Chao Phraya, regularly serving thirty eight stops from Rat Burana to Nonthaburi, covering a distance of 21 km. The route services divided into four routes: local line boat with no flag, express boat with orange flag, express boat with yellow flag and express boat with green flag. The researchers have acknowledged the problems that some of the passengers are facing on the transportation, such as lack of the information on the transportation, fare rates, the time table and the transfer connection. Thus, the researchers developed Chao Phraya Express Boat route and tourist attraction application on android to help the people that they are select to travelling by boat transportation in Bangkok with more convenient and easier for people to use in daily life [5].

This paper proposes Chao Phraya Express Boat route and tourist attraction application on android. The application function is divided into two modes: online and offline mode. The language can be displayed in two languages: Thai language and English language. This paper presents the design and implementation by using Android Software Development Kit. This application has been developed using Android Studio [6], Java [7], NetBeans [8], HTML [9], PHP [10], Adobe Photoshop [11] and MySQL [12]. The remainder of this paper is organized as follows. Section 2 describes related work. Section 3 explains the system overview and methodology. The implementation and testing is presented in Section 4. Section 5 demonstrates the result of Chao Phraya Express Boat route and tourist attraction application on android. Finally, the conclusion discussed in the Section 6.

II. Related Work

Roy Deddy Hasiholan Tobing [13] presented the application provides contents related to latest tourism information, favorite attraction spots/points of interest, or offers from some service providers. The application implements Google Map Application Program Interface (API) to provide location-based service for users. Moreover, the data used for the mobile application is fetched from server using web service. Social media is also integrated to the system to provide better experience for the users and for sharing tourism information.

Meiliana et al. [14] presented feature provides any

information about all ongoing or upcoming events in Indonesia which are gotten from the database that implemented using MySQL. Events data in the database were inputted by admin using a web-based application as the user interface and SQL code to manipulate the data. After the data is inputted, all events are viewed in Event Menu at the mobile version application. The user can view the detail location of the desired event based on Google Map API coordinate, which is stored in the database too. There are also searching option to look for the event based on name or city which the application retrieves it from the user input and search the database using SQL command.

Jian Meng and Neng Xu [15] presented mashup technology is a useful for this application. Along with web-based applications becoming richer and related technologies becoming more mature, Mashups based on open web APIs have shown the power of integrating applications and data sources to create novel and situational web services to serve needs of users. A mashup can combine two or more data sources (content or service) to provide several new services or contents to the users. More importantly, it is a lightweight web application program. The data or contents are mashed up in the mashup server side. Furthermore, no matter what the mobile client is a Web browser or not, it is able to understand the format of the data or contents. The advantage of mashup technology is greatly exploited for the application of mobile devices.

Pooja D. Watkar and Prof. M. R. Shahade [16] presented the design and implementation of a mobile application called Smart Travel Guide, with which mobile users can get tourism guidance information they need anytime and anywhere. The purpose of application find the current location of user. The Mobile Location Protocol (MLP) is an application-level protocol for receiving the position of Mobile Stations (MS: mobile phones, wireless devices, etc.) independent of underlying network technology. The MLP serves as the interface between a Location Server and a location-based application. Google apps or services may use Location History and Location Reporting data. For example, Google Maps may use it to improve your search results based on the places that you have been history of your location data from all devices where you are logged into your Google Account and have enabled Location Reporting.

Supatra Kumlangmak [17] Presented the application development for tourism promotion of rattanakosin by chao phraya tourist boat on android. This application developed with the JAVA language and manage database with phpMyAdmin, SQLite and use both connection Gson database together. Function of application functionality includes: Attractions, Near By, My tips, Time Table, River Map and Promotion.

Pitchaporn Boriboon and Pitchapar Srikaew [18] Presented Sansaab application on iOS. Sansaab is application facilitates the use of Saen Saep canal boat service. This application is created to provide information in Saen Saep canal route. There are many functions such as calculating fare, calculate travel time and alerts when close to port of destination etc.

Knung Korrakanchana [19] Presented BTS on to go application on android. The application will show tourist attractions to choose where to go. When user press select location the application will display the destination station and

the source station from the nearest station. The application can display fare and how to get from the terminal to that location.

Soontorn Auksorncherdchoo [20] presented BKK BTS Fare application on iOS. The application will surely help to calculate fares from the place of origin and destination stations. Subsequently, the application would display fares in the travels of user.

Pongsakorn [21] presented Chao phraya application on iOS. The application can find travel information by the Chao Phraya express boat. There is also an interesting functions include: map, find restaurants, transfer connection.

TABLE. I. Comparison between our application and related work

Ability of application	Related Work					
	[17]	[18]	[19]	[20]	[21]	Our work
1. Find a station nearby.	✓	✓	✗	✓	✓	✓
2. Show a schedule of departures.	✓	✓	✓	✗	✓	✓
3. Show time table.	✗	✓	✓	✗	✗	✓
4. Show connection points to other passengers.	✗	✓	✗	✗	✓	✓
5. Show an important place or station area attractions.	✓	✓	✓	✗	✓	✓
6. Can write a review that place.	✗	✗	✗	✗	✗	✓
7. Be alert when approaching the destination.	✗	✓	✗	✗	✗	✓
8. Have a phone number for emergency? Moreover, can call out immediately in case of an emergency.	✓	✗	✗	✗	✗	✓
9. Show fares.	✓	✓	✓	✓	✓	✓
10. Show the boat route.	✗	✓	✓	✓	✓	✓
11. Users can chat with other accounts.	✗	✗	✗	✗	✗	✓

III. The System Overview

The section introduces analysis and design of Chao Phraya Express Boat Route and Tourist Attraction Application on Android. The Chao Phraya Express Boat services are divided into four routes as following:

1. Local Line Boat (No Flag) (Time: 6.20 - 8.20, 15.00 - 17.30) Round trip services from Nonthaburi Pier to Wat Rajsingkorn Pier stopping at 34 piers.
2. Express Boat (Orange Flag) (Time: 05.50 - 19.00) Round trip services from Nonthaburi Pier to Wat Rajsingkorn Pier stopping at 18 piers.
3. Express Boat (Yellow Flag) (Time: 06.15 - 08.35, 15.30 -20.00) Round trip services from Nonthaburi Pier to Ratburana Pier stopping at 10 piers.
4. Express Boat (Green-Yellow Flag) (Time: 06.15 - 08.05, 16.05 - 18.05) Round trip services from Pakkret Pier to Sathon Pier stopping at 12 piers.

A. System Analysis

The Chao Phraya Express Boat application categories is shown in Table 1. When the user starts to use Chao Phraya Express Boat Route and Tourist Attraction Application, the user has to login and select the language between Thai and English language. Then, it will go to the main page. If the user has not username and password, the user has to register before login. The main function of application has four functions such as travel information, route map, time table and emergency call. After that the user can select the desired menu and the application program will display the detail to user selected in each menu.

TABLE. II. Chao Phraya Express Boat Application Categories

Application Categories				
Login	Travel	Route Map	Emergency Call	Time Table
Select Language	Type of Flag	Map	Name of phone number	Orange flag's time table
Register	Distance from Source to Destination.	Location of pier	Phone number	Green flag's time table
	Travel Time	Navigation		Yellow flag's time table
	Transfer Connection	Notification on arrival		No flag's time table
	Fares			
	Tourist Attraction			

B. Use Case Diagram

The use case diagram shows the relation between users and application as shown in Figure 1. When the users start the application, the application will enter to the main page. The main page has four different menus include travel information, route map, time table and emergency call. The travel information can search from name of pier or pier map. After select the searching method, the travel detail will show the type of flag, distance from source to destination, travel using time, transfer connection, fares and tourist attraction. The time table shows the service route and time to travel by using local line boat (no flag), express boat with orange flag, express boat with yellow and express boat with green flag. The route map shows map, location of pier, navigation and notification before arriving in destination pier. The emergency call shows the name of department and phone number.

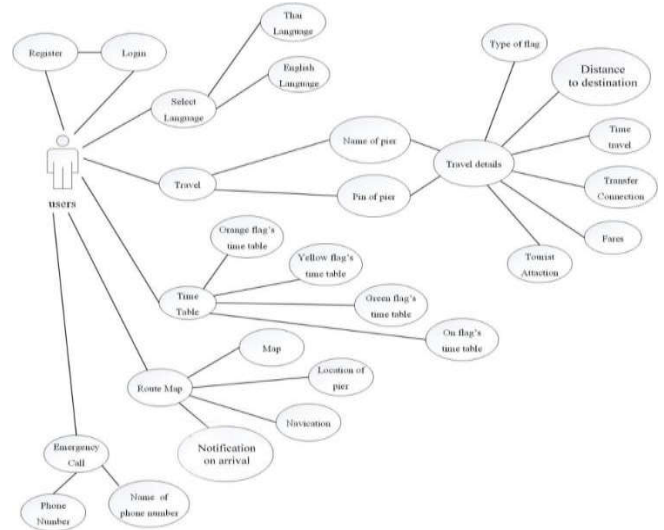
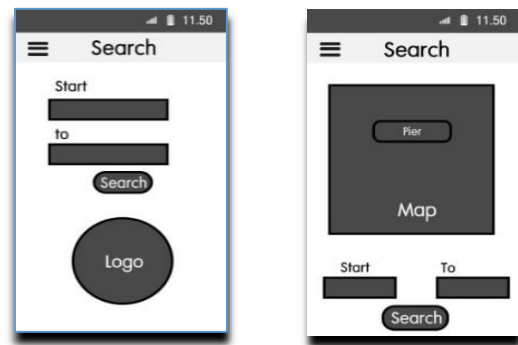


Fig. 1. Use Case Diagram of Chao Phraya Express Boat Application.



(a) Search by name of pier (B) Search by pier map

Fig. 2. Design Applications.

Design Application

The design of user interface is presented in this section. The user interface has two main screen as show in Figure 2. The application has been developed using Android Studio [6] with Java programming language [7], NetBeans for assistance in Java [8], HTML programming language [9] and PHP programming language [10]. This application using MySQL database [12] for storing data and the graphic user interface (GUI) is designed by Adobe Photoshop [11].

IV. Demonstration of Application

A. Main Function of Application

This section demonstrates recommender system for Chao Phraya Express Boat On Android. The application program will enter to the page when the users start to use the application.

Tab Bar Page

In this page, allow the user to process to the functionalities of the application by select Travel, Route map of the boat, Emergency Call and Time Table. There are four main functions such as number 1 is Travel Menu, number 2 is Route Map, number 3 is Emergency Call and number 4 Time Table. The tab bar is shown in Figure 3.

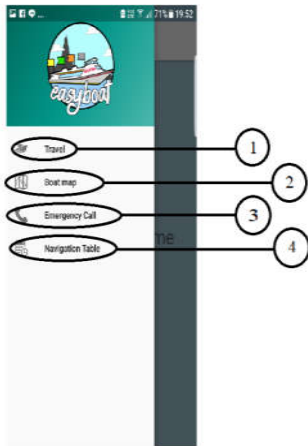


Fig. 3. Tab Bar Page.

Travel Page.

This activity is the travel page. The travel page allow the users select the starting pier and the end pier, then click the search button. After that the travel information will show the detail of travel by using Chao Phraya Express Boat. The travel page is shown in Figure 4.

Route Map Page.

The screen will display the route map of the boat. The users will be able to view the location of the pier on the map. The route map is shown in Figure 5.

Emergency Call Page.

The emergency call will display a list of name of department and emergency phone numbers. The user can click on the button icon to make a phone calls when the emergency is occur. The emergency call is shown in Figure 6.

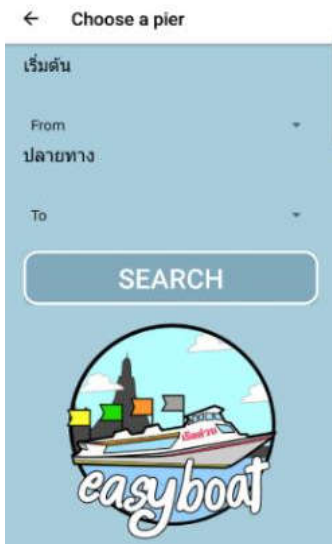


Fig. 4. Travel Page.



Fig. 5. Route Map Page.



Fig. 6. Emergency Call Page.

Time Table Page.

This screen will display the time table follow the type of boat. The user can click to select the color of the boat flag then the application will show the details of time table. The time table is shown in Figure 7.



Fig. 7. Time Table Page.

B. The Satisfaction of Users

The questionnaire is created to evaluate user satisfaction on the Chao Phraya Express Boat Route and Tourist Attraction Application on Android. The questionnaire consists of five rating scales as following.

- Level 1 Satisfaction in the lowest level.
- Level 2 Satisfaction in the low level.
- Level 3 Satisfaction in the medium level.
- Level 4 Satisfaction at the high level.
- Level 5 Satisfaction at the highest level.

For a definition of the measurement, the research has determined that the criteria used to give meaning to the concept of Beat (Beat, 1986: 195).

- - 1.50 : Satisfaction in the lowest level.
- 1.51 - 2.50 : Satisfaction in the low level.
- 2.51 - 3.50 : Satisfaction in the medium level.
- 3.51 - 4.50 : Satisfaction in the high level.
- - 5.00 : Satisfaction in the highest level.

The results of the user satisfaction evaluation from the Chao Phraya Express Boat Application is used by 30 passengers, who use the Chao Phraya Express boat service. The satisfaction evaluation questionnaire is concerned with the performances and functions of the application. The questionnaire can be summarized into three aspects: First, the usability, the users's satisfaction are considered as high ($\bar{x} = 4.48$, S.D. = 0.53). Second, the elements, the users's satisfaction are considered as high ($\bar{x} = 4.19$, S.D. = 0.64) Third, the quality, the users's satisfaction are considered as highest ($\bar{x} = 4.63$, S.D. = 0.52). The overall results of the satisfaction evaluation questionnaire are considered as high ($\bar{x} = 4.44$, S.D. = 0.59). The user satisfaction evaluation is shown in Table 3.

TABLE. III. The result of the user satisfaction evaluation

Topic assessment	\bar{X}	S.D.	Results
1. Usability			
1.1 Usability.	4.50	0.63	High
1.2 Travel search system is not complicated.	4.43	0.51	High
1.3 Application allows the user to travel by the Chao Phraya Express Boat easier.	4.43	0.73	High
1.4 The information in the applications meet the needs of users.	4.50	0.74	High
1.5 Application options allow more convenient for people traveling by the Chao Phraya Express Boat.	4.53	0.50	Highest
sum	4.48	0.53	High
2. The elements			
2.1 The design of the application screen.	4.03	0.51	High
2.2 Colors within applications and application suitability.	4.10	0.61	High
2.3 The color and font size within applications are appropriate.	4.17	0.61	High
2.4 Images and symbols, easy to understand.	4.47	0.70	High
sum	4.19	0.64	High
3. In quality			
3.1 Useful to the user.	4.83	0.38	Highest
3.2 Simple operation, convenient and	4.60	0.50	Highest

quick.			
3.3 Travel information is full details.	4.53	0.57	Highest
3.4 Overall satisfaction	4.57	0.57	Highest
sum	4.63	0.52	Highest

V. Conclusion

This paper presents the Chao Phraya Express Boat Route and Tourist Attraction Application on Android. This application was developed to search for travel information by the Chao Phraya Express Boat. The searching function is divided into two forms: searching from a name list of piers and searching from pier map. The language can be displayed in two languages: Thai language and English language. This application can display travel information, period of time on traveling, time table, fare rates, tourist attractions, and emergency calling function when in certain accidents. The researchers have uploaded the application into the Play Store on Android which are already qualified and authorized as duly competent to be officially available for the users. The overall results of the assessment of user satisfaction on the Chao Phraya Express Boat route and tourist attraction application on android are high satisfied.

References

- [1] Smartphone [Internet], available from: <https://en.wikipedia.org/wiki/>
- [2] Smartphone.
- [3] The most popular operating systems for smartphones [Internet], available from: <https://mybroadband.co.za/news/software/232485-the-most-popular-operating-systems-for-smartphones-and-pcs.html>.
- [4] the-most-popular-operating-systems-for-smartphones-and-pcs.html.
- [5] Android [Internet], available from: <https://en.wikipedia.org/wiki/>
- [6] Android Operating System.
- [7] Chao Phraya Express Boat [Internet], available from: <http://www.chaophrayaexpressboat.com/en>.
- [8] Chao Phraya Express Boat [Internet], available from: https://en.wikipedia.org/wiki/Chao_Phraya_Express_Boat.
- [9] Android Studio [Internet], available from: https://en.wikipedia.org/wiki/Android_Studio.
- [10] Kathy Sierra, *Head First Java*, O'Reilly Media, 2005.
- [11] NetBeans [Internet], available from: <https://netbeans.org/>.
- [12] Eric Freeman, Elisabeth Robson, *Head First HTML and CSS*, O'Reilly Media, 2012.
- [13] Kevin Yank, Tom Butler, *PHP & MySQL - Novice to Ninja*, Sitepoint Pty Ltd, Victoria, Australia, 2017.
- [14] Adobe Photoshop [Internet], available from: https://en.wikipedia.org/wiki/Adobe_Photoshop.
- [15] MySQL [Internet], available from: <https://www.oracle.com/technet-work/database/mysql/index.html>.
- [16] Roy Deddy Hasiholan Tobing, *Mobile Tourism Application for Samosir Regency on Android Platform*, Conference: International Symposium on Technology Management and Emerging Technologies (ISTMET), At Langkawi Island, Malaysia, 2015.
- [17] Meiliana, D. Irmanti, M. R. Hidayat, N. V. Amalina, *Mobile Smart Travelling Application For Indonesia Tourism*, International Conference on Computer Science and Computational Intelligence, 2017.
- [18] Jian Meng, Neng Xu, *A Mobile Tourist Guide System Based on Mashup Technology*, 2010.
- [19] Pooja D. Watkar, M. R. Shahade, *Smart Travel Guide: Application For Mobile Phone*, International Journal of Research In Science & Engineering Volume: 1, e-ISSN: 2394-8299, 2015.
- [20] Supatra Kumlangmak, *Application Development for Tourism Promotion of Rattanakosin by Chaophraya Tourist Boat on Android*, Silpakorn University, 2012.
- [21] Sansaab [Internet], available from: <https://itunes.apple.com/th/app/sansaab/id797892831?mt=8>.

[23] BTS On To Go [Internet], available from: <https://play.google.com/store/apps/details?id=com.kvsoftware.bkkransit&hl=en>.

[24] BKK BTS Fare [Internet], available from: <https://itunes.apple.com/th/app/bkk-bts-fare/id606821432?l=th&mt=8>.

[25] Chaophraya Application [Internet], available from: <https://itunes.apple.com/th/app/chaophraya/id591000319?mt=8>.

Sharing Experience and Knowledge: How to verify Secure Boot against Modify Attack

Yangjae Lee
SysCore Lab.
Sejong University
Seoul, South Korea
leelambjae@gmail.com

Keon-Ho Park
SysCore Lab.
Sejong University
Seoul, South Korea
imguno0629@naver.com

Daeseon Choi
Dept. Department of
Medical Information
Kongju National
University
Kongju, South Korea
sunchoi@kongju.ac.kr

Ki-Woong Park*
Dept. Information
Security
Sejong University
Seoul, South Korea
woongbak@sejong.ac.kr

Abstract— To enhance the mobility of embedded devices, the board has become smaller. However, this characteristic makes the board to be stolen easier. In this case, when the board which contains critical information is stolen, the attacker can steal the data easily because they can conduct every attack from physical attack to cyber-attack. Therefore, implementing the secure boot is an indispensable thing for embedded system security. However, does secure boot can really recognize the modify attack? In this paper, we detail our experiences which building and executing verification model to test the secure boot against modify attack. We expect that these experiences serve two benefits for readers. First, readers can get the knowledge of T2080 RDB which we used for exemplary, Second, it can raise questions about what verification model is the best for verifying the secure boot against modify attack.

Keywords— *verification method; embedded system; secure booting; security methodology*

I. Introduction

To protect boot procedure, many kinds of secure boot have released [5-7]. However, we can't really be sure that the secure boot can protect the modify attack. Therefore, we make a verification model against modify attack to verify the secure boot. In our experiences which building and executing verification model, we expect that readers to obtain the two benefits. The first benefit is knowledge of T2080RDB which we used for exemplary. Because our verification model requires prior knowledge of the service, readers can obtain the information about T2080RDB which we have investigated. The second benefit is that readers can raise questions which verification model is the best for verifying the secure boot against modify attack. Because we investigated some verification model for other service and analyzed each verification model, readers can raise the question which verification model is the best.

II. What Verification Model Most Suitable for Secure Boot Against Modify Attack?

In order to make most suitable verification model for the

secure boot against modify attacks, we analyzed other verification models for other services. The detailed procedure of each verification model is listed in Table I .

SiChoon Noh et al. proposed verification method of ensuring web application security [1]. To protect the threats, they present the verification model for web application security, the verification model procedure is consisting of four steps. Myong-Yeal Lee et al. proposed a safe smart car application plan [2]. They look at types of smart car and deriving the security threats based on various scenarios. Jeom Goo Kim. proposed an automatic method which verifies the network security system and verification method based on scenarios [3]. To verify the network security system, they found the problems of current networks system based on scenarios. Balzarotti, Davide, et al. describe the testing methodology that used in testing the security of real-world electronic voting system [4].

By analyzing the other verification model for other services, we found that there are some common features. First, most of the verification model gathered information about the services to protect. After that, they analyzed the information. For example, in the verification model of web application [1], they set the scope to protect and analyzed the target application. Second, most of the verification model find threats to the service. In the verification model for smart car [2], the anticipated threats and risks are analyzed based on existing attack cases and information about services. Third, they make the attack scenarios by linking the threats. In the verification model for real-world electronic voting systems [4], they made realistic attack scenarios according to the procedure of the voting system. Finally, they verify the security by executing the attack scenarios or attacks. In the evaluation technique of network security system, they experimented and analyzed in a small school network according to scenario-based verification method. Some verification models additionally proposed countermeasures in verification model. Analyzing the several verification models and investigating the secure boot, we draw one verification model for secure boot against modify attack. In

*: Corresponding author

This work was supported by the National Research Foundation of Korea (NRF) grant funded by the Korea government (MSIP) (NRF-2017R1C1B2003957, NRF-2016R1A4A1011761).

TABLE I . The Procedure of Each Verification Model

Target Application	Step 1	Step 2	Step 3	Step 4
[1]	Set the scope of security verification	Analyze the target application	Select the security checklists	Verify the proof of security
[2]	Look at types and policies of smart car	Make scenarios which can occur	Analyze the smart car security threats based on scenarios	Propose the countermeasures
[3]	Build the database for security checklists	Define and grade the risks of security	Establish a verification environment based on the scenario	Test the automatic verification tool and proof security
[4]	Information gathering such as copy machine, source code, and documentation.	Analysis the system. Such as information flow and vulnerability	Draw the attack scenarios according to the procedure	Execute attack and report the results

our verification model, to find the attack surface we analyzed the secure boot first. After finding the attack surface against modify attack, we found risks that can occur if attack surfaces are modified. Combining these risks, we made scenarios. Executing these scenarios, we try to verify the security of secure boot.

III. Design of Verification Model

To test the secure boot, we use T2080 RDB, which supports secure boot and be used for military application [8-10]. To make the verification model for T2080RDB secure boot, we form the verification model in four steps. First, to define which components to protect, the boot process should be analyzed. After analyzing the boot process, components to protect should be defined. Second, found the risk that can occur if components are modified. Third, make the attack scenarios that can exploit the system by combining the risk. When we make scenarios based on risks and components, numerous scenarios were derived. But verifying all the scenarios manually consumes a lot of resources. In this paper, we make two attack scenarios for the case study, which steal the data and get the total access based on the attacker’s primary goal. At the last, scenarios are actually executed on the T2080 secure boot to determine whether the attack succeed or fail. If it fails, by analyzing which function of T2080 secure boot is able to defend, assure the safety of T2080 secure boot.

A. Defining and analyzing the components to protect

In this paper, we divided secure boot process of T2080 into three steps based on the secure boot phase. The first step is the Pre-Boot Phase. When the power is applied to the system, Pre-Boot Phase checks the security status of the system. Also, Pre-Boot Phase uses Security Fuse Processor (SFP) and Pre-Boot Loader (PBL). SFP physically burn fuses during device provisioning and send One Time Programmable Master Key (OTPMK) and Super Root Key Hash (SRKH) to other hardware securely. PBL reads a command file from a location determined by the Reset Configuration Word (RCW) and performs a store of a value to the ESBC pointer register within the SoC. In the case study, because SFP is programmed in hardware, we assume that to modify the SFP is impossible [11].

The second step is the Internal Secure Boot Code (ISBC) Phase. In the ISBC Phase, check the integrity of U-boot,

Barker Code of CSF Header, and public key.

The third step is the External Secure Boot Code (ESBC) Phase. The ESBC Phase checks the integrity of the Boot Script, the Root File System (Rootfs), the Device Tree Blob (DTB), and the Linux kernel.

According to the T2080 secure boot process, we can define 8 components to protect. Table II shows a description of components to protect.

The components of Table II are used to validate the boot images in T2080RDB secure boot. By defining the which components to protect, attack points can be specified, and attacks can be blocked effectively.

TABLE II . Description of Components to Protect

Components	A Description of Components	Elements related to Security
U-boot	U-boot is bootloader, and there are secure U-boot and normal u-boot.	Secure U-boot checks the integrity of ulmage, Rootfs, and DTB.
Rootfs	The filesystem that contains a program that supports the system operating.	Rootfs can be superseded to other Rootfs which have viruses.
DTB (Device Tree Blob)	The data structure which describes the hardware components of the system.	DTB can be superseded to other DTB which recognize illegal hardware.
uImage	uImage is a compressed kernel image.	To load another kernel, ulmage can be superseded to other ulmage.
Bootscrip	Contain commands which u-boot supports	Define the address of ulmage, rootfs, DTB, and CSF Header
RSA Key Pair	Using the OpenSSL RSA function, make the public key and private key.	RSA public key is used to sign the signature of boot images. RSA private key is used decrypt the signature to verify the integrity.
CSF Header	Contain Barker Code, public key, private key, the signature of boot image.	To verify the integrity of the boot image, compare booted image and decrypted signature of CSF Header.
Memory Mapping	Address where the boot images are saved when porting the boot images to T2080RDB.	User can store boot images at any address.

B. Risks to Components to Protect

The previously defined components to protect may be modified by the physical attack such as JTAG and insertion of the external media device and cyber-attack such as viruses, worms, and trojan horses. Table III shows the risk that could arise if the components to protect were modified.

TABLE III. Risk of Attack of Components

Components	Risk of modifying
U-boot	If U-boot is modified to normal U-boot, it cannot check the integrity even DTB, ulmage, Rootfs is modified.
Rootfs	The modified Rootfs which contain virus can be mounted.
DTB	The modified DTB would recognize the unexpected device.
ulmage	The modified ulmage would disable every security solutions running on the kernel level. Allow attackers to access the stored data without any authentication.
Bootscript	The modified Bootsript can turn off the secure boot. Allow attackers to boot arbitrary boot images by modifying the address of images.
RSA key Pair	Allow attackers to generate the CSF Header using the modified private key.
CSF Header	Generate the CSF Header of the modified image for verification.
Memory Mapping	Attacker can store the modified image to any address.

C. Drawing Attack Scenario

When we generate attack scenarios based on components, there were several cases such as scenarios which only one component is modified or a scenario which various components were simultaneously modified. Therefore, there are many attack scenarios which can occur. If all the images simply substituted to another image, 2^8 scenarios can be derived as shown in Fig. 1.

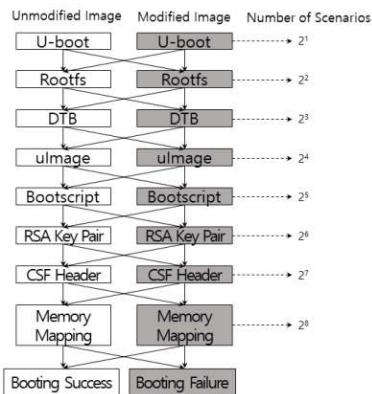


Fig. 1. Attack Scenario That Can Be Derived

If configurations of the image are changed or substituted with other images, there will be more scenarios. In this section, according to the attacker’s primary goal, we make two attack scenarios for the case study.

One of the attacker’s goal is to steal the data in T2080RDB. To steal the data, the attacker needs to turn off the secure boot of T2080RDB by substituting the secure U-boot to normal U-boot and delete the validate command in Bootsript. It can be expected that secure boot is turned off. Because secure boot is

turned off, the attacker can modify the kernel and steal data as shown in Fig. 2.

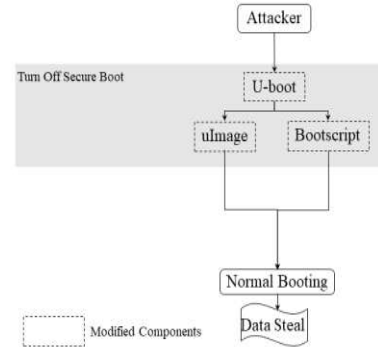


Fig. 2. Data Steal Scenario

Another attacker’s goal is to get access. To get the access, the attacker needs to create new RSA key pair and modified CSF Headers on every image such as ulmage, DTB, Rootfs, and Bootsript. Because every image is substituted to the attacker’s image, it can be expected that the attacker can get the total access as shown in Fig. 3.

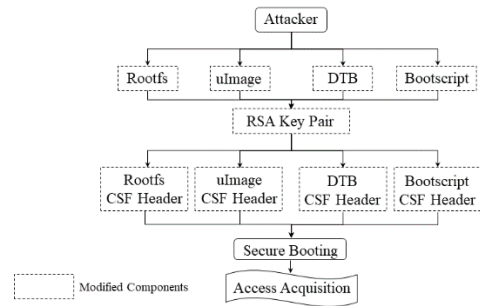


Fig. 3. Access Acquisition Scenario

Verification of security based on Scenarios

We got the two attack scenarios in the previous section. When we test the data steal attack, the attack was prevented in the RCW. Because once the RCW is programmed into ITS, it is impossible to reprogram it. Therefore, even if secure U-boot is substituted to normal U-boot and Bootsript is modified, secure boot does not turn off. As shown in Fig. 4 when we execute the attack scenario, the error message shows us that there is an error in SEC deque.

```

Error in SEC deque
RNG: Instantiation failed with error ffffffff
01: operation
02: jump
03: load_imm_u32
05: operation
    
```

Fig. 4. Error Message of Data Steal Scenario

When we test the access acquisition attack, the attack was prevented in SRKH. This is because once the SRKH is programmed into the security fuse processor, it is impossible to reprogram it. Therefore, even if a new CSF Header is created for the modified image, it cannot be decrypted because RSA public key which used to create the modified image has not been programmed into the SFP which has SRKH. As shown in Fig. 5 when T2080 secure boot verifies the images, error message was printed because the public key hash and SRKH are different.

```

ERROR :: 400 :: Public key hash comparison failed
SEC_MON already in Non Secure state.
## Executing script at e8a00000
ERROR :: 400 :: Public key hash comparison failed
SEC_MON already in Non Secure state.
ERROR :: 400 :: Public key hash comparison failed
SEC_MON already in Non Secure state.
ERROR :: 400 :: Public key hash comparison failed
SEC_MON already in Non Secure state.

```

Fig. 5. Error Message of Access Control Acquisition Scenario

IV. The Future of Verification Model

In this paper, we shared our experiences which building and executing verification model to test the secure boot against modify attack. We constructed the verification model in four steps of data collection, risk identification, scenario generation, and scenario verification. In our verification model, we could find numberless scenarios and verify the scenarios. However, this verification model is restricted to modify attack. Therefore, the verification model should be constructed according to services. Because the verification model has many forms and every service has its own verification model. If services find its own suitable verification model, it can enhance the security level of the service.

References

- [1] SiChoon Noh, IkSoo Jun, Kuinam J. Kim, Verification Method of Insuring Web Application Security. Journal of Information and Security, 3(2), pp. 11-20. 2003.
- [2] Myong-Yeal Lee and Jae-Pyo Park, An analysis on invasion threat and a study on countermeasures for Smart Car. Journal of the Korea Academia-Industrial Cooperation Society, Vol. 18, No. 3, pp. 374~380, 2017.
- [3] Jeom Goo Kim, A Study on Evaluation Technique of Network Security System. Journal of Information and Security, 9(2), pp. 33-39. 2009.
- [4] Balzarotti, D., Banks, G., Cova, M., Felmetsger, V., Kemmerer, R., Robertson, W., ... & Vigna, G. "Are your votes really counted?: testing the security of real-world electronic voting systems." In Proceedings of the 2008 international symposium on Software testing and analysis July 2008, pp. 237-248, ACM.
- [5] NXP Semiconductors, QorIQ T2080 Reference Manual, 2016.
- [6] XILINX, Zynq-7000 All Programmable SoC Technical Reference Manual, 2018.
- [7] Qualcomm Technologies, Secure Boot and Image Authentication Technical Overview, 2017.
- [8] Curtis-Wright, VPX3-133-3U-VPX-NXP-T2080-Single-Board-Computer-product-sheet, 2013.
- [9] Curtis-Wright, VPX3-152-3U-VPX-NXP-T2080-Single-Board-Computer-product-sheet, 2013.
- [10] Curtis-Wright, VPX6-195-6U-VPX-Freescale-T2080-SBC-product-sheet, 2013.
- [11] NXP Semiconductors, QorIQ SDK v2.0-1703 Documentation, 2017.

A fine-tuning CNN model for art painting style classification

Tuong Le, Mi Young Lee and Sung Wook Baik*

Digital Contents Research Institute

Sejong University

Seoul, Republic of Korea

Corresponding author: sbaik@sejong.ac.kr

Abstract—Recently with the spread of digitization of art paintings, the problem of art painting style classification has been introduced. This is an interesting problem attracted a lot of interest in research. In this study, 498 art painting in ten styles were first collected. Then, a fine-tuning CNN model for art painting style classification was proposed. The experimental results show that the performance of our model can reach 79% in terms of accuracy for our experimental dataset.

Keywords—Fine-tuning, deep learning, art painting style classification.

I. Introduction

Recently, with the continuous growth of data, machine learning has been developed and widely applied in many fields such as economic [1, 2] and computer vision [3, 4]. In machine vision, the problem of art painting style classification has been proposed by Lee and Cha [5]. This problem helps the user obtain more information on the specific artwork. In their study [5], the author collected 1633 pieces of artwork painted by 19 painters in four styles. Next, they extracted 50 feature values for each art painting. Finally, they used self-organizing map (SOM) [6] to classify the above dataset and obtained the positive results.

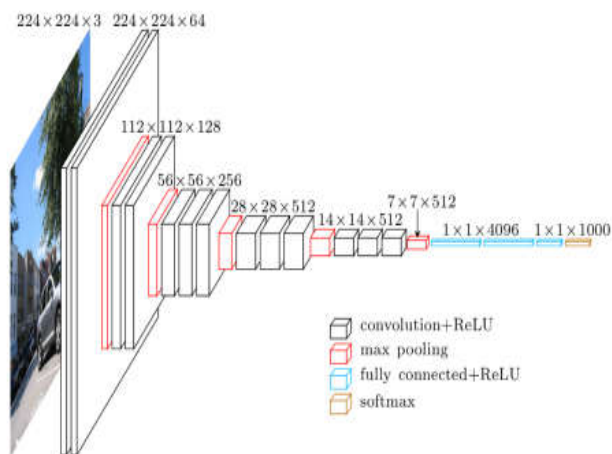


Fig. 1. Macro-architecture of VGG-16

In the last decade, CNN has been used widely especially in computer vision with high performance. Transfer learning, which use a pretrained network on a very large dataset as an initialization or a fixed feature extractor for new tasks, is widely used. There are three main categories of transfer learning: CNN as fixed feature extractor, fine-tuning CNN,

pretrained models. Among them, fine-tuning CNN has been used widely. VGG [7] is a pretrained CNN which achieves 92.7% accuracy in ImageNet [8], a dataset of over 14 million images belonging to 1000 classes. The structure and the parameters of the trained VGG model are freely available online which has two different models: VGG-16 and VGG-19. The macro-architecture of VGG-16, shown in Figure 1, consists 13 convolutional layers and 3 fully connected layers. Therefore, this study aims to using deep learning technique to improve the performance of the art painting style classification. We first collect the experimental dataset which include 498 art painting in ten styles. Then the study develops a fine-tuning CNN model, which uses VGG-16 as pretrained network, for art painting style classification effectively.

The paper is organized as follows. Section 2 introduces the experimental dataset and the proposed model. Section 3 presents experimental results. Finally, Section 4 draws a conclusion and discusses future work.

II. A fine-tuning CNN model for art painting style classification

A. The experimental dataset

The experimental dataset consists of ten classes including Baroque, High Renaissance, Primitivism, Minimalism, Surrealism, Impressionism, Expressionism, Post-impressionism, Lettrism and Muralism which have nearly 50 painting arts for each style. Several samples in each class were shown in Figure 2.

B. The proposed model

To create our model, we firstly load all convolutional and max-pooling layers with existing weights of VGG-16 (see Figure 1) using Keras which is the famous Python Deep Learning library. Next, we remove two last fully connected layers (4096, 1000) in VGG-16. Then, we added a fully connected with 256 units. Finally, output layer has ten classes which uses softmax function for classification. This model uses Mini-batch Gradient Descent optimizer with batch size $n = 16$, learning rate $\eta = 0.0001$, momentum $\gamma = 0.9$ to optimize the loss function. Figure 3 shows our model in detail.

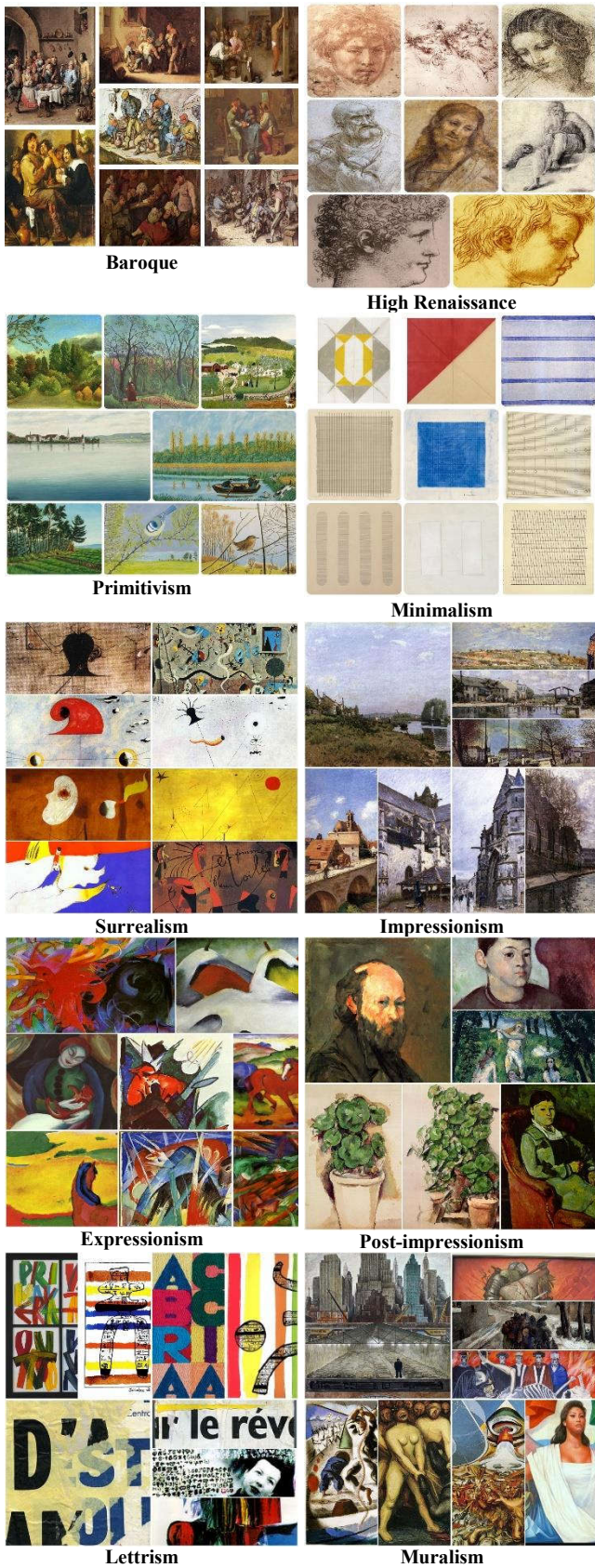


Fig 2. Samples of four art painting styles

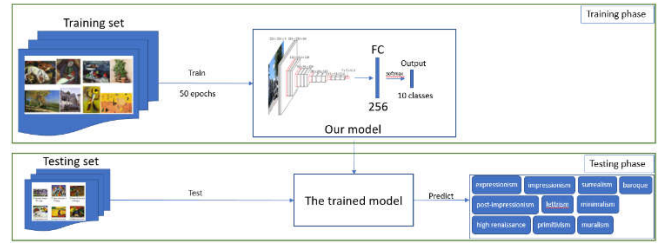


Fig. 3. The proposed model.

III. Results

To evaluate the proposed model, we use 80% pieces for training and 20% for validation to obtain the accuracy of the proposed model for art painting style classification. The experimental results show that the average accuracy of the proposed model is 79% for our experimental datasets. Figure 4 shows training loss, training accuracy, validation loss, and validation accuracy of each epoch.

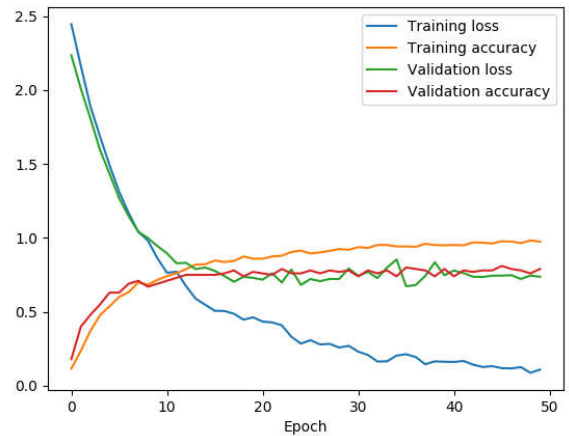


Fig. 4. Performance of the proposed model

IV. Conclusion

This paper proposed a fine-tuning CNN model for art painting style classification. The performance of our model reaches 79% accuracy for our experimental dataset. For future works, a full dataset will be collected, as well as a more powerful model will be proposed for APS classification.

Acknowledgment

This research was supported by the Korean MSIT (Ministry of Science and ICT), under the National Program for Excellence in SW (2015-0-00938), supervised by the IITP (Institute for Information & communications Technology Promotion)

References

- [1] Le T., Le H.S., Vo M.T., Lee M.Y., Baik S.W. A Cluster-Based Boosting Algorithm for Bankruptcy Prediction in a Highly Imbalanced Dataset. *Symmetry*, 10(7), 250, 2018
- [2] Le T., Lee M.Y., Park J.R., Baik S.W.: Oversampling techniques for bankruptcy prediction: Novel features from a transaction dataset. *Symmetry*, 10(4), 79, 2018
- [3] Ali M., Le H.S., Khan M., Nguyen T.T.: Segmentation of dental X-ray images in medical imaging using neutrosophic orthogonal matrices.

- Expert Syst. Appl., 91, 434-441, 2018
- [4] Le H.S., Tran M.T.: Dental segmentation from X-ray images using semi-supervised fuzzy clustering with spatial constraints. Eng. Appl. of AI, 59, 186-195, 2017
 - [5] Lee S.G., Cha E.Y. Style classification and visualization of art painting's genre using self-organizing maps. Human-Centric Computing and Information Sciences (2016) 6:7
 - [6] Kohonen T. Self-Organizing Maps. Springer, Berlin, Heidelberg, 1995
 - [7] Simonyan K., Zisserman A.: Very deep convolutional networks for large-scale image recognition. ICLR, 2015
 - [8] Deng, J., Dong, W., Socher, R., Li, L.-J., Li, K., and Fei-Fei, L. Imagenet: A large-scale hierarchical image database. In CVPR 2009, 248-2

Stock Selection by using an improved quick Artificial Bee Colony Algorithm

Dit Suthiwong⁽¹⁾, Maleerat Sodanil⁽²⁾

⁽¹⁾⁽²⁾ Faculty of Information Technology, King Mongkut's University of Technology North
Bangkok, Bangkok, Thailand

⁽¹⁾Email : s5507011966036@email.kmutnb.ac.th

⁽²⁾ Email : maleerat.s@it.kmutnb.ac.th

Abstract—Computation Intelligence have inspired many researchers to develop the capability of computer to learn and solve the complex task in real-world problems. In this work, we proposed an improved quick Artificial Bee Colony (iqABC) to deal with the Stock Selection problem. We apply a Sigmoid-based Discrete-Continuous with ABC to select appropriate features for stock scoring. The empirical study tests the performance of iqABC compare with Genetic Algorithm (GA), Differential Evolution (DE) algorithm and original Artificial Bee Colony (ABC) by using data from the Stock Exchange Thailand. The empirical results show that the novel model stock selection significantly outperforms in terms of both investment return, diversity and model robustness

keywords— *Artificial Bee Colony, Stock Selection*

I. Introduction

The Artificial Bee Colony (ABC) algorithm was first proposed by Karaboga [1] in 2005, ABC had shown competitive performance [2] on many real world problems [3]. It has an advantage in fewer control parameters, simple structure, easy to implement and good in exploration. ABC can efficiently deal with multimodal and multi-dimension problems. And it also has been successfully extended to solve multi-objective optimization problems [4]. However, the major drawback of ABC is a slow convergence speed. This is mainly caused by its solution search equation. Its search equation focus on exploration but weak on exploitation [5]. Many researchers proposed solution to improve the performance of ABC [6], [7].

A Stock Selection model is a challenge problem in finance. The investors have to make a decision based on their investment experience. Normally, the smart investors use data in the financial statement to evaluate the stock by interpreting performance and the competitiveness of each stocks compare to their competitors in same business. The example of financial data is profitability, asset ratio, net profit growth, and price ratio. In General, A Stock Selection model is comprised of two key steps, i.e., stock scoring and stock ranking. Related to the study in a Stock Selection model, it can be mainly divided into two categories: Traditional statistical regression approaches and Computational Intelligence (CI) [8] approaches. Traditional statistical regression approaches are easy to understand and implement. Example include the testing of the

forecasting of stock market returns using the dividend yield, the earnings growth, and the price earnings ratio growth [9].

However, CI approaches have shown more efficient than the Traditional statistical regression approaches [10]. Many CI models have been applied to stock evaluation, such as Genetic Algorithm (GA), Artificial Neural Networks (ANNs), ABC and Differential Evolution (DE). For GA, Huang et al. [11] utilized GA to optimize feature selection, Soam et al. [12] used GA with local search to select stock into portfolio, Chen et al. [13] applied ABC create cardinality-constrained portfolio, Tsai et al. [14] combined multiple selection methods ANN, GA and Decision Tree. Yu et al. [15] used DE with sigmoid based to solve stock scoring problem. All these example studies demonstrated that the CI approaches outperformed the traditional regression approaches.

Our proposed model is an improved quick Artificial Bee Colony algorithm (iqABC) by using sigmoid-based conversion. This modification enhanced ABC to solve a mixed discrete continuous decision variable. This paper also proposed a stock selection model by evaluate stock based on various fundamental financial data features. The detailed description of the stock selection model provides is in Section 2, The methodology of improved quick ABC is in Section 3, The empirical design, training, testing and results are in Section 4, and Conclusion is in Section 5.

II. Problem formulation

A Stock Selection is a concept of to select best stocks in to portfolio with expectation to get maximum investment return. Generally Stock Selection has two main steps, i.e, stock scoring and stock ranking. In the first step, a stock scoring can be calculated from their stock information such as profit return, amount of sale growth, etc. In the second step, a stock ranking ranks stocks according to their scores. The stock selection model in this study extended from the model proposed by Yu et al. [15] which using Differential Evolution (DE) algorithm. The proposed model uses an improved quick Artificial Bee Colony algorithm and Sigmoid conversion to handle both discrete and continuous decision variables. As shown in Fig.1, The proposed stock selection model is composed of three steps. First step is Input Preparation, Second step is Selection Model and Third step is Optimization model.

A. Input Preparation

In this step, The stock returns are calculated in terms of the natural logarithm of price ratio (i.e., $R_{i,t} = \ln(P_{i,t}/P_{i,t-1})$) where $R_{i,t}$ denotes return of stock i at current time t , $P_{i,t}$ denote price of stock i at current time t , $P_{i,t-1}$ denote previous price of stock.

Then The Z-score normalization of features j denote by $Y_{i,j,t}$ are calculated. The score $Y_{i,j,t}$ is assumed to follow a normal distribution with mean zero and deviation one. If a larger feature value implies that the direction will be up then $Y_{i,j,t}$ can be calculated according to the following form.

$$Y_{i,j,t} = \frac{V_{i,j,t} - \bar{V}_{j,t}}{D_{j,t}} \quad (1)$$

$$\bar{V}_{j,t} = \frac{1}{N} \sum_{i=1}^N V_{i,j,t} \quad (2)$$

$$D_{j,t} = \sqrt{\frac{1}{N} \sum_{i=1}^N (V_{i,j,t} - \bar{V}_{j,t})^2} \quad (3)$$

Where $V_{i,j,t}$ is the actual score of feature j and $\bar{V}_{j,t}$ is the average value of feature j across all N stocks at time t , and $D_{j,t}$ is the standard deviation of feature j at time t . If a smaller value implies that the direction will be up then $Y_{i,j,t}$ can be calculated according to the following form.

$$Y_{i,j,t} = \frac{\bar{V}_{j,t} - V_{i,j,t}}{D_{j,t}} \quad (4)$$

B. Selection Model

Stock Scoring: Feature Selection had been proposed to solve complexity of stock scoring. Various stock features including profitability, Price ratio, Growth, Efficiency can be used to calculate score. The model proposed by Yu et al. [15] applied the wrapper method and optimized solution by using Differential Evolution (DE). The model combines feature selection with the corresponding weight optimization. First, binary variable $F_j = \{0,1\}$ is utilized represent whether feature j is used in stock evaluation ($F_j = 1$) or not ($F_j = 0$), Let W_j denote the weight on the j th feature. The stock scoring $S_{i,t}$ of stock i at time t can be formulated as follows:

$$S_{i,t} = \sum_{j=1}^N F_j W_j Y_{i,j,t} \quad (5)$$

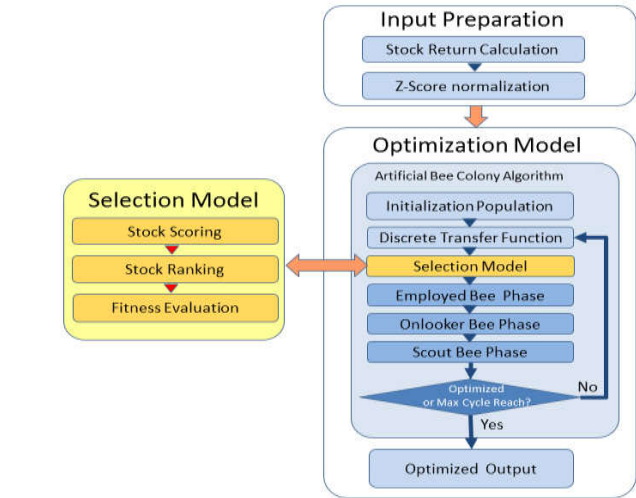


Fig. 1. Stock Selection Framework

Stock Ranking: A Stock Ranking sorts stock according to their scores. Let $r_{i,t} = \{1,2,\dots,N\}$ denote the ranking of stock i at time t , i.e., $r_{i,t} \leq r_{k,t}$ if $S_{i,t} \leq S_{k,t}$ where $i,k \in \{1,2,\dots,N\}$ represent any two different stocks. The higher rank means a high potential of price increase. Then the model creates an equal-weighted portfolio for the next period by selecting the stock with m rankings $r_{i,t} = \{1,2,\dots,m\}$ at the end of each period. Accordingly, the average return of portfolio in next period is calculated and used for evaluate the performance of all selected stocks.

$$R_{t+1}^p = \frac{1}{m} \sum_{r_{i,t}=1}^m R_{t+1}(r_{i,t}) \quad (6)$$

Where $R_{t+1}(r_{i,t})$ is the next period return of stock with current ranking $r_{i,t}$ at time t , and R_{t+1}^p is the next period return of the portfolio constructed by the proposed model.

Fitness Evaluation: To capture effectiveness of the selection model, The Information Coefficient (IC) between features and future returns has been selected as fitness function.

$$\min F = \frac{1}{T} \sum_{t=1}^T IC_t \quad (7)$$

$$IC_t = \frac{cov(r_{i,t}, r'_{i,t+1})}{\sqrt{var(r_{i,t})var(r'_{i,t+1})}} \quad (8)$$

where $r_{i,t}$ is the score ranking of stock i by the proposed model at time t , $r'_{i,t+1}$ is the actual return ranking in the next period, and T is the total number of training periods. The function $cov()$ and $var()$ are the covariance and variance estimations. IC_t is the Spearman correlation between the currently predicted ranking of stock $r_{i,t}$ and their actual return ranking $r'_{i,t+1}$ in the next period.

C. Optimization Model

To Optimize solution in term of feature selections F_j and the corresponding weights W_j , The Artificial Bee Colony (ABC) algorithm has been proposed to solve problem. Since the original ABC focus on continuous values, this study improved ABC algorithm by using the sigmoid-based mixed discrete-continuous.

The Original ABC Algorithm: In nature, Honey bees live in colonies and have a social communication. Artificial Bee Colony (ABC) algorithm [1] is a population-based evolutionary algorithm which mimic communication of Honey bees. There are three groups of bees in the colony who responsible to find and collect food to nectar. They are employed bees, onlooker bees and scouts bees. The pseudo code is shown as below.

Initialization phase
 REPEAT
 Employed bee phase
 Onlooker bee phase
 Scout bee phase
 UNTIL (cycle=maximum cycle number or Optimized)

ABC algorithm starts with population by random create food sources represent to a possible solution to the problem space. The nectar amount of a food source denotes the quality of the associated solution.

Then ABC algorithm repeat until max cycle number reach or found optimized solution. Employed bees phase takes charge of exploring the solution space in which nearby to existing food sources. Onlooker bees phase chooses a number of food sources to exploit based on the perform waggle dance of Employed bees. When there are no improvements to the food sources after several times Scout bees phase will sent scout bee out randomly to find new brand food sources. If the new food source has better nectar they will memorize the new position and forget the previous one.

The proposed model modified original ABC algorithm by using Sigmoid conversion to solve mixed discrete-continuous variable. And the proposed model also including Selection model in previous step to evaluate effectiveness of optimized solution. The pseudo code is shown as follow.

Initialization phase
 Discrete Transfer Function
 Selection Model
 REPEAT
 Employed bee phase
 Discrete Transfer Function

Selection Model
Onlooker bee phase
 Discrete Transfer Function
 Selection Model
Scout bee phase
 Discrete Transfer Function
 Selection Model
 UNTIL (cycle=maximum cycle number or Optimized)

In Initialization Phase, food sources are randomly initialize with Equation (9) in a given range.

$$x_{p,d} = l_d + rand(0,1) * (u_d - l_d) \tag{9}$$

Where x is the value of the d dimension of the p solution. l_d represents the lower bound and u_d represents the upper bound of the parameter $x_{p,d}$. In proposed model, p represents population of food sources and d represent dimension of search space. Number of dimensions are equal to number of features and number of their corresponding weights. The dimension of search space is in Fig. 2.

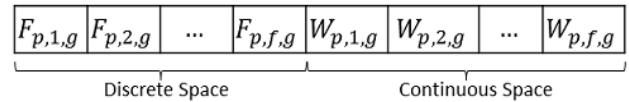


Fig. 2. Encoding

Discrete Transfer Function: The discrete term $F_{p,j,g} = \{0, 1\}$ represents the selection decision of feature j in p th solution at iteration g , and the continuous term $W_{p,j,g} \in [0,1]$ is the corresponding weight. If $F_{p,j,g} = 0$ then $W_{p,j,g}$ is accordingly set to 0.

Sigmoid Conversion method is used to identify a candidate feature as a key factor for stock scoring ($F_{p,d,g} = 1$) or a poorly information one ($F_{p,d,g} = 0$). The conversion from the continuous variable $x_{p,d,g}$ to the binary form $F_{p,d,g}$ is conducted according to the probability $P(x_{p,d,g})$ which follows a logistic distribution formula as follow.

$$F_{p,d,g} = \begin{cases} 1, & \text{if } r_{p,d,g} \leq P(x_{p,d,g}) \\ 0, & \text{otherwise} \end{cases} \tag{10}$$

$$P(x_{p,d,g}) = \frac{1}{1 + e^{-x_{p,d,g}}} \tag{11}$$

Where r is a random term following a uniform distribution on the range of (0, 1). ABC algorithm can be extended to the sigmoid-based ABC for mixed discrete-continuous problems.

Selection Model: By using food sources from initialization phase calculates with Z-score normalization of features j . The proposed evaluates fitness function by using stock scoring and stock ranking as shown in previous topic. The fitness value from Selection model is used in ABC algorithm to evaluate food sources quality by following formula.

$$fit(x_m) = \begin{cases} \frac{1}{1 + f(x_m)}, & \text{iff } f(x_m) \geq 0 \\ 1 + abs, & \text{iff } f(x_m) < 0 \end{cases} \quad (12)$$

Where x represents fitness value of the stock selection model. Each food source will be further exploited by one and only one employed bee. Then it search for the neighborhood of a target food source. This study focuses on the change of the associated v_m values for each asset selected by equation as follows:

$$v_{m,i} = x_{m,i} + \phi_{m,i}(x_{m,i} - x_{k,i}) \quad (13)$$

In equation (13) x_k is a food source selected from neighborhood randomly and i is also a randomly weight parameter. $\phi_{m,i}$ denotes a random number generated from a uniform distribution with the range of $[-1,1]$. $v_{m,i}$ is the new candidate food source which will be converted with Discrete Transfer Function and then evaluate fitness value with Selection Model. Then, a greedy selection is applied between v_m and x_m . If a food source is not be improved employed bee will increase a certain number of iteration limit by one.

Onlooker bee phase: The onlooker bees determine the food sources to search using the probability based on the quality of each food source. The probability of selection p_m can be calculated as follows.

$$p_m = \frac{fit(x_m)}{\sum_{m=1}^{SN} fit(x_m)} \quad (14)$$

According to the probability, Onlooker bees choose a food source v_m to exploit by using equation (13) similar to employed bees, its fitness value is computed by using Discrete Transfer Function and Selection model. Then, A greedy selection is used to determine between v_m and x_m .

Scout bee phase: If some of food sources cannot be improved through a certain number of iterations limit. Scout bees will be dispatched to explore new brand food sources. This make new solutions randomly generated by using Equation (9). Discrete Transfer Function and Selection executed to calculate fitness value. Then, a greedy selection is used to determine between the old solution and the new food source. If new solution is better than the old solution, then the old food source will be replaced with new food source.

I. Proposed improve quick artificial bee colony

It is known that ABC algorithm is powerful. But it still has some drawbacks such as slow convergence. Because the search equation of ABC is good in exploration but badly in exploitation. The proposed model improve. ABC algorithm by apply global best (gbest) concept in Employed Bee phase and apply quick ABC concept in Onlooker Bee phase.

A. Modification in Employed Bee Phase

Inspired by the Particle Swarm Optimization algorithm, we proposed to use global best (gbest) apply as follows.

$$v_{m,i} = x_{m,i} + \phi_{m,i}(x_{m,i} - x_{k,i}) + \psi_{i,j}(gbest_i - x_{k,i}) \quad (15)$$

In Employed bee phase, we replace equation (13) with (15). Where ϕ represents a uniformly distributed random number in $[0,1.5]$, gbest is the current global best solution in the whole swarm, and $gbest_i$ represents the i th variable of $gbest$.

B. Modification in Onlooker Bee Phase

By Comparing to nature of honey bees, Employed bees and Onlooker bees exploit foods in different ways. Employed bees exploit the food source that they visit before. Onlooker bees exploit food source based on communication from employed bee dancing (we called waggled dance.) which will be interpreted for which food sources will be selected. In Original ABC Employed bees and Onlooker bees use the same search equation (13). Karaboga [6] introduced new equation of onlooker bees phase modified. The equation for onlooker bee had been modified as follow.

$$v_{N_{m,i}}^{best} = x_{N_{m,i}}^{best} + \phi_{m,i}(x_{N_{m,i}}^{best} - x_{k,i}) \quad (16)$$

From equation (16), $x_{N_{m,i}}^{best}$ represents the best solution between the neighbors of x_m and itself N_m . The neighborhood of individual m is determined by the Euclidean distance between X_{N_m} and the other food sources. The mean Euclidean distance between x_m and the rest food sources is calculated and then compare it with A new parameter r which refers to the “neighborhood radius” is added into the parameters of standard ABC algorithm. If a solution which Euclidean distance from x_m is less than the mean Euclidean distance md_m then this food sources could be accepted as a neighbor of x_m as equation (17).

$$md_m = \frac{\sum_{j=1}^{SN} d(m,j)}{SN - 1} \quad (17)$$

This solution is similar to nature that onlooker bees selects the region which is centered by the food source x_m . The pseudocode for determine a neighbor of x_m is given as follow.

*if $d(m; j) \leq r * mdm$ then x_j is a neighbor of x_m , else not*

II. Computational analysis

Our proposed model improved quick ABC algorithm. It is compared with - Genetic Algorithm (GA), Differential Evolution (DE), and original ABC. The proposed model is coded in Matlab R2013a and run on a notebook computer with Intel Core i7-4510U CPU 2.00GHz and 4.0 GB memory.

A. Test Instance

We brought trading data from Stock Exchange Thailand from Quater1,2012 to Quater1,2017 and then calculate return from about 600 stocks. Closing price from the last trading day of the quarter are used to compare with closing price in previous quarter to calculate stock return. The testing period is formulated by 4-quarters, 8-quarters, 12-quarters and 16-quarters.

In this study, Fifteen Candidate Features has been used to test for Stock Selection. Example Stock features are Price per Earning ratio, Price per Book Value ratio, Dividend Yield, Total Assets, Revenue, Net Profit, Earning Per Share and others.

B. Parameter Setup

ABC and iqABC parameter setup are the same by using Population(P)=30, Limit=10. GA uses Population=30 cr=0.5, mr=0.6. And DE uses Population=30, Cr=0.5, beta=0.6. All algorithms will terminate when iterations reach the given maximum G = 100. All models run ten times for each case, and the average values are calculated as the final results.

C. Performance Measures

To evaluate performance of proposed model, this study evaluates in terms of the average return of the formulated portfolios over all testing periods:

$$MR = \frac{1}{T'} \sum_{t=1}^{T'} R_{t+1}^p \quad (18)$$

Where R_{t+1}^p is the next period return of the portfolio formulated at time t, and T' is the total number of testing periods.

D. Empirical Results

All algorithms are executed 10 times on each instance with a different random seeds. The test result as show in TABLE I.

It obviously seen that iqABC given high return in all periods of investment. Especially for 12-quarters testing period return from portfolio is 0.0858 or equal to 8.58% compare to market average return at 4.368%.

TABLE I. COMPARISON PORTFOLIO RETURN FOR DIFFERENT PERIODS

Algorithms	Investment periods (Quarters)			
	4	8	12	16
GA	0.04312	0.06199	0.06728	0.05922
DE	0.01224	0.01919	0.02754	0.03339
ABC	0.04068	0.06978	0.06882	0.06367
iqABC	0.04634	0.07641	0.08538	0.07906

The original ABC is second high portfolio return for 8-quarters, 12-quarters and 16-quarters testing data. The return results from ABC and GA are not much different. The main reasons for the superiority of the iqABC algorithm can be generally summarized into two following aspects. First, it

modified ABC in employed bee phase with global best guidance. Second, it modified in onlooker bee phase using neighborhood radius to improve quality of result.

III. Conclusion

The Artificial Bee Colony Algorithm had shown its powerful to solve the Stock Selection problem. For qABC, it also shows improvement for accuracy and convergence. And we have proposed iqABC which developed based on qABC. By using gbest direction concept in employed bee phase, we got the more accuracy result and more non-dominated points compare to others.

For future works, in algorithm development topic about convergence should be developed search equation and detail work in algorithm to enhance result and reduce time of execution.

References

- [1] D. Karaboga, "An idea based on honey bee swarm for numerical optimization". Technical Report, Computer Engineering Department, Engineering Faculty, Erciyes University, 2005.
- [2] D. Karaboga, B. Basturk, "A powerful and efficient algorithm for numerical function optimization: artificial bee colony (ABC) algorithm," Journal of Global Optimization, 2007.
- [3] Y. C. Liang, A. H. L. Chen, Y. H. Nien, "Artificial Bee Colony for workflow scheduling," 2014 IEEE Congress on Evolutionary Computation (CEC), 2014.
- [4] Z. Wang, M. Li, L. Dou, Y. Li, Q. Zhao, J. Li, "A novel multi-objective artificial bee colony algorithm for multi-robot path planning," 2015 IEEE International Conference on Information and Automation, 2015.
- [5] L. Cui, et al, "A novel artificial bee colony algorithm with depth first search framework and elite-guided search equation," Information Sciences, pp.367-368, 2016.
- [6] D. Karaboga, B. Gorkemli, "A quick artificial bee colony -qABC- algorithm for optimization problems," 2012 International Symposium on Innovations in Intelligent Systems and Applications, 2012.
- [7] Y. Shi, C.-M. Pun, H. Hu, H. Gao, "An improved artificial bee colony and its application," Knowledge-Based Systems, 107, pp.1431, 2016.
- [8] C. F. Huang, T. N. Hsieh, B. R. Chang, "A comparative study of stock scoring using regression and genetic-based linear models," 2011 IEEE International Conference on Granular Computing, 2011.
- [9] M.A. Ferreira, and P. Santa-Clara, "Forecasting stock market returns: The sum of the parts is more than the whole," Journal of Financial Economics, Vol. 100, No. 3, 2011.
- [10] R. C. Cavalcante, R. C. Brasileiro, V. L. F. Souza, J. P. Nobrega, A. L. I. Oliveira, "Computational Intelligence and Financial Markets: A Survey and Future Directions," Expert Systems with Applications, 55, 2016.
- [11] C. F. Huang, T. N. Hsieh, B. R. Chang and C. H. Chang, "A Comparative Study of Regression and Evolution-Based Stock Selection Models for Investor Sentiment," 2012 Third International Conference on Innovations in Bio-Inspired Computing and Applications, 2012.
- [12] V. Soam, L. Palafox, H. Iba, "Multi-objective portfolio optimization and rebalancing using genetic algorithms with local search," 2012 IEEE Congress on Evolutionary Computation (CEC), 2012.
- [13] A. H. L. Chen, Y.-C. Liang, C.-C. Liu, "Portfolio optimization using improved artificial bee colony approach," 2013 IEEE Conference on Computational Intelligence for Financial Engineering Economics (CIFER), 2013.
- [14] C.-F. Tsai, Y.-C. Hsiao, "Combining multiple feature selection methods for stock prediction: Union, intersection, and multi-intersection approaches," Decision Support Systems, 50, 1, 2010.
- [15] L. Yu, L. Hu, L. Tang, "Stock Selection with a Novel Sigmoid-Based Mixed Discrete-Continuous Differential Evolution Algorithm," IEEE Transactions on Knowledge and Data Engineering, 28, 7, 2016.

Poster Session

- Panorama Classification based on Parallax Error using Deep Learning
/ Osama Zia, JongWeonLee / Sejong University, Seoul, Korea
- Alzheimer's disease and normal control MRI classification over hippocampus region
/ Samsuddin Ahmed, Ho Yub Jung / Chosun University, Korea
- Hippocampus Localization Using Hough-CNN
/ Abol Basher, Ho Yub Jung / Chosun University, Korea
- Resilience of Features for Detecting Open Source Software in Obfuscated Android Apps
/ Byoungchul Kim, Kyeonghwan Lim, Seong-je Cho, Minkyu Park / Dankook University, Konkuk University Korea
- Magnetic Resonance Imaging Enhancement using Adaptive Histogram Equalization with Multi-scale Method
/ Waqas Ellahi, Bumshik Lee / Chosun University, Korea
- U-Net Model for Automatic Segmentation of MR Brain Images
/ Muhammad Ammar Malik, Bumshik Lee / Chosun University, Korea
- Traffic Congestion Analysis using Taxi Trajectory Data with Information Entropy
/ Mingyu Pi, Hanbyul Yeon, Seogbong Jeon, Dong gun Kim, Yun Jang / Sejong University, Korea
- Salient Event Detection in Soccer Videos using Histogram of Oriented Gradient
/ Hayat Ullah, Faisal Saeed, Mustaqeem, Muhammad Sajjad / Islamia College Peshawar, Pakistan
- Classification of Membrane Proteins using Four Phase Split Amino Acid Composition Descriptor over Random Forest
/ Abdul Jamil, Waseem Ullah, Samee Ullah, Muhammad Sajjad / Islamia College Peshawar, Pakistan
- Sequence Based Prediction of DNA binding proteins by evaluating the acidic and alkaline amino acids using Random forest
/ Samee ullah, Warda khurshid, Waseem ullah, Muhammad Sajjad / Islamia College Peshawar, Pakistan
- Our Experiences on the Design, Build and Run of CTF
/ Jun-Gyu Park, Sang-Hoon Choi, Hyun-il Kim, Hong Down, Ki-Woong Park / Sejong University, Kongju National University, Korea
- Just-Noticeable-Difference Based Edge Map Quality Measure
/ Ijaz Ahmad, Seokjoo Shin / Chosun University, Korea
- A Study on Implicit Authentication Using Sensors of Smart Device for SMS Authentication
/ Gwonsang Ryu, Daeseon Choi / Kongju National University, Korea
- Structural Perspective Analysis for Big Data As A Networks
/ Chris Soo-Hyun Eom, Wookey Lee / Inha University, Korea
- Real-time Deep ALPR for Korean License Plates using YOLO Object Detector
/ Chris Henry, Sang-Woong Lee / Gachon University, Korea
- A Web-Based Application for Constructing Deep Portfolios
/ Hye Jin Lim, Sang Il Lee, Yeong Hyeon Gu, Seong Joon Yoo / Sejong University, Korea
- A Study of Face Detection Techniques and Facial Landmarks
/ Ju Yeong Sung, Jong-Kook Kim, HwangNam Kim, JunHee Seok / Korea University, Korea
- Optimal Frequency Reuse for Progressive Image Transmission
/ Minyeong Kim, Soyoung Jang, Sungjin Kim, Seung-Hoon Kim, Seok-Ho Chang / Dankook University, Korea
- Spectrum Sensing Ratio Control Method for Improve Utilization based on the PU History
/ Gyu-min Lee, Byeong-hee Roh, Sungjin Kang, Ji Myeong Oh / Ajou University, LG Nex1, Korea
- Improvement of P & O MPPT Algorithm of Photovoltaic System Based on Least Mean Square Algorithm
/ Bong-Seog Jang, Dae-Young Lee, Il-Yong Chung, Yoon-Hwan Kim, Tae-Yeun Kim, So-Wol Yoo, Jeong-Sang Song, Sang-Hyun Bae / Mokpo National University, Gwangju Health University, Chosun University, Christian College of Nursing, Korea

- Pupil Segmentation for Gaze Applications based on Deep Learning
/ Rizwan Ali Naqvi, Sang-Woong Lee, Woong-Kee Loh / Gachon University, Korea
- Poisonous Plant Classification using Deep Learning for Smart phone Applications
/ Min-Je Kim, Su-Min Lee, Ju-Chan Park, Hye-Won Lee, Chan-Min Kwon, Il-Young Won
/ Seoul Hoseo Vocational College, Korea
- Proposal of Dog face Classification Model for Efficient Animal Character Production
/ Young-June Lim, Young-Suk Lee / Dongguk University, Korea
- Development of Hybrid Governor for FreeRTOS based on H/W low-power features
/ SungYup Lee / ETRI school University, Korea
- Performance Evaluation of Data Mining Techniques Based on Network Intrusion Detection Systems
/ Pongsarun Boonyopakorn / King Mongkut's University, Thailand

Panorama Classification based on Parallax Error using Deep Learning

Osama Zia¹, Jong Weon Lee²

Mixed Reality & Interaction Lab, Department of Digital Contents

Sejong University, Seoul, Republic of Korea

¹osama197@gmail.com, ²jwlee@sejong.ac.kr

Abstract—In this paper, a method is presented that classifies panorama images based on the presence or absence of parallax error using deep learning. Panorama images are produced using image stitching. Such images are prone to stitching errors such as parallax error, occlusion, and blending error. It is very difficult to identify such stitching errors using conventional computer vision approaches. So, we propose a deep learning-based approach to classify images based on parallax error. The technique of transfer learning is used to classify the panorama images. The VGG16 neural network architecture, pretrained on the ImageNet Dataset, is used.

Keywords— *panorama; parallax error; transfer learning*

I. Introduction

Image Quality Analysis (IQA) is an active research area. Generally, IQA methods are divided into two groups, which are reference-based methods and no-reference methods. For reference-based methods, the ground truth image is available. In this case, the distorted image is compared to the ground truth using image processing techniques such as Structural Similarity Index Metric (SSIM) [1]. For blind IQA methods, there is no ground truth image. In such cases, it is more difficult to assess the quality of the image. Some researchers have used methods such as BLIINDS2 [2] for this purpose.

A panorama image is a wide Field of View (FOV) image that is created using two or more narrow FOV images. The method used to create panorama images is known as Image Stitching. A slight inaccuracy, during image stitching, can lead to a stitching error in the final panorama image.

Usually, for panorama images, ground truth image isn't available, so reference-based methods cannot be used. The stitching errors, present in panorama images, are quite different from typical noise in images. Most no-reference methods are developed to deal with noise introduced after image compression. Such methods do not work well to analyze the quality of panorama images. Researchers have proposed various methods for no-reference IQA using deep learning. A comparison of such deep learning methods for IQA is presented in [3].

In this paper, we present a no-reference based method to classify panorama images based on parallax error using deep learning. The concept of transfer learning has been used to utilize existing state of the art neural network architecture, which is VGG16, to classify the panorama images.

II. Method

Deep Learning requires a lot of data and time to tune the millions of parameters that are present in a Deep Convolutional Neural Network (CNN). For example, the ImageNet Dataset has more than 14 million images belonging to over 20,000 classes. It is very difficult to gather such a huge amount of data for a custom classification task. However, Transfer Learning is a technique that can be used when the amount of data is quite less [4]. In Transfer Learning, the deep CNN trained on a huge dataset is fine-tuned to work on a custom dataset as shown in Fig. 1.

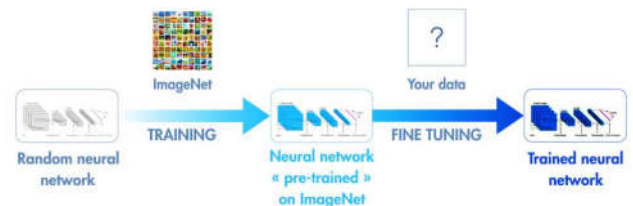


Fig. 1. Transfer Learning

For this paper, we use transfer learning technique to quickly train our system. The VGG16 pretrained on ImageNet Dataset has been used for this purpose. It has 16 weight layers, hence the name VGG16. It has about 138 million tunable parameters. The VGG16 achieved a Top-5 error rate of 7.3% on the ImageNet Dataset [5].

In Transfer Learning, the convolutional filters of a Deep CNN are used as feature extractors. The terminal fully connected layers are replaced with custom layers. For our system, we replace the fully connected layers of VGG16 by two fully connected layers, each having 128 neurons, followed by a SoftMax layer. In the initial stage, we only train the custom fully connected layers. In the second stage, we finetune the whole network using a lower learning rate so that the feature extractors can adapt to the custom dataset.

Our proposed method classifies the panorama images into one of the two classes that are parallax class and non-parallax class. In order to train the CNN, panorama images have been taken from two datasets, which are Google Street View Dataset [6] and Sun360 Dataset [7]. Google Street View Dataset has many images which have stitching errors in them as shown in Fig. 2. In contrast, Sun360 Dataset has good quality panorama images as shown in Fig. 3.



Fig. 2. Panorama Image from Google Street View Dataset



Fig. 3. Panorama Image from Sun360 Dataset

III. Experimental Results

In order to test the performance of our proposed system, we selected 1000 images from each of the Google Street View and Sun 360 datasets for the parallax class and non-parallax class respectively. The 2000 images are then divided into training set (70%), validation set (20%), and testing set (10%).

For the training set, the images were augmented in real time using the Keras library in Python. Various augmentation techniques, such as width shift, height shift, rotation, shear, zoom, and horizontal flip, were used. After augmentation, the total number of training images increased to 7000, that is 3500 images/class. Every image is resized to 224 x 224 before passing it to the network.

For the initial stage, the convolutional filters of VGG16 are frozen while the custom fully connected layers are trained. The Adam optimizer, with a learning rate of 0.001, and cross-entropy loss function are used for this stage. The system is trained for 50 epochs. For the finetuning stage, all the layers are trained. For this stage, Stochastic Gradient Descent (SGD) optimizer, with a learning rate of 10E-5, and cross-entropy loss function are used. The system is trained for 160 epochs. The validation accuracies and losses for both these stages are shown in Fig. 4.

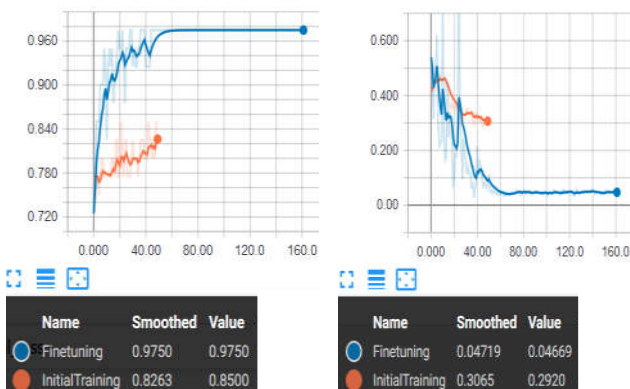


Fig. 4. Validation Accuracy (Left) and Validation Loss (Right)

Fig. 4 shows that, after the fine-tuning stage, an accuracy of 97.50% is achieved on the validation dataset. To validate this result, the testing set is passed through the system. The overall performance of the system on the validation and testing sets is summarized in Table I.

TABLE I. Experimental Results

Stage	Validation Accuracy	Testing Accuracy
Initial Training	85.00%	78%
Finetuning	97.50%	92%

Table I show that the transfer learning approach has worked well for this panorama classification task.

IV. Conclusion

In this paper, a panorama classification method based on parallax error using deep learning is presented. Panorama images suffer from stitching errors such as parallax error, blending error, and occlusion. Conventional Image Quality Analysis methods are not suited to recognize such stitching errors. We have used the pretrained VGG16 neural network to classify panorama images based on parallax error. We finetune the network by giving it training images belonging to two classes, which are Parallax Class and Non-Parallax Class. These training images have been carefully selected from Google Street View and Sun360 Datasets. The experimental results show that the network is suitable to classify the panorama images with a good accuracy.

Acknowledgment

This research was supported by MSIT (Ministry of Science, ICT), Korea under the ITRC (Information Technology Research Center) support program (IITP-2018-2016-0-00312) supervised by IITP (Institute for Information & communications Technology Promotion).

References

- [1] Z. Wang, A. C. Bovik, H. R. Sheikh and E. P. Simoncelli, "Image Quality Assessment: From Error Visibility to Structural Similarity," *IEEE TIP*, 2004.
- [2] M. Saad and C. Charrier, "DCT Statistics Model-Based Blind Image Quality Assessment," in *ICIP*, 2011.
- [3] S. Bosse, D. Maniry, K.-R. Muller, T. Wiegand and S. Wojciech, "Deep Neural Networks for No-Reference and Full-Reference Image Quality Assessment," *IEEE TIP*, 2018.
- [4] S. J. Pan and Q. Yang, "A Survey on Transfer Learning," *IEEE TKDE*, vol. 22, no. 10, pp. 1345-1359, 2010.
- [5] K. Simonyan and A. Zisserman, "Very Deep Convolutional Networks for Large-Scale Image Recognition," *CoRR*, vol. abs/1409.1556, 2014.
- [6] A. R. Zamir and M. Shah, "Image Geo-localization Based on Multiple Nearest Neighbor Feature Matching using Generalized Graphs," *IEEE TPAMI*, vol. 36, no. 8, pp. 1546-1558, 2014.
- [7] J. Xiao, K. A. Ehinger, A. Olivia and A. Torralba, "Recognizing Scene Viewpoint using Panoramic Place Representation," in *IEEE CVPR*, Providence, 2012.

Alzheimer's Disease and Normal Control MRI Classification over Hippocampus Region

Samsuddin Ahmed

Computer Engineering, Chosun University
Gwanju, Republic of Korea

Ho Yub Jung

Computer Engineering, Chosun University
Gwanju, Republic of Korea
hoyub@chosun.ac.kr

Abstract—Recently Deep learning (DL) is showing outstanding performance in classification and regression. As a result, deep based approaches are becoming one of the preferred choice for Alzheimer diseases (AD) related researches. The prime objective of this paper is to incorporate brain region that is known to be a significant biomarker for AD MRI classification. We considered left hippocampus as a distinguishing feature for separating AD from normal control (NC) MRI. And a convolutional neural network (CNN) is designed for classification task. The input to the network are the three-view patches of size 16 by 16 taken at hippocampus regions. The proposed approach showed reasonable computational efficiency as well as prediction accuracy of 97.8%. We performed our experiment on well-established Alzheimer's disease Neuroimaging Initiative (ADNI*) data. We prepared the training and test set based on the MRI scans irrespective to patients. So, it is reasonable to assume that MRI scans from a patient are randomly distributed to training and test set. The training dataset were tenfold cross validated.

Keywords—CNN; AD; Deep Learning; Dropout, Adam Optimizer, Softmax, Cross entropy

* Data used in preparation of this article were obtained from the Alzheimer's Disease Neuroimaging Initiative (ADNI) database (adni.loni.usc.edu). As such, the investigators within the ADNI contributed to the design and implementation of ADNI and/or provided data but did not participate in analysis or writing of this report. A complete listing of ADNI investigators can be found at: http://adni.loni.usc.edu/wp-content/uploads/how_to_apply/ADNI_Acknowledgement_List.pdf

I. Introduction

Previous studies [1] [5] [6] made claims that machine learning algorithms were able to predict AD more accurately than experienced clinicians. As a machine learning technique, deep learning is showing outstanding results in classification and regression. And deep based approaches has been explored for MRI classification [4], and predictions can be made for the disease status of a patient based on MRI scan [8].

The accuracy of the prediction mostly depends on the disease-representing features of the MRI. Specific to AD diagnosis, hippocampus is known to provide discerning features [11] [13]. Thus, we focus on the hippocampus region as the input feature for the CNN. We localize the hippocampus by manual observation for each MRI, then we feed 16×16 three-view patches (TVP) generated from localized region to the CNN. Our approach demonstrate reasonable computational efficiency as well as classification accuracy.

In this paper, we have summarized related works concerning deep learning based AD MRI classification researches in section II; our frameworks are described in section III; experimental setup and results are discussed in section IV and section V concludes the work.

II. Related works

As the cause of AD is not completely understood, designing analytic methods by hand-crafted features using medical experts' knowledge is a challenging task. Contrast, DL is capable of automatically learning processed features from a large set of training data. Many previous studies were conducted to further explore CNN architectures dedicated to generating robust AD features.

Gupta et al. [7] used cross-domain features to represent MRI data. They applied stacked auto-encoder (SAE) to learn a set of bases from natural images and then applied convolution network to get more effective feature representation for AD classification. In spite of being very simple, they claimed to achieve high classification performance, which is competitive with or better than contemporary approaches.

Brosch et al [3] learned a low-dimensional manifold of brain volumes by the deep belief networks (DBN) algorithm to detect the modes of variations correlating to demographic and disease parameters for AD. Their primary contributions are 1) they introduced a much more computationally efficient training method for DBNs that allows training on 3D medical images with a resolution up to 128×128×128, and 2) they demonstrated that DBNs can learn a low-dimensional manifold of brain volumes that can detects modes of variations.

Liu et al. [2] also proposed an SAE-based multimodal neuroimaging feature learning algorithm from region of interest (ROI) for AD diagnosis. To deal with multi-modality data they deployed zero-masking based data fusion strategy.

Payan et al. [4] uses sparse auto-encoder to learn feature embedding and then feed these embedding to convolution neural network for AD classification. They build a learning algorithm that is able to discriminate between healthy brains (HC) and diseased brains using MRI images as input. They investigated a class of deep artificial neural networks, and specific combination of sparse auto-encoders and convolutional neural networks. The main novelty of their approach is to use 3D convolutions on the whole MRI image.

Li et al. [8] proposed a robust multitask deep learning framework using dropout and stability selection technique to improve the ROI features representation for AD/MCI diagnosis. Shi et al. [1] developed a robust deep learning framework for multimodal AD diagnosis from MRI and PET scans. They

applied principal component analysis (PCA) to obtain features, and then utilized the stability selection technique [10] together with the least absolute shrinkage and selection operator (Lasso) method [11] to select the most effective features. These features were feed to deep learning model for further processing. They learned initial weights by adopting unsupervised learning strategy and then fine-tuned the parameters by supervised learning using AD patient labels as ground truth. During the fine-tuning phase, the dropout layer was added to improve the model's generalization capability. Finally, in the last layer SVM classifier was used for AD/MCI classification based on the learned features.

III. Methodology

The proposed approach's pipeline is depicted in fig 1. TVP Generator extracts $3 \times 16 \times 16$ patches from the region of interest of the MRI, namely hippocampus region. The patches are then feed to CNN. The CNN classify the individual TVP as AD or NC. The majority of 32 TVP predicts the AD/NC status of MRI.

A. Data Set

In this study, we used the Alzheimer's disease Neuroimaging Initiative (ADNI) database. This database was launched in 2003 as a public-private partnership. The primary goal of ADNI has been to measure progression of mild cognitive impairment (MCI) and AD from clinical and neuropsychological assessments, multi-modal data (MRI, PET) and biomarkers.

B. TVP Generation

We generate reference points $R(r_x, r_y, r_z)$ from Gaussian random number generator as in equation 1.

$$P(R) = \frac{1}{\sqrt[3]{8\pi}} e^{-\frac{(R-H)^2}{8}} \quad (1)$$

Here, $P(R)$ represents probability distributions of reference point $R(r_x, r_y, r_z)$. $H(h_x, h_y, h_z)$ is hippocampus location.

TABLE I. Manually observed location of left hippocampus

Image ID	Patient ID	Left Hippo Campus location (h_x, h_y, h_z)
S41463	100_S_0015	(145,139,65)
S20029	023_S_0030	(151,118,59)
S28430	136_S_0184	(150,129,67)

C. Convolutional Neural Network

In our proposed CNN architecture, the input is TVP, centered at the locations generated from the reference points as in fig. 1. For a single MRI, at least 32 different offsets are used to generate 32 different TVP. The CNN is train to predict individual TVP as AD or NC. Based on the collection of individual TVP decisions, the MRI is classified as AD or NC. The architecture of our CNN is shown in TABLE II. The output of third convolution layer is the feature embedding of the hippocampus region. These features are further fed to the fully connected layers to classify AD/NC. Adding dropout 0.75 in first FC layer slightly improved the accuracy. We used softmax cross-entropy as the loss function. Adam optimizer [14] and Xavier initialization [15] were used. Other related parameter values are noted in TABLE II.



Fig.1. CNN model for AD/NC classification from hippocampus atrophy

TABLE II. Architectural and training details of CNN

Layer	Specification
Input	Three View Patch of Size $16 \times 16 \times 3$; $N \times C \times H \times W = 32 \times 3 \times 16 \times 16$
Output	$[AD/NC]^T$
Convolution Layer 1	Number of Filters=64; Filter Size=5×5; Activation Function: ReLU (max (0, WX+b)) where, W is Weight, X is the input and b is bias; Maxpooling: 2×2; InputCL1=Input; outputCL1=12×12× 64.
Convolution Layer 2	Number of Filters =32; Filter Size=5×5; Activation Function: ReLU; Maxpooling: 2×2; InputCL2=outputCL1; outputCL2 =8×8×32.
Convolution Layer 3	Number of Filters =16; Filter Size=5×5; Activation Function: ReLU; Maxpooling: 2×2; InputCL3=outputCL2; outputCL3 =4×4 ×16
Fully Connected Layer1	Number of Neurons=16; Activation Function=ReLU; inputFCL1 = outputCL2; outputFCL2=16.
DropOut Layer	0.75
Fully Connected Layer2	Number of Neurons=2; ActivationFunction =softmax ; inputFCL2 = output of Dropout Layer; outputFCL2: (AD NC) ^T .
Loss Layer	LossFunction: Categorical Crossentropy
Training	Weight Initialization: Xavier; Optimization: Adaptive moment estimation(Adam) Optimizer where: Exponential decay rate for first moment estimate, $\beta_1=0.9$ Exponential decay rate for second moment estimate, $\beta_2=0.999$ Divide by zero prevention constant, $\epsilon=0.00001$ Learning rate, $\alpha=0.0001$; Batch Size: 32

IV. Experiments and Results

A. Data Preparation

In ADNI we have 351 MRI scans from 60 different patients. Among these 131 MRI are labeled as NC, 144 as MCI and 76 as AD. We combined MCI and AD as a single label named AD. From 352 scans we have selected 100 NC scans and 150 AD scans with purposive random sampling and without considering the patient IDs, which makes up 250 MRI scans for training. The remaining 31 NC and 70 AD labeled scans are used as test set. MRI scans from a single patients may appear in different set as we did not separate data by considering patient ID. The size of the MRI scans are generally $170 \times 256 \times 256$. The sizes variations in some MRIs did not affect our experiments as the scale of the

data is mostly invariant. We used tenfold cross validation to evaluate our method. In tenfold cross validation, we randomly divided the dataset in ten different subsets of equal size. We ensure to avoid class imbalance in each subset by carefully choosing samples from each class. For each run we use nine subset for training while keeping one subset for testing. In subsequent runs, we interchanges the test set with remaining nine training set. We repeated the process to ensure that each subset is used at least once as test set. The accuracy is calculated over all the correctly classified sample and total samples.

B. Hippocampus Localization

We crosscheck the manual hippocampus location, H (h_x, h_y, h_z) by repeating the manual marking at different runs, and found on average less than 1 mm error in subsequent localization. The examples of pixel coordinate for left hippocampus each MRI are shown in TABLE II.

C. AD/NC Classification

The performance of the binary classification of the CNN is presented on TABLE IV. First two columns display the precisions of the relevant classes. The following three columns show the overall accuracy, sensitivity and specificity calculated from the confusion matrix of test set. Fig. 2. Illustrates the validation accuracy and loss curve for CNN in one of the cross-validation run. The vertical axis is the accuracy (left) and loss (right) while the horizontal axis represents the number of training steps.

V. Conclusion

This work proposed an efficient framework for detecting hippocampus atrophy from ADNI MRI scans and subsequently classify the MRI into AD or NC. Instead of using whole 3D image, we examined only the left hippocampus region in details. Based only on the features from hippocampus, we were able to successfully classify MRI scans as AD or NC at 97.8% accuracy. Although the result is little below the state-of-the-arts accuracy, we were able to show that an accurate AD/NC MRI classification is possible using only a small ROI of brain such as left hippocampus.

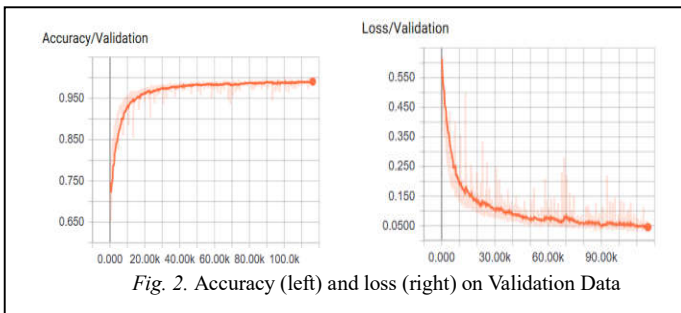


Fig. 2. Accuracy (left) and loss (right) on Validation Data

TABLE III. Performance (%) of the binary ad/nc mri classification

Precision(NC)	Precision(AD)	Accuracy	Sensitivity	Specificity
97.9	97.7	97.8	97.7	97.9

Acknowledgement

This research was supported by MIST (Ministry of Science & ICT), Korea, under the National Program for Excellence in SW) supervised by the IITP (Institute for Information & Communications Technology Promotion) (2017-0-00137).

References

- [1] J. Shi, X. Zheng, Y. L. Q. Zhang, S. Ying, "Multimodal neuroimaging feature learning with multimodal stacked deep polynomial networks for diagnosis of Alzheimer's disease", IEEE Journal of Biomedical and Health Informatics, vol. PP, no. 99, 2017.
- [2] S. Q. Liu et al., "Multimodal neuroimaging feature learning for multiclass diagnosis of Alzheimer's disease," IEEE Trans. Biomed. Eng., vol. 62, no. 4, pp. 1132–1140, Apr. 2015.
- [3] T. Brosch, R. Tam, and ADNI, "Manifold learning of brain MRIs by deep learning," in Proc. Int. Conf. Med. Image Comput. Comput. Assist. Interv., 2013, pp. 633–640.
- [4] Payan and G. Montana, "Predicting Alzheimer's disease: A neuroimaging study with 3D convolutional neural networks," in Proc. Int. Conf. Pattern Recog. Appl. Methods, 2015.
- [5] S. Liu, W. Cai, H. Che, S. Pujol, R. Kikinis, D. Feng, M.J. Fulham, "Multimodal neuroimaging feature learning for multiclass diagnosis of Alzheimer's disease", IEEE Transactions on Biomedical Engineering, vol. 62, no. 4, pp. 1132-1140, 2015.
- [6] S. Liu, S. Liu, W. Cai, S. Pujol, R. Kikinis, D. Feng, "Multi-phase feature representation learning for neurodegenerative disease diagnosis", Australasian Conference on Artificial Life and Computational Intelligence, pp. 350-359, 2015.
- [7] Gupta, M. Ayhan, and A. Maida, "Natural image bases to represent neuroimaging data," in Proc. Int. Conf. Mach. Learn., 2013, pp. 987–994.
- [8] F. Li, L. Tran, K. H. Thung, S. W. Ji, D. G. Shen, and J. Li, "A robust deep model for improved classification of AD/MCI patients," IEEE J. Biomed. Health Informat., vol. 19, no. 5, pp. 1610–1616, Sep. 2015.
- [9] H.I. Suk, S.W. Lee, D. G. Shen, and ADNI, "Hierarchical feature representation and multimodal fusion with deep learning for AD MCI diagnosis," NeuroImage, vol. 101, pp. 569–582, Nov. 2014.
- [10] Hinrichs, V. Singh, G. F. Xu, S. C. Johnson, and ADNI, "Predictive markers for AD in a multi-modality framework: An analysis of MCI progression in the ADNI population," NeuroImage, vol. 55, no. 2, pp. 574–589, 2011.
- [11] Q. Zhang, Y. P. Wang, L. P. Zhou, H. Yuan, D. G. Shen, and ADNI, "Multimodal classification of Alzheimer's disease and mild cognitive impairment," NeuroImage, vol. 55, pp. 856–867, 2011.
- [12] Amoroso, N., Rocca, M. L., Bellotti, R., Fanizzi, A., Monaco, A., Tangaro, S., Weiner. (2018). Alzheimer's disease diagnosis based on the Hippocampal Unified Multi-Atlas Network (HUMAN) algorithm. BioMedical Engineering OnLine, 17, 6. <http://doi.org/10.1186/s12938-018-0439-y>
- [13] B. Olsson, R. Lautner, U. Andreasson, A. Öhrfelt, E. Portelius, M. Bjerke, M. Hölttä, C. Rosén, C. Olsson, G. Strobel, E. Wu, K. Dakin, M. Petzold, K. Blennow, H. Zetterberg; CSF and blood biomarkers for the diagnosis of Alzheimer's disease: a systematic review and meta-analysis; The Lancet Neurology, Volume 15, Issue 7, 2016, pp. 673-684
- [14] P. D. Kingma, B. Jimmy, "Adam: A Method for Stochastic Optimization", 3rd International Conference for Learning Representations, San Diego, 2015
- [15] X. Glorot, Y. Bengio, "Understanding the difficulty of training deep feedforward neural networks." In In Proceedings of the International Conference on Artificial Intelligence and Statistics (AISTATS10). Society for Artificial Intelligence and Statistics, 2010.

Hippocampus Localization Using Hough-CNN

Abol Basher

Department of Computer Engineering
Chosun University
Gwangju, South Korea

Ho Yub Jung

Department of Computer Engineering
Chosun University
Gwangju, South Korea
hoyub@chosun.ac.kr

Abstract— The memory loss is known to have a link to the atrophy of hippocampus. In this paper, we present Hough Convolutional Neural Network (H-CNN) based localization of hippocampus from MRI data. From large size of volumetric MRI data, the localization of hippocampus is highly complicated. However our localization method works efficiently on MRI data. H-CNN calculate the relative offset from random reference point to the ground truth hippocampus location and provides accumulated average position. We have trained our network using 250 MRI, validate on 50 MRI and test on 50 MRI. This data separation has been performed according to MRI serial number. The accumulated average test loss is 4.62mm.

Keywords—H-CNN, Hippocampus, Localization, Offset.

*Data used in preparation of this article were obtained from the Alzheimer’s Disease Neuroimaging Initiative (ADNI) database (adni.loni.usc.edu). As such, the investigators within the ADNI contributed to the design and implementation of ADNI and/or provided data but did not participate in analysis or writing of this report. A complete listing of ADNI investigators can be found at:

http://adni.loni.usc.edu/wpcontent/uploads/how_to_apply/ADNI_Acknowledgement_List.pdf

I. Introduction

An extensive research on medical imaging are being carried out in recent years. Brain MRI is one of the *most* studied field in medical image analysis, and hippocampus localization in MRI has been researched in various groups [1] [3] [4]. Our method combines the Convolution Neural Network and Hough Transformation and offers generalized technique to predict hippocampus location in MRI.

Convolutional Neural Network (CNN) is good at learning hierarchical representation of the input data without requiring any handcrafted features. Taking that advantage of CNN, we have designed simple H-CNN [1] to locate hippocampus. H-CNN learns the feature maps from input training patches and offers a prediction. The offset between the reference point and manually localized left hippocampus position is used as ground truth for our network. H-CNN predicts the offsets from the patches that are created from the random reference points and thus locates the hippocampus.

The remaining research work has been organized in the following sections. In section II, we have introduced H-CNN related works. In section III, the functional methodology of H-CNN as well as the dataset preparation have been explained. The training procedures of H-CNN with validation and testing

procedures have been described in section IV. In section V, we have summarized the paper.

II. Related Works

Hough CNN is based on Hough forest [2] which performs a generalized Hough transform using random forest. Hough transform convert the input image into Hough image that is also known as a Hough space where each point in the Hough space corresponds to a hypothesis about the object of interest in the original image space at a certain location [7][8]. Hough forest makes a codebook based on local appearance of image or video frames. It generates a decision tree learned from training data and each leaf of the tree provides a probabilistic vote in the Hough space [6]. Codebook based Hough voting strategy is efficient to locate specific object with limited number of training samples where each patch is sampled independently, and the combined votes estimate the center of object [2].

Juergen Gall et al. [2] have developed a method using Hough Forests for object detection such as pedestrian detection from unconstrained images and videos. They have improved the general Hough transform and combine with other methods like the Implicit Shape Model [9] and local appearance codebooks. Angela Yao et al [6], using Hough transform voting strategy, have proposed a framework to detect human action. The codebook shares features between the action classes and vote for the action centers in a probabilistic manner.

The method we have developed in this paper is related to number of existing works that were developed for object recognition, localization and segmentation. The work most related to our model is Fuesto Milletari et al.’s [1] approach on brain regions segmentation using H-CNN. Fuesto Milletari et al. [1] have introduced H-CNN based segmentation for MRI and CT. Firstly, a binary segmentation volume is constructed from background and foreground classification. Binary segmentation volumes are used to train the networks and obtained a features vector and a vote with segmentation patch where segmentation patches represents foreground and background. The feature vector is compared with the database to retrieve the nearest neighbors. Once the neighbors are identified, the vote with their associated segmentation patches has been used to localize and segment the interested regions. According to [1], 26 regions have segmented from brain MRI. They used H-CNN for MRI segmentation, in contrast, we focus on the localization of hippocampus using H-CNN in this paper.

III. Hippocampus Localization

A. Method

Let us assume that we can calculate offset from several random points to one certain interest point, and average those offsets. We can move to new location by averaged offset to generate new reference point. And we keep continuing offset calculation cycle for the same interest point, then after few cycles we can end up at our interest point. Using this approach, H-CNN, trained to predict offset value to hippocampus location, is able to accurately output the hippocampus position from any random MRI position.

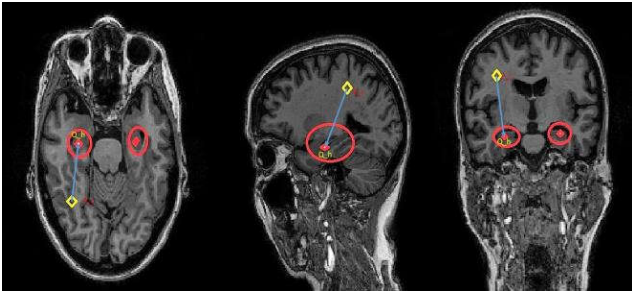


Fig. 1. Offset calculation from random reference point to the manually localized left hippocampus position.

Let us consider a volumetric MRI is $I: \mathbb{R}^3 \rightarrow \mathbb{N}$ and three axis in the MRI is X, Y and Z. For any random point $P(a_x, b_y, c_z)$ and manually localized left hippocampus position $Q(u_x, v_y, w_z)$ are within the MRI. Then offset between the random point P and the hippocampus location Q will be X_{gt}, Y_{gt}, Z_{gt} .

$$\begin{aligned} X_{gt} &= (u_x - a_x) \\ Y_{gt} &= (v_y - b_y) \\ Z_{gt} &= (w_z - c_z) \end{aligned} \quad (1)$$

X_{gt}, Y_{gt}, Z_{gt} are used as ground truth for H-CNN. For any MRI, random reference point's three-view patches and offsets to hippocampus can be generated. And offsets are used as input features and ground truths, respectively.

B. Dataset

The ADNI* dataset have 131 Normal Control (NC) MRI, 76 Alzheimer's disease (AD) MRI, and 144 Mild Cognitive Impairment (MCI) MRI. 351-MRI exists in this dataset. ADNI MRI data have been used to train, validate and test our network. In ADNI MRI dataset, the MRI's pixel dimension is around 1mm in each axis. The most of the MRI's height, width, depth in ADNI dataset are 256, 256, and 170 respectively. 350-MRIs have been selected for training, validating and testing the proposed H-CNN: 250 MRI for training set, 50 MRI validation set, and 50 MRI test set. We have used the MRI serial number to divide the data into training set, validation set and testing set. This dataset consists of 60 patients that is why there are chances to have same patient's MRI scan in training, testing and validation set.

The patches have been generated using a range of 16 pixel from the manually localized left hippocampus points. So for every direction, maximum 16 pixel from the hippocampus location is considered and random reference points are generated. Using those points as a center, three-view (Sagittal, Axial,

Coronal) 32x32 2-D patches are extracted and merged into three channel reference patches. 60% training patches' centers are kept within 8x8x8 cubic region from the hippocampus location. Approximately, 3,000 Patches are created from each MRI for training. For training, validating and testing, the generated total patches are 750,000, 200,000 and 200,000 respectively. Separate MRIs are used for training, validating and testing. The corresponding ground truths are the offsets from the random three-view patch point to the manually marked hippocampus position.

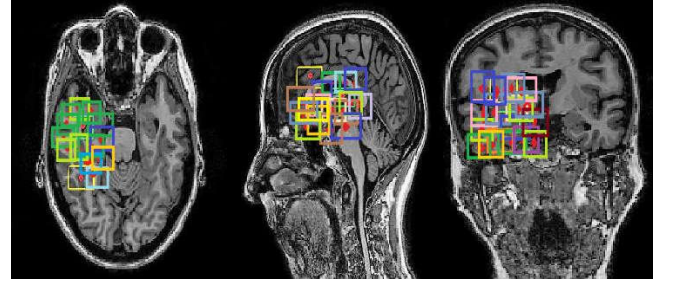


Fig. 2. Using random reference point as a center, the 3-channel 32x32 2-D patches has been generated from the MRI.

IV. Experiment And Evaluation

A. Training and Validation

The H-CNN architecture is shown in Table I. After each convolution block and fully connected block, Rectified Linear Units (ReLU) [10] has been used as an activation function. We have used Adam optimizer [11] for our network optimization. For Adam optimizer, all the parameters are kept as default except for the learning rate and decay factor. The learning rate and decay factor are 0.001 and 0.009 respectively for proposed H-CNN. Three channel patches from MRI are fed to H-CNN. From training patches, H-CNN learns the features map and predicts offsets. A graphical overview of the network, input and output is shown in Fig. 3.

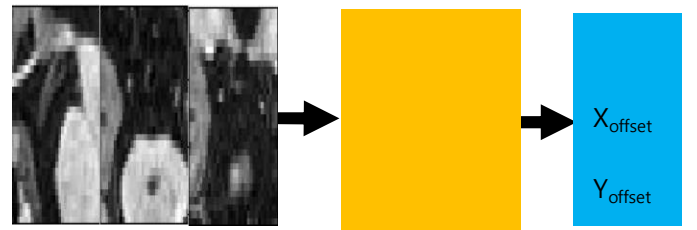


Fig. 3. 3-channel 32x32 patches has been feed to the H-CNN as input and returns $X_{offset}, Y_{offset}, Z_{offset}$ as output from H-CNN.

TABLE I. NETWORK ARCHITECTURE

Layer	Parameters Details
Layer 1	Conv1: Kernel size = 3 Number of filters = 8 Input size = 32x32x3 Pooling 1: Kernel size = 2, Stride = 2 Activation function: ReLU
Layer 2	Conv2: Kernel size = 3, Number of filters = 16, Input size = 16x16x8, Pooling 2: Kernel size = 2, Stride = 2 Activation function: ReLU
Layer 3	Conv3: Kernel size = 3, Number of filters = 32, Input size = 8x8x16 Activation Function: ReLU
Layer 4	Conv 4: Kernel size = 3, Number of filters = 64, Input size = 8x8x32 Activation function: ReLU
Layer 5	FC Layer 1: Number of filter = 256 Activation Function: ReLU
Layer 6	FC Layer 2: Number of filter = 128 Activation function: ReLU
Layer 7	Dropout = 0.6
Layer 8	FC Layer 3: Number of filter = 3

A L1 distance loss function has been used for our network. The loss function is shown in equation (2). Euclidean distance is computed between offsets predicted by H-CNN and ground truth offsets.

$$\text{Loss} = \sqrt{((X_{\text{offset}} - X_{\text{gt}})^2 + (Y_{\text{offset}} - Y_{\text{gt}})^2 + (Z_{\text{offset}} - Z_{\text{gt}})^2)} \quad (2)$$

$X_{\text{offset}}, Y_{\text{offset}}, Z_{\text{offset}}$ is the offset that has been predicted by H-CNN and $X_{\text{gt}}, Y_{\text{gt}}, Z_{\text{gt}}$ is the ground truth offset that has been calculated from random reference point to manually marked position of hippocampus. The network has been trained for 30 epochs. The training loss and validation loss are shown in Fig. 4.

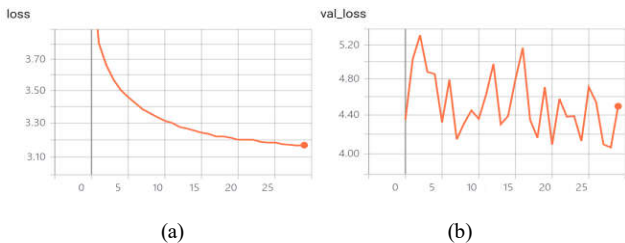


Fig. 4. (a) Training loss (b) Validation loss

B. Testing

For testing, 200,000 patches have been feed to our trained model. The average test loss is 4.62mm. The training, validating and testing have been carried out on HP Workstation Intel Xeon Processor (3.10 GHz) with 32 GB RAM along with INVIDIA Quadro MD4000 GPU (8GB).

V. Conclusion

In this work, we applied H-CNN to localize the left hippocampus. The average accumulated loss for test set is 4.62 mm for 200,000 samples from 50 MRI. For future improvements, we look to re-analyze our network parameter selections and network size as well as consider scaling and rotation data augmentation. In this research work, we divide the dataset using MRI serial number. In future research, we will separate the dataset according to the patient identification number, more like the real-world problem.

Acknowledgment

This research was supported by MIST (Ministry of Science & ICT), Korea, under the National Program for Excellence in SW) supervised by the IITP (Institute for Information & Communications Technology Promotion) (2017-0-00137).

References

- [1] Fausto Milletari, Seyed-Ahmad Ahmadi, Chritine Kroll, Annika Plate, Verene Rozanski, Juliana Maiostre, Johannes Levin, Olaf Dietrich, Birgit Ertl-Wagner, Kai Botzel, and Nassir Navab, "Hough-CNN: Deep Learning for Segmentation of Deep Brain Regions in MRI and Ultrasound," arXiv:1502.02506v1[cs.CV] 9 Feb 2015.
- [2] Juergen Gall, Angela Yao, Nima Razavi, Luc Van Gool, and Victor Lempitsky " Hough Forests for Object Detection, Tracking and Action Recognition," IEEE Transaction On Pattern Analysis And Machine Intelligence.
- [3] Alexandre de Brebisson and Giovanni Montana, "Deep Neural Network for Anatomical Brain Segmentation," CVPR2015 .
- [4] Adrian Payan and Giovanni Montana, "Predicting Alzheimer's Disease: a neuroimaging study with 3D convolutional neural networks," arXiv: 1502.02506v1[cs.CV] 9 Feb 2015.
- [5] D. Ballard, " Generalizing the hough transform to detect arbitrary shapes ," Pattern Recognition, vol.13, no. 2, pp. 111-122, 1981.
- [6] A. Yao, J. Gall and L. Van Gool, " A hough transformed-based voting framework for action recognition," in IEEE Conf. Computer Vision and Pattern Recognition, 2010.
- [7] R. Okado, "Discriminative generalized hough transform for object detection," in Int'l Conf. Computer Vision, 2009
- [8] O. Barinova, V. Lempitsky, and P. Kohli, " On the detection of multiple object instances using hough transforms," in IEEE Conf. Computer vision and Pattern Recognition, 2010.
- [9] B. Leibe and B. Schiele, "Interleaved object categorization and segmentation," in British Machine Vision Conf., 2003, pp.759-768.
- [10] Vinod Nair and Geoffrey E. Hinton, " Rectifier Linear Units improve Restricted Boltzmann Machines" ICML, 2010.
- [11] Diederik P. Kingma and Jummy Lei Ba, " ADAM: A method for stochastic optimization," arXiv: 1502.02506v1[cs.CV] 30 Jan 2017.

Resilience of Features for Detecting Open Source Software in Obfuscated Android Apps

Byoungchul Kim
Dept. of Software Science
Dankook University
Gyeonggi-do, Republic of Korea
gurukbc@dankook.ac.kr

Seong-je Cho
Dept. of Computer Science and Engineering
Dankook University
Gyeonggi-do, Republic of Korea
sjcho@dankook.ac.kr

Kyeonghwan Lim
Dept. of Computer Science and Engineering
Dankook University
Gyeonggi-do, Republic of Korea
limkh120@dankook.ac.kr

Minkyu Park
Dept. of Software Technology
Konkuk University
Chungju, Republic of Korea
minkyup@kku.ac.kr

Abstract— As the use of Open Source Software (OSS) increases, OSS license violations increase because software developers adopt OSS arbitrarily without obeying open source license's terms and security threats of software vulnerabilities can also increase if popular OSS has severe bugs or weaknesses. Recently lots of Android apps adopt OSS. Therefore, we must be able to detect whether OSS in question is included in Android apps without notice. Code obfuscation makes this detection more difficult. Features used for the detection should be resilient to code obfuscation. We explore which feature are resilient to which obfuscation technique. This paper considers the features such as class hierarchy, Android components, and control flow graph. Our experiment result can lead to an efficient detection technique considering multiple features simultaneously.

Keywords—Android, Open Source Software, Similarity detection, Feature, Code obfuscation

I. Introduction

As the use of Android smartphones increases, so do the number of apps being developed. As a result, the use of Open Source Software (OSS) has been increasing to reduce costs and shorten development time. Using OSS can cause OSS license violation [1] and security problems due to OSS vulnerability. To solve these problems [2], it is necessary to be able to detect whether apps contain OSS or not.

We can use software features to calculate similarity between two software. OSS detection tools based on features have been developed, but their detection rates are low. Most of the released apps are obfuscated, thus features are also transformed. For example, SimiDroid [3] uses the Android app components as features. When the obfuscation tool DashO [4] is used to perform renaming obfuscation, the content of the AndroidManifest.xml file of the APK is also obfuscated. The file is a target of comparison. Using SimiDroid [3], the similarity between original APK and obfuscated APK must be low.

The resilience to obfuscation of feature used by OSS detection tools is directly related to the effectiveness of the tool. LIBSCOUT [5], LIBPECKER [6], and Kim et al. [7] argue that class hierarchy, class dependency, and control flow graph (CFG) with partial method signature are resilient to

obfuscation. However, one feature cannot be resilient to all obfuscation techniques.

To calculate the similarity of software, several studies using many features were performed. Lim et al. [8] compare the original APK with the obfuscated APK using the class hierarchy of LIBSCOUT [5] and compare APKs that are not identified similar using the control flow graph feature of Kim et al. [7]. In this multilevel detection technique, resilient features should be used for each type of obfuscation. In this paper, we first apply various obfuscation techniques to Android apps using DashO [4] which is one of popular tools for obfuscating Android apps. By comparing the detection results of three OSS detection tools (SimiDroid [3], LIBSCOUT [5], and CFG-based DexDump[7]), we then analyze the resilience of features which are used for measuring the degree of software similarity by the three tools.

II. Related Work

OSS detection tools use various features and the detection performance and resilience to obfuscation are different. LibScout [5] uses class hierarchy as feature, LIBPECKER [6] class dependency, and SimiDroid [3] Android component. Originally LibScout and LIBPECKER are tools for third-party library detection, not OSS detection, but feature extraction and feature comparison can also be applied to OSS detection.

LibScout is resilient against some obfuscation schemes, however, has limitation when applied to large-scale library detection, because it extracts too relaxed class profile and it is hard to handle developer customization, and dead code elimination [6]. On the contrary, LIBPECKER can construct strict class signatures and encode class dependencies into a signature for each class and each class member. LIBPECKER's signature is harder to conflict compared to the relaxed class profile in LibScout. Besides, LIBPECKER employs fuzzy class matching and adaptive class similarity threshold and weighted class similarity to handle code customization and dead code elimination. Unfortunately, LIBPECKER is not open to the public.

TABLE I. Comparison with Related Studies

	Main feature	Purpose	Code obfuscation
LibScout [5]	Class hierarchy (Package tree)	Detecting 3 rd -party libraries in apps. Pinpointing exact library versions.	Considering Identifier renaming and API hiding
LIBPECKER [6]	Class Dependency	Detecting 3 rd -party libraries in apps	Not specifying which obfuscation tools are used. More resilient to code-based obfuscation than LIBSCOUT
SimiDroid [3]	Android component, method, and resource	Detecting Android OSS	Not considering obfuscation techniques and tools
WuKong [9]	Code Clustering	Detecting app clones by filtering lib code	Considering apps obfuscated by ProGuard[10]
[7]	Control flow graph (CFG)	Detecting Android OSS	Applying only trivial obfuscation, String Encryption, Class Encryption, Reflection
[8]	Class hierarchy + CFG	Detecting obfuscated Android OSS	Considering apps obfuscated by ProGuard[10]
This Study	Class hierarchy, CFG, Android component	Exploring how much SW birthmarks are resilient to obfuscation techniques for Android OSS detection	Applying renaming, string, control flow Graph by DashO[4]

SimiDroid [3] is a framework for multi-level comparison of Android apps which can help to understand similarities/changes among app versions and among repackaged apps. It implemented several similarity comparison schemes that were borrowed from descriptions in the state-of-the-art literature, covering code-based and resource-based similarity comparisons. The comparison schemes includes method-based, component-based, and resource-based comparison.

In addition, WuKong [9] detects app clones with high accuracy by filtering library code that is detected by code clustering techniques. That approach relies on the assumption that app developers do not modify the library, however, the assumption is not realistic because dead-code elimination during app building will necessarily modify the library code. In addition, the approach only provides binary classifications because it cannot pinpoint the exact library versions used in the apps. Kim et al. [7] proposed a technique for generating a control flow graph from source codes as a feature. Lim et al. [8, 14] tried to increase detection rate using the Kim's proposed method after LIBSCOUT to calculate the similarity between the original APK and its corresponding APK obfuscated by ProGuard [10]. Table I shows the summaries of our study compared to the previous studies.

III. OSS Detection Technique

To verify resilience of features to code obfuscation schemes, we devise an OSS detection technique by utilizing open-source Android apps and their obfuscated version. We obfuscate Android apps by using DashO [4], which provides app hardening and shielding, reducing the risk of intellectual property theft. In this paper, we adopt three types of obfuscation, identifier renaming, string encryption, and control flow transformation by using DashO.

We then use three software detection tools that use different kinds of features. These tools include LIBSCOUT [5] using class hierarchy, SimiDroid [3] using Android components, and Kim et al. [7] using control flow graphs. The method of Kim et al. [7] is referred to as Dexdump for convenience of discussion. This is because Dexdump [11] is used to extract control flow graphs.

Figure I illustrates the OSS detection process. First, 67 open-source APKs obtained from F-Droid [12] are obfuscated using DashO. For each app, string obfuscation, renaming obfuscation, and control flow graph obfuscation are applied separately. As a result, three obfuscated apps are generated for each app. We measure the similarity of a pair of original and obfuscated apps using the three detection tools.

The Dexdump method, which extracts the control flow graph as a feature, are applied to only 40 apps. This method sets a threshold value on the number of nodes of graph because the overhead is too large when the number of nodes is too large and the accuracy of comparison is low when the number of nodes does not exceed minimum. APK may not contain enough branches in the method depending on its characteristics. In that case, the number of nodes will not exceed the threshold and will be excluded from the experiment.

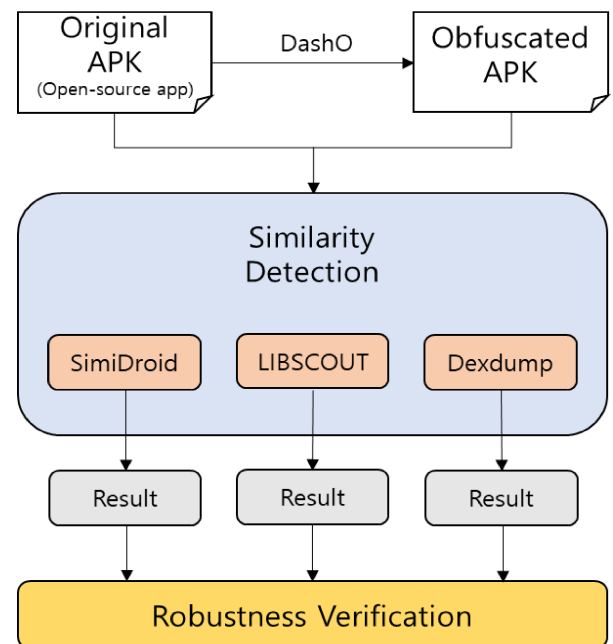


Fig.1. OSS Similarity Detection Process

TABEL II. Detecion Rate of Three Tools

Type of Obfuscation	Type of Tool		
	SimiDroid	LIBSCOUT	Dexdump
Renaming	22/67(32.83%)	3/67(4.47%)	35/40(87.50%)
String	66/67(98.50%)	5/67(7.46%)	34/40(85%)
Control flow graph	66/67(98.50%)	66/67(98.50%)	11/40(27.5%)

IV. Experiment Results

TABEL II shows the results of similarity measure between the original APK and the obfuscated ones. In the case of LIBSCOUT removes the arguments of a method and use it as a method signature. However, DashO inserts many methods that do not exist in the original APK code when string obfuscation is applied. As a result, the similarity between the original APK and the String obfuscated APK is very low. SimiDroid, on the other hand, is stronger in String obfuscation than LIBSCOUT because it uses the contents of AndroidManifest.xml file as features.

LIBSCOUT and SimiDroid show high degree of similarity to control flow graph obfuscation, while low degree of similarity to renaming obfuscation. It is because renaming obfuscation includes class hierarchy obfuscation, partial string obfuscation, and obfuscation of Android components.

In the case of Dexdump, it shows robust results for renaming and string obfuscation because it measures the similarity based on the control flow graph. On the other hand, it shows low similarity for the control flow graph obfuscation. This is because DashO directly inserts branch statements such as if-else statements into the code and the control flow graph is directly affected by the number of branch statements.

Dexdump also shows a lower degree of similarity in detecting string obfuscation than SimiDroid. This is because Dexdump uses method signatures as feature partially in addition to control flow graph.

V. Conclusion & Future Work

In this paper, we use three OSS detection tools and DashO obfuscation tools to verify which feature is resilient to which type of obfuscation. Class hierarchy feature is not resilient to renaming obfuscation and string obfuscation, and is resilient to obfuscation of control flow graph. In the case of Android component feature, it is not resilient to renaming obfuscation and is resilient to string obfuscation and obfuscation of control flow graph. Control flow graph feature is not resilient to control flow graph obfuscation and is resilient to renaming obfuscation and string obfuscation.

As mentioned in Section II, LIBPECKER[6] is known

to recognize a library even after a certain amount of code obfuscation is applied while existing works cannot. We plan to implement LIBPECKER's technique and detect obfuscated OSS module. In addition to, it is necessary to develop a tool that uses multiple features in steps. We can use multiple features resilient to each type of code obfuscation in combination. We will also study a method to give different weight to feature depending on characteristics of Android apps.

Acknowledgments

This research was supported by (1) the MIST(Ministry of Science and ICT), Korea, under the National Program for Excellence in SW supervised by the IITP(Institute for Information & communications Technology Promotion)(2017-0-00091), and (2) Basic Science Research Program through the National Research Foundation of Korea(NRF) funded by the MIST (no. 2018R1A2B2004830)

References

- [1] Synopsys, "2018 Open Source Security and Risk Analysis," Report of Synopsys Center for Open Source Research & Innovation, 2018.
- [2] OPEN SOURCE SECURITY RISKS, REWARDS AND REGULATION ,https://www.blackducksoftware.com/files/webmedia/webinars/ThomasEggar_ControlRisks_15.pdf ,Black Duck Webinar, 2014
- [3] LI, Li; BISSYANDÉ, Tegawendé F.; KLEIN, Jacques. "Simidroid: Identifying and explaining similarities in android apps," In Trustcom/BigDataSE/ICSS, 2017 IEEE, 2017. p. 136-143.
- [4] DashO,<https://www.preemptive.com/dasho>
- [5] BACKES, Michael; BUGIEL, Sven; DERR, Erik. "Reliable third-party library detection in android and its security applications," In: Proceedings of the 2016 ACM SIGSAC Conference on Computer and Communications Security. ACM, 2016. p. 356-367.
- [6] ZHANG, Yuan, Detecting third-party libraries in Android applications with high precision and recall. In: 2018 IEEE 25th International Conference on Software Analysis, Evolution and Reengineering (SANER). IEEE, 2018. p. 141-152.
- [7] G. Kim, J. Sim, and S. Cho, "A Study of Detecting Open-Source Software Module for Android Applications", in Proc. of the KIISE Korea Computer Congress, 2017, 125-127.
- [8] K. Lim, B. Kim, and S. Cho, "Detection of Obfuscated Open Source Android Apps", in Proc. of the KIISE Korea Computer Congress, 2018, 723-725.
- [9] WANG, Haoyu, et al. "WuKong: a scalable and accurate two-phase approach to Android app clone detection," In Proceedings of the 2015 International Symposium on Software Testing and Analysis. ACM, 2015. p. 71-82.
- [10] Proguard, <https://www.guardsquare.com/en/proguard>
- [11] Dexdump, <https://github.com/plum-umd/dexdump>
- [12] F-Droid, <https://f-droid.org/en/>
- [13] Deguard, <http://apk-deguard.com>
- [14] K. Lim, J. Han, B. Kim, S. Cho, M. Park, and S. Han, "Open-Source Android App Detection considering the Effects of Code Obfuscation," The 3rd International Symposium on Mobile Internet Security, Aug.-Sep. 2018.

Magnetic Resonance Imaging Enhancement using Adaptive Histogram Equalization with Multi-scale Method

Waqas Ellahi

Department of Information and Communication Engineering
Chosun University
309 Pilmun-Daero, Dong-Gu, Gwangju 61452, Republic of
Korea
waqasellahi@chosun.kr

Bumshik Lee

Department of Information and Communication Engineering
Chosun University
309 Pilmun-Daero, Dong-Gu, Gwangju 61452, Republic of
Korea
bslee@chosun.ac.kr (Corresponding author)

Abstract— Many diseases are diagnosed using Magnetic Resonance Images (MRI). The contrast between different regions or tissues in the MRI is an important factor for medical doctors to clearly visualize the region of interest in the image. In this paper, a visual quality improvement scheme is proposed on an existing MRI enhancement method. The existing MRI enhancement scheme uses Laplacian pyramid (LP) for edge preservation and singular value decomposition (SVD) for low frequency area enhancement in MRI. The Contrast-limited adaptive histogram equalization (CLAHE) is recommended instead of the Global Histogram Equalization (GHE) technique in the SVD enhancement module. The mean structural similarity index (MSSIM) and peak-signal-to noise (PSNR) metrics are used for evaluation. The experiment results show that the proposed recommendations improve image enhancement as well as preserves the edges of the image.

Keywords— Laplacian pyramid (LP); singular value decomposition (SVD); Contrast-limited adaptive histogram equalization (CLAHE); Global histogram equalization (GHE);

I. Introduction

Various modalities of medical imaging like Ultrasound, Computer Tomography (CT) and Magnetic Resonance Imaging (MRI) are used for diagnosing various kinds of diseases. Each medical imaging modality has their pros and cons. CT has the capability of rapid acquisition of images. On the other hand, MRI is a non-invasive method and does not harm the patient unlike CT. The radio waves and magnetic fields are used to capture the image of human organ in the MRI. MRI is mostly used to determine abnormalities in the pathology or structuring of the brain tissues [1]. The brain is the most complex organ of the human body and is made up of a composition of different neurons. The human brain controls all necessary actions of the body where it receives and understands information and relays required action to other organs of the human body.

The structure of different tissues of the brain are affected in many dangerous diseases. These diseases can be diagnosed by brain anatomy, for example hippocampus, ventricles and cerebral cortex areas are affected in the Alzheimer disease. Sometimes contrast between background and different tissues of the brain is inadequate due to RF coil imperfection or problem with image acquisition [2]. This inadequate

contrast might create problems for the medical inspector to diagnose the disease of the patient. The disease can easily be identified by improving the contrast of the MRI. Therefore, the MRI contrast enhancement considered as an essential pre-processing before any subsequent work. There has been a lot of works already done to enhance the visual quality and edge information in the MRI images.

The most common methods for MRI contrast enhancement are based on histogram equalization [3-4] and morphological operation [5-6]. In histogram equalization, different kinds of enhancement methods are applied such as Global Histogram Equalization (GHE), Local histogram equalization (LHE) and Adaptive Histogram Equalization (AHE). GHE accumulates the histogram of the pixel values in the image and then change all image pixel values. Whereas, GHE takes into description the global information and cannot adjust the local information of the image. Local Histogram Equalization (LHE) carries out block-overlapped histogram equalization. LHE classifies a sub-block and recovers the information. Then, the histogram equalization is used for the center pixel of the sub-block. In AHE, each pixel is customized based on the pixels that are in the neighboring region of that pixel. The morphology provides an approach based on geometrical shape in image processing. Dilation and erosion are the basic operations that are used to define the opening and closing operations. The first combination is erosion before dilation, called closing. The second combination is dilation before erosion, called opening. Closing morphological filtering is applied for image contrast enhancement when processing the pixels in the dark region of the image. With closing morphological filtering, the pixel contrast in the shadow regions can be enhanced to effectively improve pixel information. Since the light region remains unchanged, the contrast of the enhanced image is relatively apparent and the enhanced image is relatively natural. Opening morphological filtering is used during processing of the pixels in the light region of the image. With opening morphological filtering, the contrast can be stretched in the light region of the image, and the whitening is unlikely to occur. Opening morphological filtering retains the dark details of the image and prevents abnormal expansion of dark